The Dissertation (or Treatise) Committee for Kristen M. Lamb Certifies that this is the approved version of the following dissertation (or treatise):

Understanding the Assembly of Simple ssRNA Virus Nucleocapsids

Committee:

Stanley J. Watowich, Ph.D., Supervisor

Werner Braun, Ph.D.

Wlodzimierz M. Bujalowski, Ph.D.

Andres F. Oberhauser, Ph.D.

Stanley Lemon, M.D.

Bidadi V. Prasad, Ph.D.

Dean, Graduate School

Understanding the Assembly of Simple ssRNA Virus Nucleocapsids

by

Kristen Michelle Lamb, B.S.

Dissertation

Presented to the Faculty of the Graduate School of

The University of Texas Medical Branch

in Partial Fulfillment

of the Requirements

for the Degree of

Doctor of Philosophy

The University of Texas Medical Branch

December, 2010

Acknowledgements

Those who helped support me are those from my personal life and know full well of my gratitude for their support over the years. Their names remain private as they are from my private life.

Understanding the Assembly of Simple ssRNA Virus Assembly

Publication No._____

Kristen Michelle Lamb, Ph.D.

The University of Texas Medical Branch, 2010

Supervisor: Stanley J. Watowich

Abstract: The assembly of simple ssRNA viruses from the initial interactions critical for nucleocapsid formation until the morphogenesis which occurs at each maturation stage of the virus's "life" can entail a wide range of possibilities at every given stage. By whatever seeding event initiates the nucleocapsid formation, the nucleocapsid, encasing the nucleic acid, then undergoes changes associated with the virus maturation process, which can involve, becoming enveloped, interacting with additional virus/host proteins, becoming subsequently stripped of its envelope, and/or exposure to changes in ion concentration or pH change. My studies focused on two viruses, Hepatitis C Virus (HCV), focusing on the physical characteristics of core protein and *in vitro* nucleocapsid assembly; and Venezuelan Equine Encephalitis Virus (VEEV), focusing on *in vivo* formation of pre-viral nucleocapsid structures and briefly the subsequent post-entry nucleocapsid stage. Experimentally, it was found that H124 expressed better in *E. coli* expression systems than H158 and H36-169, which was attached to MBP. Purified H158 was found to be largely unstructured and exist as a multimer, even at a concentration of 1 mg/mL, making crystallization attempts with it a vain and unprofitable goal. The nucleocapsid-like-particles produced with H158 or H124 both showed size heterogeneity within the reactions, and given the scale of the reactions, projected purification yields would make cryo-EM reconstructions of these impractical. Therefore, focus shifted to VEE nucleocapasids, formed *in vivo*, enabling the experimental scale and biological relevance to increase substantially. VEE pre-viral nucleocapsid cryo-EM reconstructions were successfully achieved, but at low resolution. Given, again, the heterogeneity of the system at this maturation stage, it is more an insight into one, maybe two, structures,

which exist within the population. Thus, more questions are formed for the formation of ssRNA virus nucleocapsid formation.

Table of Contents

List of Figures

Introduction

Chapter 1: Introduction to Flaviviruses, Alphaviruses, and Nucleocapsid Assemblies

INTRODUCTION TO VIRUS ASSEMBLY-FOCUSING ON SSRNA NUCLEOCAPSID ASSEMBLY

The assembly of nucleocapsids within simple single-stranded (ss)RNA viruses is dependent on the structural and physical properties of the coat and ssRNA of which it is comprised. For the coat protein's part, it needs to form contacts with both itself, in potentially different conformations necessary to form pseudo-hexamers and pentamers in the nucleocapsid protein shell, depending on its triangulation number (Nguyen *et al*., 2009), as well as the ssRNA it encases in many cases. The ssRNA itself must be folded either by assisted folding from the coat protein as in Satellite tobacco mosaic virus (Larson and McPherson, 2001); or an RNA chaperone as in HCV, HIV, and hepatitis delta (Cristofari *et al*., 2004; Huang and Wu, 1998; Rein *et al*., 1998); or it must collapse onto itself Woodson (Schneemann, 2006; Woodson, 2000). The difference between assisted RNA folding and chaperoning is that in assisted RNA folding the RNA has yet to be completely transcribed when a protein, usually the coat protein, begins helping the RNA into a fold conducive for encapsidation, and in the case of chaperoning, a protein, again usually the coat protein, interacts with the RNA post-transcription and melts its current structural elements and refolds it into the correct fold for encapsidation (Herschlag, 1995). The nucleocapsid itself is formed beginning with a nucleation event which occurs either from coat-coat interactions, as in the case of Herpes simplex viruses forming procapsids (Newcomb *et al*., 2001, 2000) or foot-and-mouth disease virus (Yafal

and Palma, 1979), which result in a protein shell which is then filled with the ssRNA (Chiu *et al.*, 1997), or by coat-ssRNA interactions, as in the case of Sindbis virus nucleocapsid assembly (Linger *et al.*, 2004), which results in coat proteins assembling around the core-ssRNA to form the nucleocapsid/virus (Larson *et al.*, 1998; Larson and McPherson, 2001). In addition, the size of the ssRNA plays a role in the determining the size and shape of the nucleocapsid particles (Schneemann, 2006). These basic principles of assembly are employed when the nucleocapsid assembles, but are reorganized during virus maturation to accommodate the nucleocapsid's changing roles.

Of the crystal structures available, the majority of coat proteins which adhere to tiling theory well are nearly identical, with β-barrel folds (Mannige and Brooks, 2008; Nguyen *et al.*, 2009; Rossmann and Johnson, 1989), though their sequences have no similarity (Chiu *et al.*, 1997). As of April 2007, this was the case for the coat protein structures available in the VIPER database, which was inclusive of eight virus families (Carrillo-Tripp *et al.*, 2009; Mannige and Brooks, 2008). After finding the structure of Hepatitis B Virus Core protein's largely alpha-helical structure, (Böttcher, *et al*., 1997), commented that the alpha-helical core's fold is "quite different from the standard β-sheet jelly-roll packing in many small viral capsids" (Böttcher *et al.*, 1997). This is, by no means, to suggest that the β-barrel coat is a paradigm in nucleocapsid assembly, as there are notable coat proteins which have predominantly alpha helical character, such as Narcissus Mosaic virus coat protein (Wilson *et al.*, 1991), Bromovirus capsid protein (Choi and Rao, 2000), and Rice Dwarf core protein P3 (Nakagawa *et al.*, 2003). Whatever the structure of the coat protein, it seems that non-covalent interactions drive the coat proteins into a few conformations to accommodate the coat-coat interactions necessary to produce the icosahedral structure prominent in ssRNA nucleocapsid

structures (Nguyen *et al*., 2009). From a theoretical perspective, in order to produce nucleocapsids of triangulation numbers greater than 1, the coat protein needs to adopt a few different conformations, which can largely be attributed to flexible regions near the N and C-terminals (Nguyen *et al*., 2009). A couple of theories, demonstrated computationally, have attempted to explain how protein subunits conglomerate effectively into an icosahedral structure. Two of these are the "local rules" theory (Berger *et al*., 1994; Schwartz *et al.*, 2000) and the "conformational switch" theory (Kellenberger, 1976). While the two do not necessarily contradict each other, they articulate what drives protein subunits to assemble differently. According to "local rules theory," the assembly of an icosahedral structure should be looked at as depending on interactions between protein subunits, like approximate interaction angle, angle lengths, and torsional angles of the given conformations the protein subunits occupy (Berger *et al.*, 1994). So, even though, a given coat protein subunit may occupy a variety of different conformations, it will only be the most energetically favorable conformation which interacts with a given subunit (Berger *et al.*, 1994). It further states that while you can build the pentamers and hexamers required for triangulation numbers greater than 1 by assembling hexamers and pentamers independently with the protein subunits, that computationally, this is possible still given what arrangement or interaction is the most favorable given the conformation of the growing assembly (Berger *et al.*, 1994). "Conformational switch" theory would go further to say that when, for instance two subunits, coat monomer or multimer, interact that they could cause conformational changes with each other, which therefore make the binding to the next subunit unique to how the first two interacted (Kellenberger, 1976). Still, conditions, like temperature and coat protein concentration, are factors which affect assembly (Dokland, 2000; Krol *et al.*,

1999; Nguyen *et al*., 2009; Prevelige *et al*., 1993; Salunke *et al*., 1989; Savithri and Erickson, 1983; Schwartz *et al*., 2000), and may affect the difference between triangulation number or success of the assembly at all (Nguyen *et al*., 2009). While this had not been demonstrated outside of computer simulations, it has been found that various viruses assemble using a given number of protein subunits, which could be either a monomer or some given multimer. Examples of this are T=3 black beetle virus which assembles from trimers (Reddy *et al.*, 1998), Hepatitis B core which is assembled using dimers after a nucleation event (Zlotnick *et al.*, 1999), and bacterophage P22 capsid which is capable of forming its T=7 structure using monomers (Tuma *et al.*, 2001). This still leaves the question unanswered of how pentamers and hexamers are possible if not formed independently and then collapsing onto each other to form a structure. According to Brooks and supposedly cross-referenced with structures in VIPER (Carrillo-Tripp *et al.*, 2009), there is nominal difference, about 1 Å rmsd (Nguyen *et al*., 2009), between comparable Cα atoms in subunit interactions which make up a pentamer versus a hexamers. It has also been suggested that coat protein may play a part in error checking during nucleocapsid assembly (Nguyen *et al*., 2009). This is because the coat proteins multimers act as "subassemblies" which conglomerate into icosahedral shells (Xie and Hendrix, 1995). Subassemblies without correct folds simply fail to make the correct bonds and remain in the assembling nucleocapsid (Xie and Hendrix, 1995). An articulate example of how virus subassemblies constitute preformed hexamers and pentamers (Kerner, 2008), suggests that the specificity of how the subassemblies conglomerate lie in the capability of the performed hexamers to be comprised of 2 types of sides, 3 types of sides, or 6 types of sides. The pentamers' sides must all be equivalent. According to Kerner, hexamers can only bind to other hexamers with certain side(s) and can only bind

to pentamers with given sides(s), due to their capability to make critical interactions with these sides and the inability to do so with other sides. Kerner also says that the possibility of "handedness" comes about when the virus is comprised of the most differentiated hexamers, e.g. with 6 different sides (Kerner, 2008). While, given that some coat proteins are inherently capable of forming these correct subassemblies or otherwise capable of forming icosahedral assemblies *in vitro* (Lopez *et al.*, 2009; Myers *et al*., 1999), this is not always the case, and chaperones (Chromy *et al*., 2003; Satyanarayana *et al.*, 2000; van der Vies *et al*., 1994; Wrobel *et al.*, 2000) are necessary for the coat protein to adopt the correct folds for assembly.

How coat proteins are arranged on icosahedral nucleocapsids, similar to proteins on the surface of any virion, have long been thought to be governed by the theory laid out by the Casper-Klug theory (Caspar and Klug, 1962). The basic assumptions are that viral structures are largely icosahedral, and therefore have at least 60 subunits on 20 triangular faces, and that to accommodate more than 60 protein subunits that these 20 faces can each be divided into smaller structural units, which is where we get the idea of different triangulation, "T" numbers from (Caspar and Klug, 1962). Helical structures have also been postulated and determined experimentally, such as TMV (Namba and Stubbs, 1986) and the nucleocapsids of mouse mammary tumor virus (Sarkar and Moore, 1970), but they do not seem to predominate. The preoccupation with icosahedral symmetry is that a virus with this geometry would be giving the maximum enclosure volume, empty space which nucleic acid could be packed, given the size of the protein subunit used to produce it (Caspar and Klug, 1962). In order to keep the overall icosahedral order, only certain triangulation numbers are allowed, according to the following equation by Casper and

Klug, H^2+HK+K^2, given that H and K must both be non-negative integers. This is illustrated in Fig. 1.1.

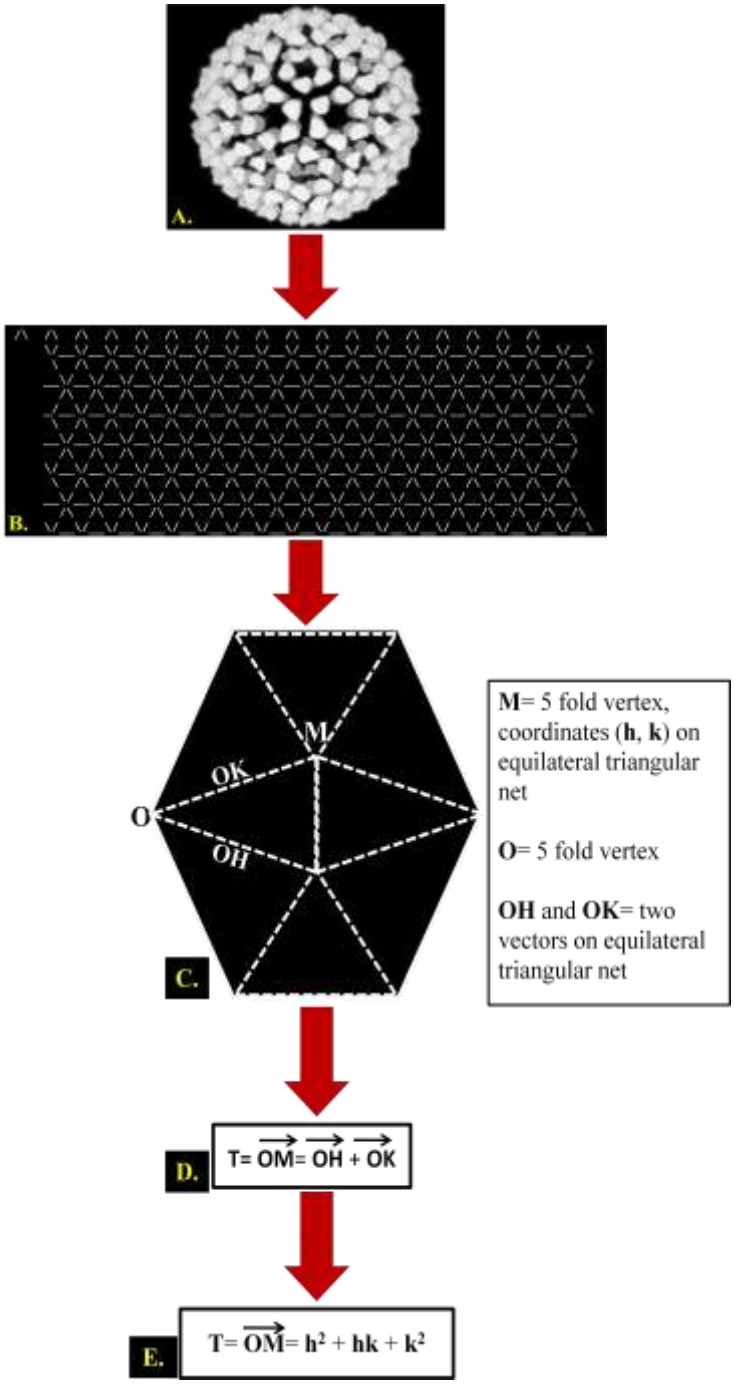

Fig. 1.1. The geometry of triangulation numbers

A. Example of an icosahedral nucleocapsid structure of triangulation number >1. Shown here is the VEEV mature nucleocapsid, originally reconstructed by A. Paredes (Paredes *et al*., 2001). B. An icosahedral structure can be produced by taking an equilateral triangular net and folding it in such a way to produce an icosahedral structure. That being said, the positions on the icosahedral face made by the equilateral triangular net can be described by positions on this "net." C. Triangulation number is calculated from vector OM, the distance between two neighboring 5-fold vertices. These distances are related to the "net" discussed in (B). D. The resulting vector equation for the triangulation number E. Resulting vector equation after expanding the vector equation using the (h, k) coordinates for OK and OH. Content modified from http://www.virology.wisc.edu/virusworld/tri_number.php.

This equation may seem impractical when faced with a newly reconstructed virus or other structure. Simpler ways to determine the triangulation number exploit other aspects of the icosahedral symmetry. For instance, an icosahedron is made up of 60 subunits making up 20 equilateral triangles in the total icosahedral structure. Structures with quasi-equivalence and a triangulation number greater than one have a total of 60T subunits making up 20T equilateral triangles. Thus, 60T subunits/20T equilateral triangles, suggests that there are 3T subunits per equilateral triangle in a given icosahedral structure of triangulation number, T. One of these 20T "equilateral triangles" can be used to reproduce the whole structure, since each of the equilateral triangles must be identical. This is, therefore, called the asymmetric unit (asu) of the structure. Thus, one can simply count the number of subunits in a given asymmetric unit to determine the triangulation number. This is illustrated in Fig. 1.2 below.

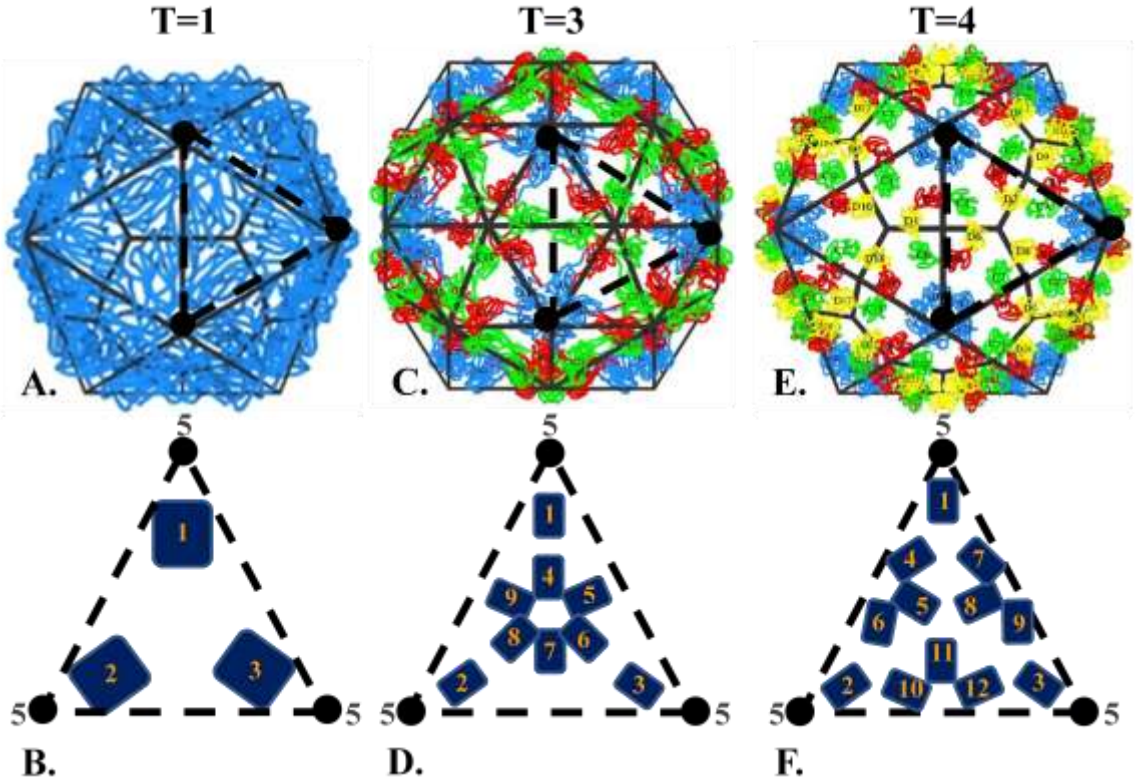

Fig. 1.2. Easy way to determine T-numbers

The broken lines in (A-F) represent one asu of the given structure. Orange numberings in (B, D, F) count number of protein subunits in asu. Gray numbers in (B, D, F) represent vertices of 5-fold axes. A. Example of a T=1 virus, Satellite Panicum Mosaic Virus, image taken from Viper database, entry number 145. B. Number of protein subunits within the asu of a T=1 virus. C. Example of a T=3 virus, CCMV Swollen Form Model 1, image taken from Viper database, entry number 203. D. Number of protein subunits within asu of a T=3 virus. E. Example of a T=4 virus, Semliki Forest Virus, image taken from Viper database, entry number 37. Viper database is discussed in (Carrillo-Tripp *et. al.*, 2009). Database available online at http://viperdb.scripps.edu/data_analy.php.

To put this into perspective with virus coat proteins on an icosahedral surface, it means that each perceived vertex in a tessellation determined by the theory is a location of a protein unit, adapted from (Twarock, 2004). Given this quasi-equivalence, it would allow for the following possible number of protein subunits, 60, 180, 240, and 420, for T= 1, 3, 4, 7, respectively, reviewed in (Twarock and Hendrix, 2006). Thus, the building

blocks of the icosahedral structure are like triangular geometric units, which are further divided into smaller-triangular units. The protein units occupying the same relative geometric position within the triangular building blocks must be equivalent to each other, which is what gives us the term "quasi-equivalence" (Caspar and Klug, 1962). Casper and Klug's theory of how protein units (be it protein monomer, homo- or heterodimer, etc.) are arranged to form an icosahedral shell for virions and/or nucleocapsids has held true for the majority of cases determined thus far by crystallography or cryo-EM. However, exceptions, such as L-A virus (Caston *et al.*, 1997) and the polyoma virus (Rayment *et al.*, 1982), suggest that the Casper and Klug theory of quasi-equivalence may need to be more generalized to explain biological systems in a more encompassing manner. To accommodate these exceptions, "Tiling Theory" has been formulated (Keef *et al*., 2005; Twarock, 2004, 2006) and generalizes the theory of quasi-equivalence, such that the building blocks are no longer limited to regular triangles, as in Casper and Klug's model, but can be more of a kite, dart, or rhombus shape (Twarock, 2004). So, back to the coat proteins, it means that they are capable of interactions with each other which can form "tiles" of one of several shapes and can still adopt the icosahedral symmetry theorized to be the most advantageous geometry for virus assembly (Caspar and Klug, 1962).

Assembly of nucleocapsids is not limited just to interactions with coat proteins, and functions of the coat protein are not limited to interactions with other coat proteins. The coat protein also modulates what nucleic acid is encased within the nucleocapsid by having higher binding affinity for ssRNA of the appropriate virus (Schneemann, 2006). Thus, it contributes to virions ultimately packaging only its own genome during assembly as opposed to foreign nucleic acid. Despite the advantage of a maximized interior due to

icosahedral symmetry, encasing the length of viral RNA is still an obstacle, and thus frequently needs help conforming to a shape to enable this. For this, coat proteins, due to what has been found to be otherwise enigmatic large unstructured portions of its structure, may also give it the capacity to act as ssRNA chaperones (Ivanyi-Nagy *et al.*, 2006; Poynard *et al.*, 2000; WHO and Viral Hepatitis Prevention Board Antworp, 1999). The interactions between the coat protein and the ssRNA remain a factor beyond the nucleocapsid's assembly, given that within the whole, mature virion, it is still evident that 13-44% of the RNA is still in contact with the inner capsid protein shell post-nucleocapsid assembly (Chiu *et al*., 1997).

The ssRNA has structural components itself, making it an active participant in the nucleocapsid assembly process or the structure itself. As mentioned above, the ssRNA makes substantial contacts with the interior surface of the protein shell of the nucleocapsid (Chiu *et al.*, 1997). These contacts are critical in many cases to the stability of the nucleocapsid, given nucleocapsids' vulnerability to RNase (Tellinghuisen and Kuhn, 2000). The suggestion of their ssRNA digestion experiments is that ssRNA and coat protein interactions within the nucleocapsid are essential to the nucleocapsid structural stability. This may be the case for some viruses. Examples of viruses which have structural contacts with the viral nucleic acid and the coat protein, include Rous sarcoma virus (Dupraz and Spahr, 1992), Hantaan virus (Severson *et al.*, 2005; Xu *et al.*, 2002), Cucumber Mosaic virus (Kaper and Geelen, 1971), and Kunjin virus (Khromykh and Westaway, 1996). The contacts with the coat protein and the induced structure it imposes are not, however, the only structural contributions viral nucleic acid has on the process of nucleocapsid assembly. Prior to interactions with the coat, the ssRNA itself has structural features which aid in the assembly process. During the encapsidation

process, some ssRNA viruses' secondary and tertiary structures are imperative to the RNA's recognition by the coat protein (Schneemann, 2006), and as such are critical in some cases to the selectivity of nucleic acid packaged by the virus. These ssRNA structural elements also initiates interactions which are important for ssRNA folding induced by the coat protein, which if this is adulterated by a ssRNA misfold, then the resulting nucleocapsid structure would either be malformed or incapable of assembling (Ivanyi-Nagy *et al.*, 2006). In some extreme cases, nucleic acid has been found to be capable of adopting icosahedral symmetry, as in the case of Turnip Yellow Mosaic Virus (Larson *et al.*, 2005). In this case, the authors suggest the possibility that the RNA's sequence itself enables it to adopt the structure, given the minimal interaction the RNA has with the coat protein (Larson *et al.*, 2005). There still remains to be hard evidence that nucleic acid is capable of forming such high ordered symmetry on its own.

After its initial assembly, nucleocapsids likely undergo changes during assembly, envelopment, disassembly, and general change in conditions when the newly formed virus infects. Examples of this include, Cowpea chlorotic mosaic virus (CCMV) (Liepold *et al.*, 2005), Red Clover Mosaic Virus (RCMV) (Sherman *et al.*, 2006), bacteriophage HK97 (Lata *et al.*, 2000), and bacteriophage λ capsids (Dokland and Murialdo, 1993). These are illustrated in Fig. 1.3.

Changes have also been found between the isolated Venezuelan equine encephalitis virus (VEEV) nucleocapsid (Paredes *et al.*, 2003) and the mature VEEV nucleocapsid (Paredes *et al.*, 2001), suggesting that merely stripping the nucleocapsid of the envelope and interaction with the E2 protein can cause changes in the nucleocapsid. In order to better understand the structural characteristics and changes which nucleocapsids undergo for two ssRNA viruses, we investigated hepatitis C virus (HCV)

of the Flaviviridae family (notated not italicized according to the Linnean system of nomenclature, though almost exclusively noted today in peer-reviewed articles italicized according to the International Committee on the Taxonomy of Viruses), and then Venezuelan equine encephalitis virus (VEEV) of the Togaviridae family.

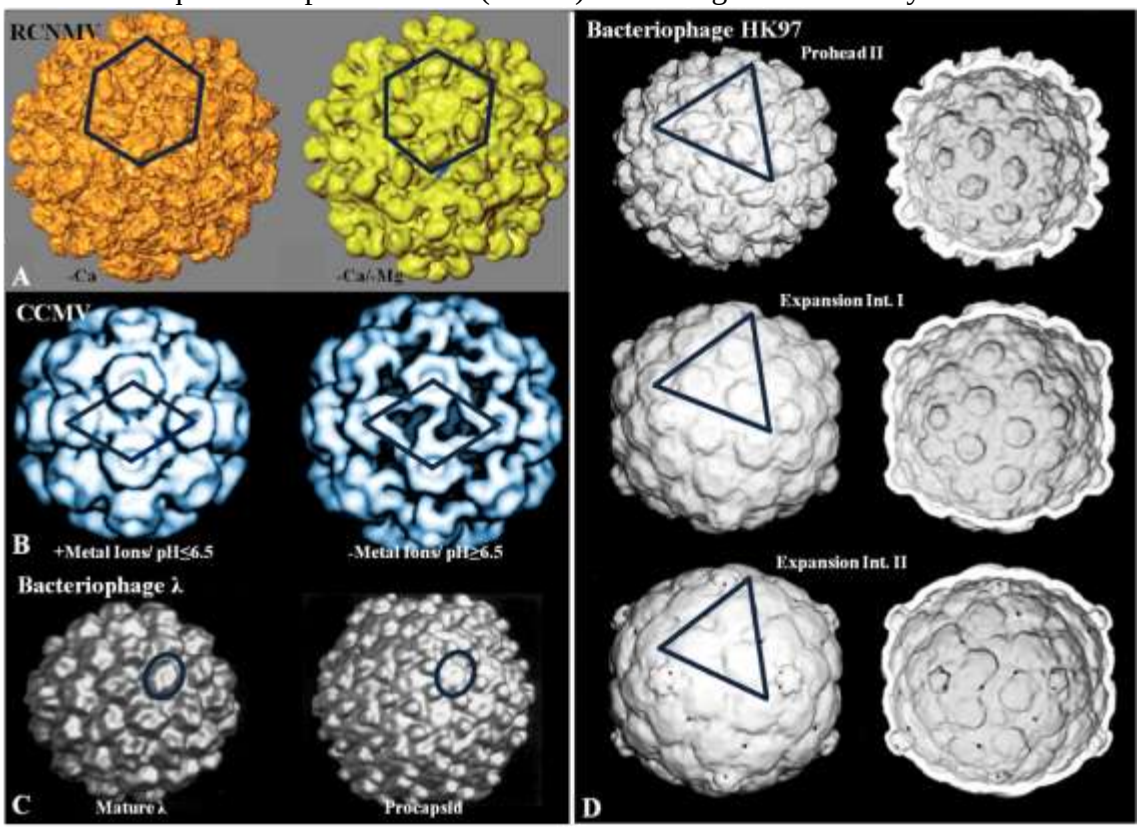

Fig. 1.3. Examples of virus structures which undergo structural transitions

A. Red Clover Necrotic Mosaic Virus (RCNMV) changes due to the presence or absence of magnesium. Figure adapted from (Sherman *et al.*, 2006). Difference between the pseudo-hexamers in the two structures is noted. B. Cowpea Chlorotic Mosaic Virus (CCMV) changes structurally due to +/- metals and pH changes. Figure adaptation from (Liepold *et al*., 2005). The second structure seems to be shifted up and out relative to the first. Hence, the second structure is considered the "expanded" form. C. Bacteriophage λ undergoes changes after the tail and DNA are incorporated into the procapsid. Shown are the procapsid and mature structures. Figure adapted from (Dokland *et al.*, 1993). D. Three maturation stages of bacteraphage HK97. Figure adapted from (Lata *et al.*, 2000). Of note is the difference between all the structures at the 3-fold axis of symmetry.

Biology owes the structures and their implications, discussed above, almost entirely to one technique, cryo-EM. The origin of cryo-EM can be traced back to the first transmission electron microscope (TEM) in 1931, developed by Max Knoll and Ernst Ruska (Freundlich, 1963). Resolution by a light microscope was limited by the wavelength of light, and electrons, with a much shorter wavelength, could achieve, theoretically, sub-atomic resolution of a given specimen. The first electron microscopes were of lower voltages than are used today, ~50-60 kV in the 1940's, with a theoretical resolution limit of 10 Å (Cosslett, 1947). Unfortunately, it would not be until the 1970's that the first reconstructions were achieved (Crowther *et al*., 1970) and not until the 1980's in which it became more common place. Still from the time of its conception in 1931 until the 1970's improvements in the theoretical resolution were achieved largely by improving the microscope voltage and magnetic lenses which centralize the beam. Today, sub-angstrom resolutions are theoretically possible (Lentzen and Urban, 2006). The TEM reconstructions became more common place in the 1980's due to the advent of computerized systems, such as (Hainfeld *et al*., 1982), which could handle data storage and analysis.

Since Crowther's introduction to reconstructions using TEM and negatively stained virus sample (Crowther *et al*., 1970) and his subsequent publication of procedures for doing three-dimensional reconstructions (Crowther, 1971), a number of advancements in orientation determination, raw data pre-processing procedures, specimen preparation, and the computerization of TEM microscopes and accessory systems has made producing these reconstructions more practical to a wider range of scientists. By the late 70's, integrated computer programs for processing electron micrographs for biological

structures became available (Smith, 1978), and a package which still has a variation around today, IMAGIC, had its initial version (van Heel, 1979). Companies which offered commercially available TEMs, Phillips, JEOL, and Hitachi, had been well-established for decades, but by the 1970's they started building models, which were easier to use and more economical, http://authors.library.caltech.edu/5456/1/hrst.mit.edu/hrs/materials/public/ElectronMicroscope/EM_HistOverview.htm. While the solutions would not be apparent until much later, the idea of electron dose causing damage to the specimen was noted around this time (Cremers *et al*., 1979). This issue, along with the problem of sample dehydration would be noted as two of the major problems limiting resolution in its day (Baumeister, 1982). Up to this point, reconstructions were produced from negatively-stained biological specimens. The dehydration issue would be solved by vitrifying samples, without stain or fixation (Adrian *et al*., 1984). Data became easier to store, manage, and analyze with the new computer systems and data becoming digitized from the late 1970's to 80's (Smith, 1978; Hainfeld *et al*., 1982). By the 1980's TEMs produced commercially began to regularly feature micro-processor-controlled instruments, making the microscopes themselves less difficult to operate, http://authors.library.caltech.edu/5456/1/hrst.mit.edu/hrs/materials/public/ElectronMicroscope/EM_HistOverview.htm. The 90's saw the remaining major hurdle, electron irradiation damage, noted in (Baumeister, 1982) find practical approaches to the issue (Koster *et al*., 1992; Dierkenson *et al*., 1993). Energy-filtering of the beam's scattered electrons improved the pursuit of higher-resolution structures (Schroder *et al*., 1990). The 1990's also saw the emergence of two methods for finding orientation of particles which are still used today, common-lines method (Fuller *et al*., 1996) and the model-based

approach (Baker and Cheng, 1996). Common lines are evident when particles are not oriented along the direction of the 2, 3, 5 fold axes vertices. This is when the axis vertices are easier to detect, and thus one can find how a given particle is oriented relative to these lines. It is, however, difficult to determine a particle's orientation by this method when it is close to a symmetry axis, because the axis lines are not apparent and therefore cannot be exploited (Fuller *et al*., 1996). In the model-based approach, an initial model is used to produce possible orientations the raw data could have. Given the model, projections are produced and compared with the raw data to determine which model-derived projection correlates best, thus giving the orientation along the surface of the structure (Baker and Cheng, 1996). The concern with this approach is the affect model-bias can have on the resulting structure. Whether it be due to technological limits, imperfections in the microscope, or plasticity or heterogeneity in the sample itself, EM and even cryo-EM frequently gave us only vague ideas of what was occurring structurally. With the advent of pseudo-atomic modeling, as discussed in (Baker and Johnson, 1996), docking crystal structures into EM densities, the implications for these densities became more pronounced. As for the commercially available microscopes, the 90's had the merger of Phillips Electron Optics with FEI, with the Phillips name dropped in all subsequent microscopes produced by the company, and the theoretical resolution limit of 1 Å being finally reached by microscopes thanks to the field emission guns (FEG) and other advancements, http://authors.library.caltech.edu/5456/1/hrst.mit.edu/hrs/materials/public/ElectronMicroscope/EM_HistOverview.htm. By this time, computers and graphical user interfaces were standard in TEMs. Thus far, the early 2000's have given us EM processing approaches aimed at being more automated, such as AUTO-3DEM (Yan *et al*., 2007) and the EMAN

packages (Ludtke *et al*., 1999; Tang *et al*., 2007). The model-based approach, still used today in EM programs such as the EMAN packages, previously mentioned, as well as those by Tim Baker, summarized in http://cryoem.ucsd.edu/programs.shtm, has been evaluated and the concern with model-bias or, alternatively, reference-bias can be addressed via the cross-validation approach discussed in (Shaikh *et al*., 2003). The past few decades have seen electron microscopy incorporate newly-developed computer science technology, and TEM-design has achieved theoretical resolving capabilities. The question then becomes what can cryo-EM and three-dimensional reconstruction do for the further advancement of biological knowledge and keep its status as an important technique for the coming years. A quote given in 1992 about where the future of EM lies may still give insight to the answer. According to Hewan-Lowe, "if diagnostic EM is to remain a viable entity, its future role in tumor diagnosis lies in exploiting the relevance of the correlation between structure and function of subcellular organelles" (Hewan-Lowe, 1992). In a more generalized approach to medical science, it would suggest that the future is in understanding how the structures determined relate to the biological function of the specimen. Thus, the endeavor becomes not just to determine a structure, but to utilize microscopy and specifically cryo-EM to comprehend structural changes as it relates to biology.

Flaviviridae Background-with a Focus on Hepatitis C Virus

Hepatitis C virus (HCV) is a blood-borne, enveloped, positive-sense single-stranded RNA virus (Family: Flaviviridae, genus: *Hepacivirus*) (Fields *et al*., 1996; Mandell *et al*., 1995; Miller and Purcell, 1990; Robertson *et al*., 1998). The major routes of infection are contamination with blood and plasma derivatives (Courouce *et al*., 1994;

Esteban *et al.*, 1989; Ludlam *et al.*, 1989; Maisonneuve *et al.*, 1990, 1992; Ponz *et al.*, 1991; Seeff and Dienstag, 1988; Williams and Dodd, 1990), needles and syringes from injected drug use (Alter and Moyer, 1998; Bolumar *et al.*, 1996; Carruthers and Loxley, 1995; Chetwynd *et al.*, 1995; Esteban *et al.*, 1989; Roggendorf *et al.*, 1989), sexual contact depending on the titer of the carrier (Alter *et al.*, 1989, 1990; Melbye *et al.*, 1990; Wejstal, 1999), healthcare work (Cotton, 1991; Hofmann and Kunz, 1990; Hopf *et al.*, 1990), and mother to child (Zanetti *et al.* , 1999). There is a low occurrence of transmission via household contact (Deny *et al.*, 1992). The onset or acute phase of the infection is frequently asymptomatic (Tong *et al.*, 1995), but can include abdominal discomfort, nausea, vomiting, fever, and jaundice (Marcellin, 1999; Tong *et al.*, 1995). The major concern with this virus is the high prevalence of it establishing a chronic infection, about 54-86% or 40-85% (Sabahi, 2009; Teoh and Farrell, 2004), of which 17-55% can develop cirrhosis of the liver (Sabahi, 2009), and hepatocellular carcinoma can result in about 1-23% of chronic cases, as mentioned in (Sabahi, 2009). These statistics are illustrated in Fig. 1.4 below. The disease is widespread and has infected 170 million people worldwide or about 3% of the human population according to the World Health Organization http://www.who.int/csr/disease/hepatitis/whocdscsrlyo2003/en/print.html. The current treatment available is a combination treatment of peg-IFNα and ribavirin (Hadziyannis *et al.*, 2004; Hoofnagle and Seeff, 2006; Werling and Tulassay, 2006), but this is neither able to clear the virus and in some cases, as in genotype 1, is only effective ~30% of the time (Di Bisceglie and Hoofnagle, 2002).

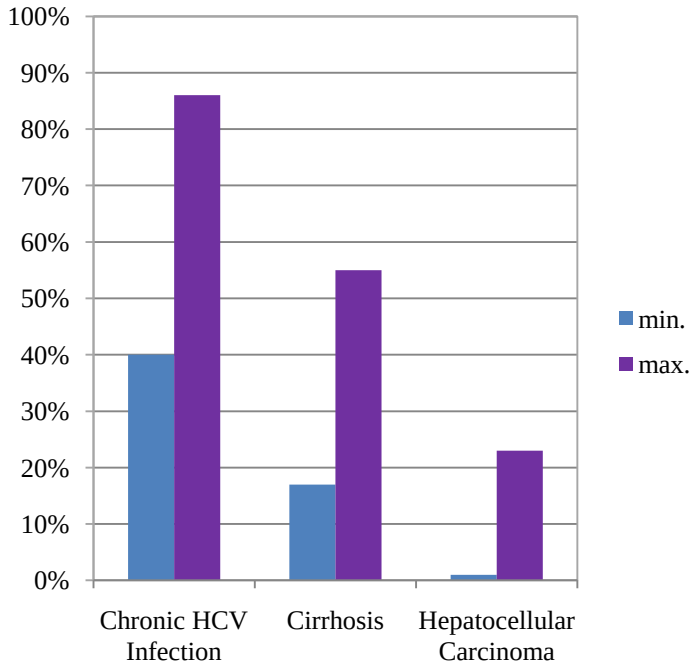

Fig. 1.4. Medical consequences of infection with HCV

Data for the following major medical consequences of infection with HCV has been ambiguous, thus the percentage of total persons initially infected with HCV to develop the following complications is presented as max and min values.

HCV virions enter host cells via clatherin-mediated endocytosis (Blanchard *et al.*, 2006), using one of the following receptors or co-receptors binding to the viral E2 protein, CD81 (Knipe *et al.*, 2001; Pileri *et al.*, 1998) and low-density lipoprotein receptor (LDLR) (Monazahian *et al.*, 1999). Other cellular co-receptors which have been implicated include glycosaminoglycans, DC-SIGN, which can bind both of HCV's envelope proteins (Pohlmann *et al.*, 2003), and L-SIGN (Gardner *et al.*, 2003; Lozach *et al.*, 2003; Pohlmann *et al.*, 2003), SRBI (Barth *et al.*, 2005; Scarselli *et al.*, 2002), and claudin-1 (Evans *et al.*, 2007). More specifically, it is thought that HCV interacts with

the host's lipids within their blood and then bind to one of the co-receptors to infect a new cell. Entry within the cell utilizes clathrin-mediated endocytosis (Blanchard *et al.*, 2006). The endosome's low pH, which engulfed the newly entered virion, triggers the fusion event which likely involves the HCV E1 protein, given its similarity to paramyxovirus glycoproteins with the same function (Flint *et al.*, 1999). Little seems to be known of the details of the uncoating of the nucleocapsid and the specifics behind the release of the vRNA into the cell, but it is interesting to note that the core protein which comprises the viral nucleocapsid has been shown to associate with the 60S ribosomal subunit (Santolini *et al*., 1994). This interaction may play a part in the ssRNA's release. Once the ~9.6 kB +ssRNA genome is released into the infected cell's cytoplasm (Bradley *et al.*, 1983, 1985, 1991), negative-sense RNA (-RNA) is transcribed from the positive-sense RNA (+RNA), and the genome's highly structured 5'NCR facilitates plus-strand RNA replication (Knipe *et al*., 2001). Translation of the +RNA, which utilizes the +RNAs IRES element (Jubin *et al.*, 2000; Lyons *et al.*, 2001; Tsukiyama-Kohara *et al.*, 1992) as well as other structural elements in the 5'NCR (Fukushi *et al.*, 1994; Honda *et al*., 1996; Kim *et al.*, 2002), then results in three structural proteins, E1, E2, and core protein, as well as seven non-structural proteins p7, NS2, NS3, 4A, NS4B, NS5A, and NS5B (Knipe *et al*., 2001). The scope of this publication is mainly on the core and nucleocapsid formation, thus, focus will be truncated to that at this point. The core protein is cleaved from the remaining polyprotein by a signal peptidase in the ER lumen Selby 1993 (Grakoui *et al.*, 1993; Selby *et al.*, 1993), resulting in the immature 21 kD form (at aa 191) of the protein. Further processing by an intramembrane presenilin-type aspartic acid protease (SPP, or signal peptide peptidase) (Weihofen *et al.*, 2002) results in the mature form of the core protein, which is 19 kD and is cleaved somewhere between

aa179 and 181 (Hussy *et al.*, 1996). This mature form of the core protein is involved in interactions with the viral genomic +ssRNA to form the nucleocapsid. A summary of biophysical properties and interactions involving specific amino acids with HCV core protein are shown in Fig. 1.5 below.

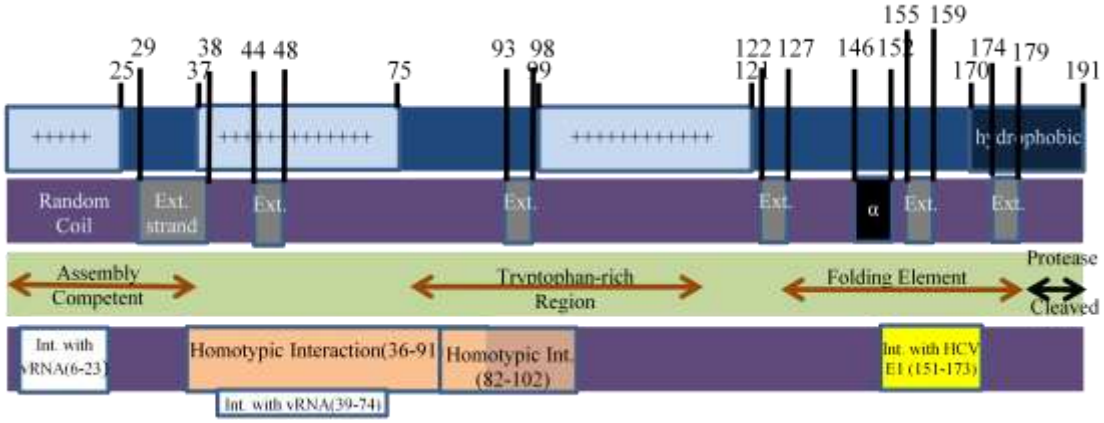

Fig. 1.5. Hepatitis C core protein biophysical properties and functions

The biochemical characteristics of the amino acids present in the core protein are shown above in the Line A. (+) represents amino acids with positively charged R-groups. The predicted structural characteristics of the protein given dynamic light scattering data (Kunkel and Watowich, 2004) is shown in Line B. Functionalities of the protein's different regions are given in Lines C and D. The sequence noted as "protease cleaved" denotes the region which is cleaved so that the remaining core protein is considered in its "mature" form.

Nucleocapsid assembly involves both specific and non-specific binding between the core protein and the viral RNA and multimerization of core proteins. Binding between the core protein and the ssRNA is likely the first step in nucleocapsid assembly, if it follows the trends for other alphaviruses (Hong *et al.*, 2006; Linger *et al.*, 2004). For the binding of RNA, the core protein's N-terminal sequence is a largely basic sequence, comprised of two conserved basic regions at aa6-23 and aa39-74 (Bukh *et al.*, 1994). However, HCV is not known to package nucleic acid other than its own. To account for

this observation, it has been shown that the core protein binds most efficiently to a highly conserved sequence, 31 nts long, in loop IIId of the 5'UTR (Tanaka *et al.*, 2000). It is also suggested that interactions between the core and loop I of the 5' UTR at nt 23-41 may also be a point of recognition for the core protein (Tanaka *et al.*, 2000). Multimerization of the core protein is not essential to nucleocapsid formation, which occurs due to C-terminal sequences between aa125-179 (Kunkel and Watowich, 2002), however, it may be essential to the protein's stability in the cell, due to the fact that aa1-124 is largely unstructured (Kunkel and Watowich, 2002). Between aa125 and 179, there are key folding elements which enable the core to fold and become multimeric (Kunkel and Watowich, 2004). Yeast two-hybrid system showed that the first 113 amino acids are involved in homotypical core interactions (Matsumoto, 1996), and further investigation showed that aa36-9Ånd aa82-102 were more specifically responsible (Matsumoto *et al.*, 1996; Nolandt *et al.*, 1997). This is upstream from the key folding element (Kunkel and Watowich, 2004) for the core protein. While the core's folding maybe important for the core protein *in vivo*, *in vitro* it has been found that the N-terminal end is enough to assemble nucleocapsids (Fromentin *et al.*, 2007; Klein *et al.*, 2005; Majeau *et al.*, 2004). HCV nucleocapsid-like-particles (nlps) which have been isolated *in vitro* have been found to be ~33 nm in diameter, which would be consistent with what has been recovered from the blood of infected humans (Takahashi *et al.*, 1992). The virus obtains its envelope from the ER lumen, with core proteins interacting with the E1 at aa151-173 (Lo et al., 1996). Virus from infected humans have diameters between 30 and 80 nm (Prince *et al.*, 1996). Seventy-percent of the population had diameters between 60-70 nm, and were considered the viable HCV virions (Prince *et al.*, 1996). It is suspected that the lower diameter particles, ~30 nm, are nucleocapsids, as opposed to full virions.

Aims and rationale A major hurdle in studying HCV has been the lack of a suitable cell-culture system which can sustain an infection, thus current studies which have been done have been done *in vitro* with *E. coli* expression systems or by HCV replicon cell culture systems. There is currently no structure available for either the core protein in a crystal structure, nor the nucleocapsid in cryo-EM. The current HCV whole virion reconstruction was not in existence at the time the experiments began. Thus, the aims were to determine the structure of a construct of core protein, and also to determine the structure of the HCV nucleocapsid. Within the first aim of finding the structure of a construct of the HCV core protein, the first objective was to express constructs which, given the current biophysical data of the core protein, may be both structured and without the tendency to aggregate. This suggests that I believed that the core protein does have a segment which does contain structure, and yet does not aggregate. Within the second aim of finding the structure of the HCV nucleocapsid, this first required the isolation or assembly of HCV nucleocapsids. The studies undertaken here utilized *in vitro* assembled nucleocapsid-like-particle (nlp) system to provide assembled nucleocapsids for structural determination thereof. The *in vitro* system was used only due to the current cell-culture systems at the time yielding titers insufficient for isolation of nucleocapsids *in vivo*. The rationale behind using crystallization is straightforward given that it is the standard biological technique for resolving protein structures at atomic resolution. The rationale behind using cryo-EM to resolve the structure of nucleocapsids is that cryo-EM reconstructions are regularly used with crystal structures in obtaining pseudo-atomic modeling, enabling the determination of the positions of the proteins comprising protein complexes, in this case nlps comprised of proteins and ssRNA. Tomography or single particle reconstruction could have both been

used in this case, but these studies did not continue to this point. The hypothesis was that if a core construct structure as well as the nlp structures were both determined, and the crystal structure docked into the cryo-EM (single particle or tomogram) structure, then what we would see would likely mimic what has been found for the protein in Fig. 1.3. Fig. 1.3 leads us easily to believe that if such a docking were to accurately be done, then the E1 interaction region, with a nearby alpha-helix would likely be found on the surfaces of the nlp structure; the nlp exterior with presumed pentamers and pseudo-hexamers, characteristic of icosahedral structures, would likely be held together by homotypic interactions around aa82-102 and see extended strands interacting; the more N-terminal amino acids would fold into the more interior parts of the nucleocapsids, interacting the other core proteins, keeping the nucleocapsid protein shell enclosed, but also dipping into the nucleocapsid cavity to interact with the interior nucleic acid.

Having these structures would greatly increase our understanding of assembly which was, thus far, poorly understood. In addition, such structural knowledge may lead to another type of therapy, given that the genetic variability is one of the challenges associated with treating HCV, and that the core protein has the most conserved sequence of the proteins, across genotypes and subtypes. Unfortunately, these studies presented several road blocks which lead to the abandonment of efforts with this system and the shift in focus to another simple ssRNA virus, Venezuelan equine encephalitis virus. Given this change in systems and also specific aims to be achieved, the central hypothesis becomes broader and more generalized. The hypothesis is generalized to that simple ssRNA viruses' nucleocapsids are comprised of coat proteins which are capable of arranging into ordered structures on their own, and that the arrangement of coat proteins can exhibit plasticity as seen in whole virions discussed earlier.

Togaviridae Background- with a Focus on Venezuelan equine encephalitis virus

Venezuelan equine encephalitis virus (VEEV) is a mosquito-borne, single-stranded RNA enveloped virus (Family: Togaviridae, genus: *Alphavirus*) (Tsai, 1991; Weaver *et al.*, 2004) which causes highly debilitating flu-like infections which can lead to neurological complications in ~10% of those infected, when the virus invades the central nervous system. Fatalities are less than 1%, with children being more vulnerable to the virus progressing to central nervous system (CNS) infection and encephalitis. Outbreaks are re-occurring in Central and South America (Aguilar *et al.*, 2004; Estrada-Franco *et al.*, 2003; Rico-Hesse *et al.*, 1995; Weaver *et al.*, 1996, 2004), and the virus has stretched as far north as Texas, USA (Weaver *et al.*, 2004). The Center for Disease Control also notes this virus to be a potential biological weapon (Hawley and Eitzen, 2001; Hilleman, 2002; Klietmann and Ruoff, 2001) with no effective anti-viral treatments or vaccines currently available for wide-spread distribution.

Alphaviruses, in general, enter host cells by receptor-mediated endocytosis, reputedly laminin-binding protein (Ludwig *et al*., 1996), or glycosaminoglycans (Bernard *et al*., 2000; Wang *et al.*, 2003) in cell cultures, but this is likely an incomplete understanding of the receptor, given the lack of explanation for restricted host range (Weaver *et al.*, 2004). The endosomes interior exposes the virus to an acidic environment, which causes the envelope proteins to undergo rearrangements, and the viral envelope to be absorbed into endosome. As a consequence, the nucleocapsid ("post-entry" nucleocapsid) is released into the cytoplasm. The post-entry nucleocapsid (nc) readily disassembles in the cell's cytoplasm. This is potentially facilitated by the capsid proteins binding to 60S ribosomes (Wengler *et al*., 1992, 1996). Icosahedral three-dimensional (3D) reconstruction of isolated nucleocapsids (Paredes *et al.*, 2003) shows

an increased diameter relative to the nucleocapsid within the intact virion ("mature" nucleocapsid) (42 nm compared to 38 nm). The hexamers in the isolated nucleocapsid are more "cup-shaped" (Paredes *et al.*, 2001, 2003) as opposed to flattened ones found in the mature nucleocapsids. These two structures, as well as their T=4 symmetries, in Fig. 1.6 below. Even though the "isolated nc" does not mimic a nucleocapsid state *in vivo*, given that the true post-entry nc is exposed to an acid pH prior to its formation, this difference between a mature nc and an isolated nc is evidence that the nucleocapsid likely undergoes structural changes within the cell during the virus's "life cycle."

VEEV genomic RNA is ~11,400 nucleotides in length, and codes for four nonstructural proteins on its 5' end and three structural proteins on its 3' end (Strauss and Strauss, 1994). Alphavirus negative-sense-RNA is transcribed from the viral, positive-sense RNA on the cytoplasmic surface of endosomes. These negative-sense RNA are used as templates for genomic RNA and sub-genomic positive-sense RNA, which codes for the structural proteins E1, E2, and the capsid protein. The viral genome is translated in the cytosol to produce polyprotein which is cleaved to produce four nonstructural proteins (nsP1-4) (Lemm and Rice, 1993). Translation of the sub-genomic RNA produces a polyprotein which is cleaved to become the structural proteins, E1, E2, and the capsid proteins (Melancon and Garoff, 1987). The capsid protein, cleaved from the polyprotein, interacts with newly formed viral RNA to form pre-viral nucleocapsid. The current thinking is that it is the initial high affinity interaction between specific amino acids in the capsid protein and the ssRNA encapsidation signal which provide the "seeding" complex for nucleocapsid assembly (Warrier *et al.*, 2008). The capsid protein helix I is important to this initial stages of nucleocapsid assembly, due to the lack of the helix impairing nucleocapsid formation (Hong *et al.*, 2006), and has been further found that it

is more involved in the dimerization of capsid proteins which is imperative to the initial nc assembly process (Hong *et al*., 2006; Warrier *et al.*, 2008). These two events comprise the two most essential steps in pre-viral nucleocapsid assembly (Warrier *et al.*, 2008). Nucleocapsids were able to form *in vitro* into a structure which was similar to the mature nc (Paredes *et al.*, 2001; Tellinghuisen *et al.*, 1999), but the structure(s) of the resulting pre-viral nc product(s) have yet to be isolated and examined *in vivo*. Amino acids 19-264 of the Sindbis capsid protein, another Alphavirus, interact with artificial vesicles made of neutral or negatively charged phospholipids (Wilkinson *et al.*, 2005). This suggests that the capsid protein not only interacts with the E2 protein, but also is involved with interactions with lipids in the envelope in which it is encased (Wilkinson *et al.*, 2005).

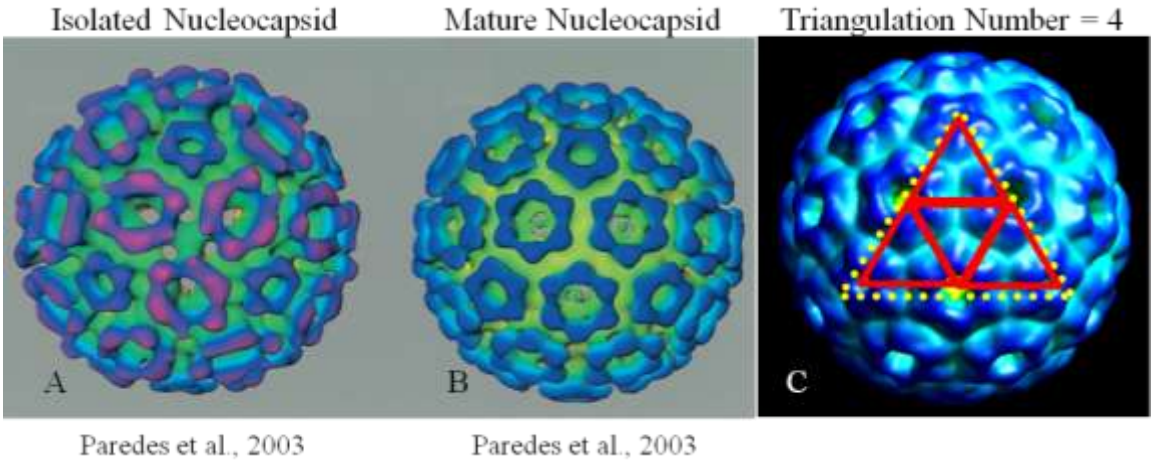

Fig. 1.6. Known VEEV nucleocapsid structures have T=4 Symmetry

A. Isolated nucleocapsid produced by stripping the membrane off whole virion, but without changing the pH, as would occur in the endosome. B. Mature nucleocapsid from the cryo-EM map of whole virion. C. Illustrates why these structures are considered T=4. Panels (A-B) are adapted from Paredes *et al.*, 2003. Panel C is a lower-resolution version of A. Paredes's mature nucleocapsid structure from Paredes *et al*., 2001.

The question of whether pre-viral nucleocapsids have structure upon assembly led to two leading hypothesis on the matter. One hypothesis is that pre-viral nucleocapids are capable of forming well-structured precursors to the mature nucleocapsid which is enveloped later in assembly. This is supported by electron microscopy (EM) data showing pre-viral nucleocapsids in the cytoplasm of Semliki Forest Virus-infected cells (Acheson and Tamm, 1967). This classic hypothesis of alphavirus assembly implies that an ordered pre-viral nucleocapsid is formed in the cytoplasm and migrates to the cell surface to interact with E2-E1 heterodimer, and becomes incased with the viral envelope as it buds (Bykovsky *et al.*, 1969; Garoff, 1974; Garoff and Simons, 1974; Garoff *et al*., 1974). Another hypothesis proposes that a disordered capsid-viral RNA complex migrates to the cell surface and the T=4 symmetry is imposed by capsid-E2 interactions during or after enveloping the virion (Forsell *et al.*, 1996; Frolov *et al*., 1997). Therefore, according to proponents for the latter hypothesis of alphavirus assembly, pre-viral nucleocapsid ordered structure is unnecessary for alphavirus production (Forsell *et al*., 1996). Supporting that, *in vitro* obtained alphavirus nucleocapsid-like-particles (nlps) have been shown to not have icosahedral symmetry (Mukhopadhyay *et al*., 2002; Tellinghuisen and Kuhn, 2000). This suggests that there may be other factors, absent from their *in vitro* system but present in cell cultures, which could facilitate the pre-viral nucleocapsid's structure. Fig. 1.7 below illustrates the different VEEV nucleocapsid maturation stages, as well as the query of whether or not pre-viral nc's are structured.

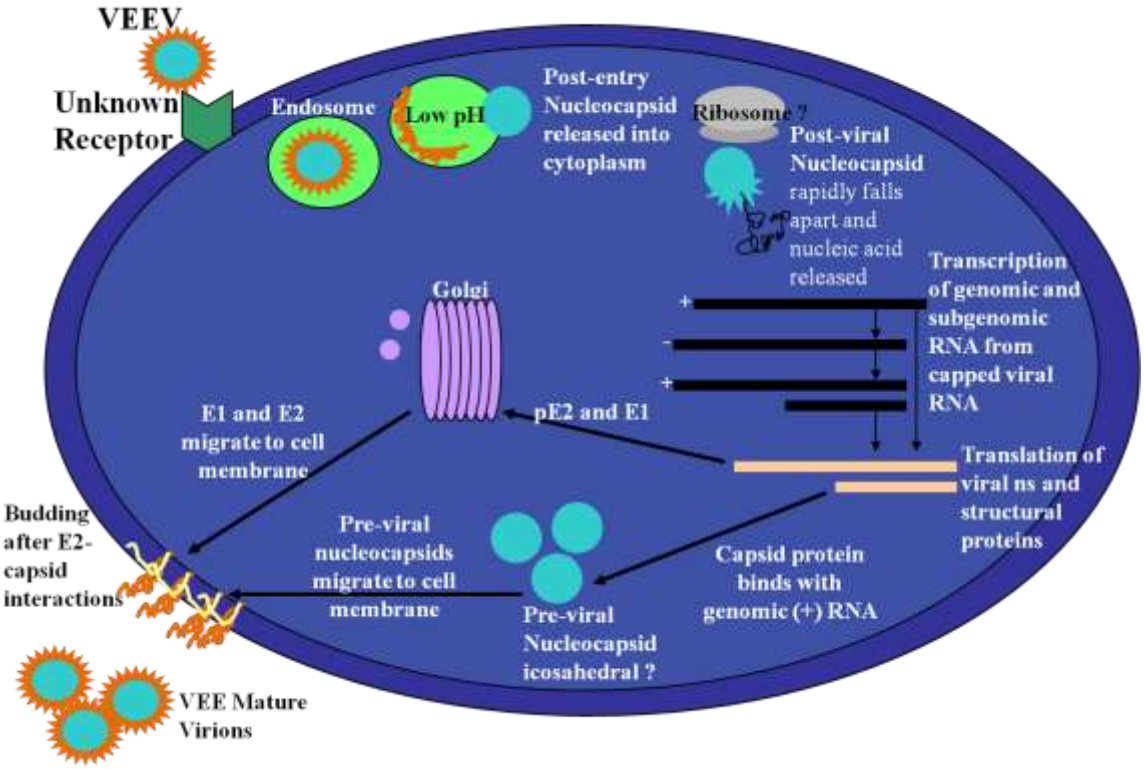

Fig. 1.7. VEEV "Life" cycle, including the articulation of various maturation stages

Above is a summary of where pre-viral, post-entry, and mature virions (which encase mature nucleocapsids) are in relation to the VEEV "life" cycle.

The attenuated strain of the Trinidad Donkey strain, TC-83, is frequently used for research on alphaviruses and VEEV, specifically, because it enables researchers to work under BSL-2 conditions. The attenuated strain has no changes in the amino acid sequence of the capsid protein, but has single amino acid changes in the E1 and NSP4 proteins, and five amino acid changes in the E2 protein (Kinney *et al.*, 1993). Most likely TC-83 is very similar structurally to wild type of VEEV, at least at cryo-EM level of resolution. More directly, the structure of the pre-viral nucleocapsid particles would be structurally

similar to that which would be isolated in the wild-type. There is, of course, the possibility that the ssRNA-capsid protein may have minor differences due to the small changes in the nucleic acid sequence between the TC83 and the wild-type strain, but these are unlikely to show structure differences at the resolution determined for the cryo-EM structure elucidated.

The cryo-EM structure of the whole enveloped VEEV-TC83 has T=4 icosahedral symmetry, according to cryo-electron microscopy reconstruction (Paredes *et al.*, 2001), and is ~70 nm in diameter. Interior to its envelope, the mature nucleocapsid shows flattened pentamers and hexamers, also arranged in a T=4 icosahedral symmetry; meaning the nucleocapsid has four quasi-equivalent capsid protein subunits. The mature nucleocapsid's geometric arrangement and shape of pentamers and hexamers in its structure line up well with those on the envelope surface. In the isolated nucleocapsid, its pentamers and hexamers are shifted in relation to those of on the envelope surface (Paredes *et al.*, 2003). The capsomeres are arranged most symmetrically relative to the mature nucleocapsid (Paredes *et al.*, 2001). The question remains of how the nucleocapsid may potentially change from when it is initially formed to the mature nucleocapsid, when it is encased within the mature virion, and then when it is released within a newly infected cell as a post-entry nucleocapsid. It is suspected that the nucleocapsid would undergo structural changes given its changes in environment and function at each given stage.

Aims and rationale Given that there was a question as to whether or not the pre-viral nc was structured or not, the first aim was to determine the structure of pre-viral nc's by cryo-EM. The target resolution was 15 Å, which is the minimal resolution at which crystal structures can be docked into EM densities. This relates to a later aim. The

rationale behind finding the pre-viral nc structure goes beyond finding whether or not the pre-viral nc's are structured or not. Nucleocapsid structures at this stage and comparable stages in other viral systems are rare, as discussed earlier, and to find one of these may divulge information which is applicable to other systems. The structure, if found, would also determine whether nucleocapsids show plasticity, as has been seen for non-enveloped viruses, discussed earlier and illustrated in Fig. 1.3. The second aim of this project was to determine the structure for another maturation point in the VEEV "life cycle," post-entry nc's to at least 15 Å resolution. The rationale here would be to better understand whether or not structural changes occur in the VEEV nucleocapsids at different stages and, if so, what those changes are. The third and final aim was to dock the known C-terminal crystal structure into the EM densities of the cryo-EM maps from aims 1 and 2. The reason for this to understand, at a pseudo-atomic level, the changes which may be apparent in the cryo-EM reconstructions of pre-viral and post-entry nc's. The hypothesis was that VEEV nucleocapsids are capable of forming an icosahedral structure at the pre-viral nc stage, and that through the viral "life cycle," the nucleocapsid undergoes structural changes which ultimately facilitate the virus nucleocapsid at its function at each level.

We report here on a structure of vaccine strain VEEV (TC83) pre-viral nucleocapsid which is likely a predominant species in a distribution. We have isolated pre-viral nucleocapsids from VEEV-infected cells prior to the virus's extensive budding, and achieved ~40Å resolution by cryo-EM and image analysis. Given the volume estimations of the pre-viral nc reconstruction along with the mature nc (Paredes *et al.*, 2001) as well as the docking of the C-terminal domain of the capsid protein (PDB file 1EP5), it suggests that the pre-viral nc structure we found could accommodate 240 C-

terminal domains, thus suggesting that this predominant species may be a species on a pathway leading to the T=4 mature nucleocapsid (Paredes *et al.*, 2001).

Chapter 2: Materials and Methods

EXPRESSION OF H124, H158, AND H36-169

H124, HCV core protein residues 1-124, was produced from transformed BL21DE3 cells with cDNA encoding HCVC 1-124 residues within a pET30 plasmid (Novagen), previously produced in the laboratory (Kunkel *et al.*, 2001). Growth of H124 pET30/BL21DE3 was adapted from a laboratory protocol written by Marta Lorinczi. Stored glycerol stock of H124 pET30/BL21DE3 cells were used to grow an overnight culture in 2xYT/kanamycin (KAN) (30 µg/mL, final concentration) at 37°C. The overnight culture was used to inoculate fresh 2xYT/KAN media. Typically, about 4L of culture was used per-prep. Culture was grown to an OD_{600} of ~0.8 at 37°C at ~300 rpm. IPTG (1 mM) was then added for protein induction. Induction was allowed to persist for 3 hours at room temperature with the shaker remaining at the same speed. Afterwards, cells were collected by pelleting the induced cultures by centrifugation at room temperature for 30 minutes at ~3,000 xg. At this stage, the pellets can be stored at -80°C. The pellet(s) were resuspended in lysis buffer (35 mL lysis buffer/ 1L culture, treated 1 hour). Lysis buffer includes 8 M Urea pretreated with Dowex MR-3 beads (1g beads/ 100 mL solution), 25 mM sodium phosphate pH 7.0, 250 mM NaCl, 2 mM EDTA, 2 mM DTT. Resuspended pellets were sonicated on 20% duty cycle pulse for 10 minutes on ice. If more lysis buffer was required to break up the cells, then a few more pulses with the sonicator followed. Tubes with sonicated resuspended pellets were centrifuged again at ~5,000 xg for 30 minutes at 4°C. The supernatant was saved and stored at 4°C for chromatography later. The lysis pellet was resuspended in the lysis buffer and sonicated again on ice, and centrifugation again followed. The supernatant again was saved and stored at 4°C.

The first stage of purification of H124 by HPLC chromatography is cation exchange chromatography. The Biocad chromatography machine was used for this with the following buffers: buffer A (0.25 M Hepes pH 7.0), buffer B (8 M of Dowex beads-treated Urea, 1.5 M NaCl), buffer C (8 M of Dowex-beads treated Urea). All buffers were filtered with a 0.2 micron filter prior to use. The cation exchange column used was the POROS 20-S. Fractions resulting from this run which contained H124 were pooled and dialyzed against refolding buffer (20 mM Tris pH 7.0, 150 mM NaCl, 5 mM DTT) on ice or at 4°C. Protease inhibitors, including leupeptin (0.05 mM final concentration), pepstatin A (0.001 mM final concentration), and PMSF (0.5 mM final concentration) were added to the final protein sample to reduce protein degradation.

H36-169, HCV core protein residues 36-169, was originally produced in the lab from prior work from Marta Lorinczi and Meghan Kunkel (Kunkel and Watowich, 2002). The original cDNA for H36-169 was in a pET Blue plasmid (Novagen), however, the plasmid containing the H36-169 cDNA was changed. The H36-169 pET Blue plasmid was isolated from the original BL21(DE3) cells it was transformed into using the QIAprep Spin Miniprep Kit (Qiagen) according to kit instructions. Zynoclean Recovery Kit was used to recover the isolated plasmids from 1% agarose gels. Digestive enzymes, HindIII and EcoRI, were used to digest pMAL-c2X and the H169 pET Blue plasmid. These were recovered, again, from another 1% agarose gel with the Recovery Kit mentioned earlier, and the H36-169 was ligated into the pMAL vector. Perfectly Blunt Cloning Kit (Novagen) was used to transform Tuner Competent Cells (Novagen) with the newly ligated H36-169 pMAL. Other competent cell lines attempted for the expression of H36-169 included BL21 DE3, Rosetta, and Nova Blue cells (all from Novagen). Overnight cultures of the H169 pMAL/Tuner cells were grown in LB or 2xYT medium

with 34 µg/mL carbamecillin (Cb) at 37°C. From this, 4-6 1 L LB/Cb media flasks were grown up to an OD_{600} of ~0.8 at 37°C and rotating at ~300 rpm. After the optical density reached 0.8, 1 mM IPTG was added, and induction was carried out at 37°C. This was the case for most of the preps, though an induction at room temperature was also attempted. Various induction times were attempted to optimize H36-169 expression (from 3 hours to 12 hours). In some preps, the addition of 1% wt/vol glucose pre-induction, and changing of the media so that the glucose was removed during induction, was also attempted. After the induction period, the cells were isolated from the media and lysed in a similar manner as described for H124 or by resuspending the pelleted induced cells in (40 mL/ 1 L culture) lysis buffer (25 mM sodium phosphate, 20 mM Tris-HCl pH 7.0, 2 mM DTT, 10 mM magnesium chloride, lysozyme (0.05 mg/mL), RNase A (0.01 mg/mL), DNase I (0.01 mg/mL), and PMSF (0.1 mg/mL) followed by sonication in a similar manner as described earlier. After the sonicated sample was centrifuged, as described with the H124 prep, the remaining pellet was resuspended in lysis buffer with 1% Triton-X100 and resonicated. This procedure was repeated again, and all soluble lysates were combined for the purification of H36-169.

Purification post-lysis utilized an amylase-bead column from New England BioLabs to isolated H36-169 via affinity to MBP fused to the HCVC construct. Protocol was followed at 4ºC using the company's protocol for utilization of the beads, available at http://www.neb.com/nebecomm/products/protocol31.asp. The column, as well as all buffers used in the isolation, was chilled to 4ºC prior to use. Column volume was ~3-4 mL, and 1.5 mL fractions were taken.

H158, HCV core protein residues 1-158, cDNA was available in the laboratory in at pET Blue1 (Novagen) plasmid. This was then transformed into one of two competent

cell lines, Rosetta DE3 pLacI and BL21(DE3) (Novagen). Growth and induction of the transformed competent cells with the H158 pET Blue1 plasmid were done as described above for H169. Induction, however, was allowed, in the case of the cells containing the H158 pET Blue1 to proceed for 6 hours, before they were centrifuged down, as previously described for H124 and H169, and lysed. The induced cells were lysed as described for H124. Purification of H158 from other cellular contents from the *E. coli* cells included the cation exchange column as well as the reverse phase HPLC column described in the purification on H169.

STRUCTURAL STUDIES OF H158

Circular Dichroism (CD) spectroscopy Purified H124 was used as a control in this experiment, given that its CD spectroscopy has been previously described by (Kunkel and Watowich, 2004). Three different buffers were utilized, and both H124 and H158 were dialyzed into them prior to use. They were, 10 mM potassium phosphate buffer pH 7.4, 150 mM potassium chloride, and 5 mM β-mercaptoethanol; 10 mM potassium phosphate buffer pH 7.4, 100 mM potassium chloride, and 1 mM β-mercaptoethanol; and 10 mM potassium phosphate pH 7.4 and 50 mM potassium sulfate. The undiluted concentration of H124 and H158 were 1 mg/mL. Wavelength scans of the protein samples were taken on a CD spectrophotometer (Aviv Instruments) of the initial buffer (no H124 or H158 content), the undiluted protein sample, the protein sample diluted 2-fold, the protein sample diluted 4-fold, and the protein sample diluted 5-fold. Wavelength scans between 190.00 nm to 300.00 nm were taken at a constant temperature of 25°C. Ten scans were taken per experiment with an average time of 2.0 seconds between wavelength steps.

Dynamic Light Scattering Experiments H158 was dialyzed into one of two buffers (10 mM potassium phosphate pH 7.0, 150 mM potassium chloride, and 5 mM β-mercaptoethanol) or (10 mM potassium phosphate pH 7.0 and 50 mM potassium phosphate). The concentrations of the undiluted protein samples were determined via absorbance at a wavelength of 280.0 nm, taken at a constant temperature of 25°C. Concentrations of H158 between 0.58 and 0.21 mg/mL, respectively, for buffers mentioned above. Concentrations were determined on a Beckman DU-600. Light scattering measurements were taken on a DynaPro-MS/X, dynamic light scattering instrument (DLS) using the Dynamics Program for data analysis. Measurements were taken at 25.0°C +/-0.2°C using the automated temperature control system on the instrument. The light source utilized was an 822.6 nm semiconductor laser, and scattered light was collected at a 90° angle. Data was collected for each sample for 3 minutes, with autocorrelation functions created every 5 seconds.

ASSEMBLY OF NUCLEOCAPSID-LIKE-PARTICLES (NLPS)

The following was added to rabbit reticulocyte lysate for the production of nlps: H124 or H158 sample (between 0.4 mg and 0.05 mg final concentration) in refolding buffer (20 mM Tris pH 7.0, 150 mM NaCl, 10 mM β-mercaptoethanol, protease inhibitor cocktail tablet (one tablet per 15 mL solution), 0.004 mg (final concentration) tRNA from brewer's yeast, RNase inhibitor (ribonucleoside vanadyl complexes 0.01 M final concentration). Controls included rabbit reticulocyte lysate with refolding buffer; rabbit reticulocyte lysate, tRNA (0.004 mg final concentration), and refolding buffer; rabbit reticulocyte lysate, refolding buffer, and H124 or H158 (between 0.4 mg and 0.05 mg final concentration). All NLP reactions were done in epitubes cooled on ice and then

placed in a 37°C water bath for 2 hours. Afterwards, the reactions were cooled to 4°C for at least 15 minutes. Alternatively, nlp reactions were done as similarly as described in (Kunkel *et al.*, 2001) with H158 and H124.

Purification, if performed, included a 10-50% sucrose gradient of nlp reactions which was ultacentrifugated (Beckman L7 or Beckman L8-80M with an SW41 rotor) at 270,000 xg for 2.5 hours at 4°C. Half-mL fractions were collected thereafter from the ultracentrifuge tube. Fractions of interest, given SDS-PAGE gel results, were dialyzed against refolding buffer at 4°C.

ELECTRON MICROSCOPY AND IMMUNO-GOLD LABELING OF HCV NLPS

NLP reactions and controls were centrifuged at 5388 xg for 10 minutes. Pellets were resuspended in refolding buffer (mentioned earlier). Supernatants were centrifuged at 18, 340 xg, and resulting pellets were resuspended in refolding buffer. Supernatants were saved, and all samples, resuspended pellets and supernatants were placed on ice until EM grids were made. Sample (10 µL) was floated atop carbon-formvar coated 200 mesh copper grids for 10 minutes, and subsequently floated atop 2% uranyl acetate for 45 seconds. Grids were air-dried. Negatively-stained grids were viewed one of the following microscopes, Phillips 201 (Phillips), JEM 1010 (JEOL), and JEM 2010 (JEOL), at 60, 80, and 200 keV, respectively.

For immuno-gold labeling, the supernatant/resuspended pellet where nlps predominate only were used for this. Procedures were adapted from those provided (personal communication) by V. Popov (UTMB) for purified rickettsial suspension. Sample (10 µL) was float atop formvar/carbon-coated 200 mesh nickel grids for 5 minutes. Grids, now blotted with sample, were incubated with primary antibody, rabbit polyclonal antibody against H179 from serum, diluted 100-fold in 1% BSA-PBS (bovine

serum albumin-phosphate buffered saline solution). Incubation with primary antibody was allowed to proceed for 30 minutes at room temperature in a wet chamber. The grid was then washed 4 times with 1% BSA-PBS (10 µL each). The grid was then exposed with secondary antibody, 1:20 diluted in 1% BSA-PBS for 30 minutes at room temperature in a wet chamber. The secondary antibody was Auroprobe goat anti-rabbit antibody chelated with 5 nm gold particles. Afterwards, the grid was washed 3 times with deionized water (10 µL/wash). The sample was then fixed using 10 µL of 2% gluteraldehyde for 10 minutes. The grid was washed with deionized water as before and stained in 2% uranyl acetate for 30 seconds before air drying. Grids were viewed on the Philips 201 TEM and JEM 2100. Images were taken either on film or via slow-scan CCD camera (Ultrascan 895, Gatan), respectively.

ELECTRON MICROSCOPY AND IMMUNO-GOLD LABELING OF HCV H77-JFH AND J6CFNS2-NS3 JFH CULTURE SAMPLES

Samples of the following two HCV cultures, H77-JFH and J6CFNS2-NS3 JFH, were obtained from Dr. Stan Lemon's laboratory. The supernatants from the virus cultures were concentrated by the Lemon lab, and 10 µL of each sample was used for making negative stain grids and doing immuno-gold labeling using techniques described in the previous section.

PURIFICATION OF VEEV PRE-VIRAL NUCLEOCAPSIDS

BHK cells at 80% confluence were infected with VEEV TC-83 at multiplicity of infection of one infectious particle per cell. Cells were lysed with 0.1% deoxycholic acid in isolation buffer (25 mM HEPES pH 7.4, 100 mM potassium acetate, 1.7 mM magnesium acetate, Roche protease inhibitor cocktail tablet, and 5 mM ribonucleoside

vanadyl complexes or RNAase inhibitor from human placenta). Cell lysate and debris were separated by centrifuging at 2000 rpm (Jouan CR312) at 4°C for 20 minutes. Sample supernatants were concentrated onto 25% sucrose or iodixanol cushions with centrifugation (Beckman L7 or Beckman L8-80M with an SW41 rotor) at 115,604 x*g* for 3 hours at 4°C. Pre-viral nucleocapsids were purified with density separation using a 10%-60% continuous sucrose or iodixanol gradient centrifuged at 115,604 x*g* for 3 hours at 4°C. Fractions containing pre-viral nucleocapsids were identified by Coomassie blue staining and Western blotting of SDS 16%-polyacrylamide gels.

PURIFICATION OF VEEV-TC83

The procedure here is largely taken from (Weaver, personal communication, and as described in Paredes 2001). BHK-21 cells were grown to 80% confluency in MEM (Minimal Essential Media) media with 10% FBS (Fetal Bovine Serum) and normocin antimicrobial at 37°C. At the time of infection, the media was changed to MEM with 5% FBS and containing no antimicrobial and cells were infected with stock VEEV-TC83 at MOI (multiplicity of infection) of 1. Infection was allowed to continue for 48 hours at 37°C. The media from the infected BHK cell flasks were collected and combined, and centrifuged at 2000 rpm (Jouan CR312) at 4°C. Supernatants were collected and virus was precipitated from it using 2.3% NaCl and 7% PEG 8000. Precipitation occurred at 4°C for 24 hours. This was then centrifugated at 3000 rpm (Jouan CR312) for 30 minutes at 4°C. The resulting pellets were resuspended in TEN buffer (10 mM Tris pH 7.4, 1 mM EDTA, 100 mM NaCl and loaded onto a 20-70% continuous sucrose gradient made with the same buffer, with protease inhibitor cocktail added according to manufacturer's instructions and RNase from human placenta. All buffers used were filtered through 0.2 micron filters prior to use. Sample was ultracentrifugated at 270,000 xg Beckman L7 or

Beckman L8-80M with an SW41 rotor sing for 1 hour at 4°C. Turbid band with virus was collected from the gradient and diluted slightly such that it could sit atop a 30%/70% sucrose cushion (made with solutions described for the gradient). This underwent ultracentrifugation for 2 hours at 4°C. The interface between the two sucrose layers (turbid in appearance) was collected. The sucrose from the sample was dialyzed away using simple dialysis on ice against the TEN buffer or using the Amicon Ultra-4 concentrators.

PURIFICATION OF VEEV ISOLATED NUCLEOCAPSIDS AT PH 7.4

Whole VEEV-TC83 was isolated as described above as well as in (Paredes *et al*., 2001). Sucrose from the final purification step was removed either by dialysis or by using Amicon Ultra4-concentrators (Millipore) in sequential runs of dilution with TEN buffer (described previously) and concentration with the Ultra-4. Concentration was done at 4°C at 3000 rpm (Jouan CR312) when Ultra-4's were used. In the case of production of post-entry nc's at pH 5.5, the whole virion in sucrose was dialyzed against a buffer with the same EDTA and NaCl concentrations, but using 10 mM MES, as opposed to Tris. After sucrose is removed, then a volume of Triton-X100 which will equal 2% vol/vol given the end volume of the dialyzed, isolated whole virus sample is added for 15 minutes on ice.

THIN-SECTIONS OF VEEV-TC83-INFECTED BHK CELLS

Thin sections of BHK cells were examined for virus budding around the VEEV post-infection times used to isolate nucleocapsids. Little or no budding observed at these times would suggest that particles isolated from cells were predominantly pre-viral nucleocapsids (as opposed to particles from mature virus). The thin-sectioning protocol with poly/bed 812 solutions for infiltration was adapted from previous reports (2, 8, 19,

22). Briefly, 19 hrs post-infection, cells were fixed with freshly prepared PFGPA solution (1.25% paraformaldehyde, 2.5% glutaraldehyde, 0.03% $CaCl_2$, 50 mM cacodylate buffer pH 7.3) for 1.5 hours at 4ºC, and then stored at 4ºC in 100 mM cacodylate buffer. Cells were scraped from flasks and pelleted in a benchtop centrifuge at 2000 rpm for 10 minutes at room temperature. Cell pellets were fixed with osmium tetroxide (13, 22), followed by ethanol dehydration. Cells were gradually infiltrated with poly/bed 812 solution, beginning with a mixture of propylene oxide (EM grade) and poly/bed 812 solutions, and followed by 100% poly/bed 812. The resin was polymerized at 37°C. Eighty to ninety nm-thick sections were cut with an ultra-microtome (Sorvall MT6000) and placed on nickel grids (formvar/carbon) and negatively stained with Reynolds lead citrate (from Mallinckrodt's sodium citrate and EMS's lead nitrate) and 2% uranyl acetate.

The protocol for immuno-labeling was adapted from (Anderson *et al.*, 2005). Briefly, cell pellets were embedded in LR white without post-fixation with osmium tetroxide, and thin sections were immuno-labeled with a primary polyclonal antibody against the C-terminal domain of the VEEV capsid protein (Watowich, personal communication) and secondary anti-rabbit antibody IgG (H & L) linked to 5 nm gold particles. Negative controls were run of uninfected BHK cells for both immuno and non-immuno-labeled thin sections. Thin sections were imaged using a Philips EM 201 microscope.

NEGATIVE STAINING AND IMMUNO-GOLD LABELING OF PRE-VIRAL AND ISOLATED NUCLEOCAPSIDS

Pre-viral NCs Following pelleting, pre-viral nucleocapsid samples were dialyzed against isolation buffer to remove excess sucrose and then negatively stained

with 2% uranyl acetate on copper (carbon/formvar) grids. Fractions containing pre-viral nucleocapsid particles were selected for further analysis. The identity of VEEV nucleocapsids was tested using immuno-gold labeling with primary polyclonal antibody raised against the C-terminal domain of the VEEV capsid protein and secondary antibody linked to 5 nm gold particles. Images of negatively stained capsids and immuno-labeled sections were taken on a JEM 2100 electron microscope (JEOL) at 200 keV.

Isolated NCs After allowing the Triton-X100 detergent to strip the membrane of the isolated whole virion, dialyzed into the pH 7.4 buffer for at least 15 minutes, 10 μL of sample was taken and used for immuno-gold labeling in the same manner as has been described for pre-viral nc immuno-gold labeling.

VITRIFICATION AND LOW-DOSE IMAGING FOR CRYO-EM

Vitrified pre-viral nc's, post-entry nc's, and whole VEEV-TC83 were used for imaging and 3D reconstruction. Samples were applied to holey carbon film on copper grids (Quantifoil R2/2, Micro Tools GmbH, Jena, Germany), excess liquid removed by blotting with filter paper, and grids were plunged into liquid ethane (Lepault *et al*., 1983). Grids were transferred to liquid nitrogen and kept at cryogenic temperatures until examined on a cryo-electron microscope (cryo-EM). For microscopy, grids were placed in a pre-cooled cryo-specimen holder (Gatan 626) and transferred to the cryo-electron microscope. Grids were maintained at -180°C during the microscopy session. Micrographs were recorded with a slow-scan CCD camera (Ultrascan 895, Gatan) using low-dose conditions (Amos *et al*., 1982) on a JEM 2010 (JEOL) electron microscope operating at 200 keV. Images were recorded with an electron dose of 15-20 electrons/$Å^2$ and defocus values ranged from -1.5 to -3.0 microns. The first zero of the contrast

transfer function (CTF) of the microscope, even at highest defocus value used, occurred at ~27 Å.

PROCESSING OF CRYO-EM MICROGRAPHS

Pre-viral NC (39 nm diameter reconstruction) Well-preserved pre-viral nucleocapsid particles were boxed out from the low-dose micrographs using the Boxer program within the EMAN electron microscopy imaging package (Ludtke, Baldwin, and Chiu, 1999). Images were preprocessed, which included normalization in contrast (Sorzano *et al.*, 2004) and correcting for the microscope contrast transfer function (Huang *et al.*, 2003; Zhu *et al.*, 1997). Boxed particle projections from the micrographs were used to construct the pre-viral nucleocapsid map using similar methods to (Baker *et al.*, 1999). The nucleocapsid density was extracted from the reconstruction of mature VEEV (Paredes *et al.*, 2003) and used as the initial reference model for the pre-viral nucleocapsid. The EMAN programs OOR and Pftsearch were used to find origins and relative orientations of individual particle projections (Baker and Cheng, 1996; Cheng *et al.*, 1994; Fuller *et al.*, 1996). Iterative refinement of particle origin and orientations were performed and model bias decreased with successive iterations. Particles that were clearly damaged or correlated poorly with the 3D reconstruction model produced in refinement were removed from the reconstruction. Out of the initial 500 particles boxed out, 80 were used in the final reconstruction.

Pre-viral NC (43 nm diameter reconstruction) Well-preserved particles were boxed out from micrographs using the Boxer program in the EMAN package (Ludtke *et al*., 1999). Based on visual inspection, ~300 particles of similar size were manually selected from an initial set of ~580 particles for 3D reconstructions. Particles were discarded if they were different in size, distorted, damaged, or had other defects. Further

processing was performed with a modified version of the PFT protocol (Zhang *et al.*, 2003). Images were normalized to have zero average value and the same standard deviation. Particle orientations and their origins were determined based on a reference 3D map generated from image data using the AUTO-3DEM package (Yan *et al*., 2007). The orientations/origins were iteratively refined using either AUTO-3DEM package or using individual refinement programs from that package or OOR program (Yan *et al*., 2007). After each iteration step, poorly correlating particles were discarded and the best particles retained for continued refinement. The final reconstructions used an image set containing ~90 pre-viral nucleocapsid particles.

To avoid model bias in the 3D map of the VEEV pre-viral nucleocapsid, additional independent reconstructions were performed using various starting maps scaled to the diameter of the VEEV pre-viral nucleocapsid. Three different capsid maps were used, corresponding to VEEV mature nucleocapsid (Paredes *et al.*, 2001), Western equine encephalitis virus (WEEV) mature nucleocapsid (M. Sherman, personal communication), and red clover necrotic mosaic virus or RCNMV (Sherman *et al.*, 2006). The VEEV and WEEV mature nucleocapsid maps had T=4 symmetry, while the RCNMV map was T=3. Starting maps with different T numbers help verify that the image dataset yielded a stable consistent reconstruction regardless of the capsomer lattice used for initial particle alignment and orientation search. Resolution of the reconstructions was estimated using Fourier shell correlation with 0.5 threshold (Rosenthal and Henderson, 2003).

Pre-viral NC (Alternate Method) Reconstructions began with the same 300 boxed particles mentioned in the previous section, and pre-processing was done as described above. No CTF correction was employed, and the same programs, Boxer,

PFTSEARCH, and EM3DR were used in this method. No refinement iterations were done, with OOR. The initial reference map used was VEEV mature nc, mentioned earlier. The main difference with this method versus the method described above is that after finding the origins and orientations with PFTSEARCH in each iteration, only those particles with the highest combined correlation coefficients are chosen with the AUTO-SELECT program. The percentage chosen at this stage ranged from the best 10-25%, which was then used to produce the next reconstruction using EM3DR. This next iteration, however, began, again, with the initial 300 particles, and again the best oriented particles were chosen for producing that iteration's output map.

Isolated NC (pH 7.4) Particles were boxed out and pre-processed in the same manner as the pre-viral nucleocapsids (initial model). The particles, however, were separated into different datasets according to their averaged diameters, measured using the point tool in RobEM, http://cryoem.ucsd.edu/programs/robem_usersguide_v3.15.pdf. Diameters included in each dataset began as being separated out into ~41.6-48 nm and ~49-55.5 nm diameter datasets, and were later separated into datasets with diameters 39-42 nm, 42.5-45.5 nm, 46.8-50.7 nm, 52-55.5 nm. The number of particles in the datasets were 232, 85, and then 34, 123, 91, and 51, respectively given the diameter cut-offs for the datasets above. Diameter cut-offs were based on a plot of the number of boxed particles in the dataset with given measured diameters and resulting reconstruction results from the first two diameter dataset results. Reconstructions for each dataset were produced using the PFT protocol mentioned earlier, minus refinement procedures with OOR.

Whole Virus VEEV-TC83 Boxing and particle picking were done as similarly described for the pre-viral nucleocapsid reconstructions. The intact Sindbis

virus was used as an initial starting model for all TC83 reconstructions. Micrographs were obtained by M. Sherman on a JEM 2200 (JEOL) and images were taken on a CCD similar to what was previously described. Separate reconstructions beginning with the same starting reference model and the same chosen particles were used to produce reconstructions differing only in the CTF correction mode in PFTSEARCH and EM3DR programs, within the PFT protocol, referenced earlier. Three-hundred forty-two particles were used in the reconstructions.

Resolution estimation Resolution was estimated based on Fourier Shell Correlation (FSC) criterion using the well-accepted threshold of 0.5 (Baker *et al*., 1999). To accomplish this, odd and even maps were written with em3dr, and then the program, PSF, was utilized to determine the correlation between the two.

ExPASY Capsid Sequence Alignments

The known sequences in Semliki Forest virus core and Sindbis virus core proteins which are involved in binding to ribosomes (Wengler and Wurkner, 1992). The ribosome-binding-region sequences of both of these alphavirus core proteins were obtained from the Protein Data Bank (PDB) and were compared with the full length PDB acquired sequence of VEEV core protein sequence. ExPASy Server alignment tool, SIM and LALNVIEW (Duret *et al*., 1996) was utilized to find if a region exists within the VEEV-TC83 core protein with sequence similarity with either/both of these region sequences and by what degree.

Radial Slices of Pre-viral (39 nm diameter) and Mature NC Maps

Successive radial cuts were made into both the initial pre-viral nc map and the mature nc map (Paredes *et al.*, 2001). The mature nc map was first manipulated using

low-pass filtering in EM3DR to reduce the resolution of the mature nc such as to make it more comparable to the pre-viral nc map. It is from this reduced resolution mature nc map which radial cuts were made for comparison with those of the pre-viral nc map. The radial cuts were made using Chimera. Individual slices correspond to cutting into the map by about 3 nm per cut. Radial cut-offs at which major changes were noticed were compiled for each map for comparison.

ISOLATION AND "REFOLDING" OF TC83 VRNA

Viral RNA (vRNA) was isolated from purified and dialyzed TC83 in TEN buffer. One of two RNA isolation procedures was used. One employed the use of the Qiagen RNeasy Mini Kit. The procedures used were provided in the kit. The alternate method was followed from "Purification of viral DNA" section of (Yang *et al.*, 1997). Both procedures were conducted under RNase-free conditions.

"Refolding" of vRNA was attempted immediately after isolation. Conditions were intended to mimic the HCV nlp reactions mentioned above with or without the RRL. Controls, which included all put vRNA contents of the reaction, underwent procedures in parallel. Freshly prepared vRNA was heat shocked at 32°C from 10 minutes to 2 hours. Afterwards, the reactions were placed on ice for 20 minutes and subsequently stored at 4°C. Samples for negative staining were taken after the reaction was chilled on ice or after sitting at 4°C for 30 minutes.

DOCKING USING ELIQUOS AND SCULPTOR

The C-terminal end of the VEEV capsid protein was docked into the mature nc electron density maps at 8.7, 12, 16, 20, and 24 Å resolution using Eliquos for computing probable positions and Eliquos for viewing and manual docking (personal

communication with J.J. Heyd). Capsid protein structures were obtained from the PDB. The 8.7 Å VEEV mature nc map (unpublished Zhong Li) was used to produce the lower resolution maps using EM3DR from the EMAN package (Ludtke *et al*., 1999). Half-maps of each resolution map were produced for the docking using the same program. Cuts of each map were also made using Chimera (Pettersen *et al*., 2004), so 2, 3, and 5 fold axes of symmetry could be docked without the remainder of the structure. All three monomers in the crystal structure (PDB file 1EP5) were attempted in docking the 8.7 Å mature nc map. The monomer which gave a docking closest to the accepted docking (Zhong Li, unpublished) was accepted as the monomer for the rest of the docking attempts. All waters and surrounding ions in the crystal were removed in the pdb file prior to any docking attempts. The Laplacian filtering option in Eliquos and automated docking were used for maps with better than 15 Å resolution. Hessian filtering was used for maps with resolutions worse than 15 Å resolution, generally, but it was also tried with the 12 Å resolution map. Noise was generally not added to the low resolution cryo-map in Eliquos, but this was attempted in the case of the 16 Å mature nc map using Laplacian filtering. Positions chosen during interactive docking and Hessian filtering were chosen based on two criteria: the highest correlation value, given the results by the Eliquos run, and the best position to visibly fit the low resolution cryo-area. The 8.7 Å mature nc docked with the C-term capsid protein was compared with that of Xong Lee's (unpublished data) and was throughout used as the docked proteins to overlay subsequently docked maps onto in Chimera to determine its success. Potential salt bridges and other potential interactions were determined using features to highlight amino acids of choice and measure distances in Chimera.

DOCKING USING CHIMERA

An asymmetric unit was extracted from the pre-viral nucleocapsid electron density map using the program cut_cyl_map (M. Sherman, personal communication). Minimum and maximum radii were chosen that bounded the capsid protein shell. Chimera (Pettersen *et al.*, 2004) was used to position monomers of the C-terminal domain of the VEEV capsid protein (PDB entry 1EP5; S. Watowich, personal communication) into density corresponding to an icosahedral face of the pre-viral nucleocapsid map. The "space-filling" viewing option of Chimera was used to visualize docked proteins. The 3-fold symmetry of the particle was used to position symmetry-related capsid proteins within the icosahedral face.

VOLUME CALCULATION OF PRE-VIRAL NC (43 NM DIAMETER) MAP

Pre-viral nucleocapsid volumes were calculated using the program Chimera (Pettersen *et al.*, 2004). The outer radius was designated as the exterior edge of the nucleocapsid. The inner radius was specified to include only the part of the density map that corresponded to the C-terminal domain of the capsid protein. We compared calculated volumes from pre-viral and mature nucleocapsid maps using comparable radial cutoffs given the common features in the maps. Density thresholds were also equivalent, and comparisons between the two maps were made using a series of threshold values. Protein volume was calculated using the partial specific volume for a globular protein and the mass of the C-terminal domain of the VEEV capsid protein (PDB entry 1EP5; Watowich, personal communication).

Chapter 3: HCV Results

EXPRESSION OF H124, H158, H36-169

H124 expression and purification rationale The expression of H124 was for the production of nlps. Previous studies by M. Kunkel showed that nlps were successfully formed with H124 and tRNA (Kunkel *et al.*, 2001), thus H124 was purified.

H124 purification was successful, just as previously done in the laboratory. Expression of H124 yielded purified protein with concentration up to 5 mg/mL, given the absorption at 260 nm/280 nm. Procedures for H124 production were followed just as those described previously by Meghan Kunkel and Marta Lorinczi. The reverse phase chromatography step was omitted, given that the protein was pure enough after the cation exchange column. The SDS-PAGE results showing these steps are shown in Fig. 3.1 below. Confirmation of the identity of the protein purified was given by the Western Blot, shown in Fig. 3.2.

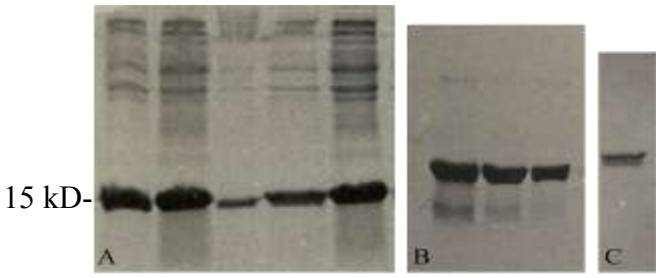

Fig. 3.1. Purification of H124 from cell culture

A. Cell lysates. B. Cation exchange fractions. C. Dialyzed H124. (A-C) H124 runs at ~15 kD.

The identity of H124 as an HCVC construct was confirmed via Western Blotting.

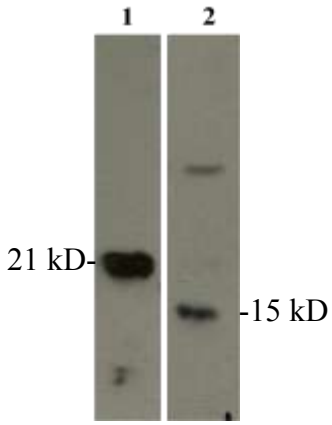

Fig. 3.2. Western Blot of purified H124

Lane 1. Positive Control, H179 purified by M. Kunkel. Lane 2. Purified H124

H158 expression and purification rationale Structural studies aimed at crystallization trials for HCVC, however, required a structured but non-aggregating construct of HCVC. This could not be achieved by H124 or H179 (the full, mature length protein), which were examined previously by M. Kunkel in the laboratory. H124 does not aggregate, but is unstructured; and H179 aggregates, but is structured (Kunkel and Watowich, 2004). The idea was to pick constructs which would be more structured than H124, thus the constructs attempted included amino acids associated with the folding element portion of the protein. To prevent aggregation, the constructs were shorter than H179, which tended to aggregate (Kunkel and Watowich, 2004). Thus, H158 was chosen due to these criteria, hoping to achieve a construct which would be suitable for crystallization trials.

H158 purification yielded adequate, pure protein. Expression of H158, shown in Fig. 3.3, yielded purified protein of ~1 mg/mL in concentration. Induction of protein expression was best at 37°C for 6 hours. A long induction time did not improve yielded protein and a shorter induction time yielded less. Purification post lysis of *E. coli* cells needed both the cation exchange column as well as the reverse phase column to purify the protein from other cellular proteins in the cell lysis mixture.

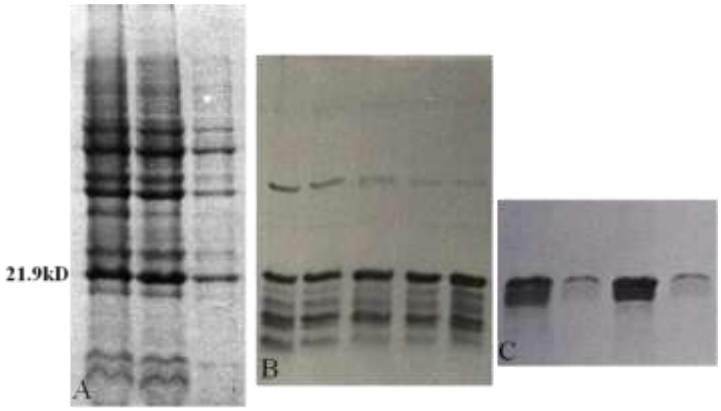

Fig. 3.3. SDS-PAGE gels illustrating the purification of H158

A. SDS-PAGE gel contains cell lysates. B. SDS-PAGE gel of cation exchange fractions. C. SDS-PAGE gel of reverse phase chromatography fractions containing H158. (A-B) H158 runs at ~20 kD on SDS-PAGE gels with 16% acrylamide separating gel. Expected MW= 17.3 kD.

Given that the purification went well, it had to be confirmed that the identity of band assumed to be H158 was HCVC content. This was done by Western Blotting, Fig. 3.4.

H36-169 expression and purification rationale H36-169 was an attempt, again, to achieve a structured construct, given CD and Light Scattering results of H158. It includes amino acids further down from aa158, hoping to include yet more of the protein which would allow it to fold.

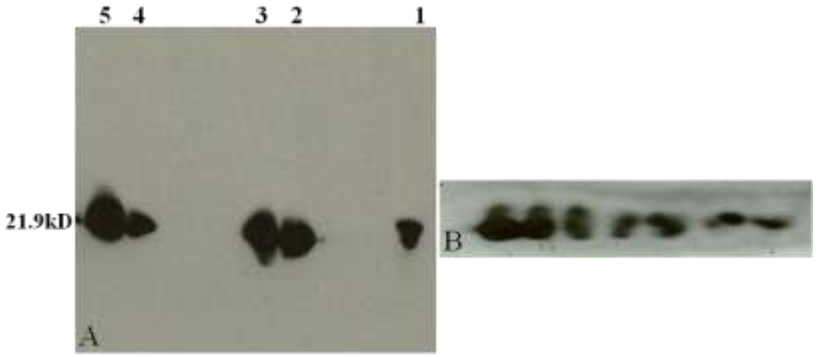

Fig. 3.4. Western Blot of H158

A. Lane 1. Positive Control, H179 purified by M. Kunkel. Lanes 2, 5 Induced H158pETBlue1/RosDE3pLacI colonies at 37ºC. Lanes 3, 4 Uninduced H158pETBlue1/RosDE3pLacI cells. B. Western blot of cation exchange fractions.

H36-169 expression poorly expressed in E. coli. Expression of H36-169, shown in Fig. 3.5, was largely unsuccessful, with the final concentrations being <0.5 mg/mL. Changing competent cell lines did not improve expression substantially and attempts at improving expression via induction/ lysis conditions were unsuccessful.

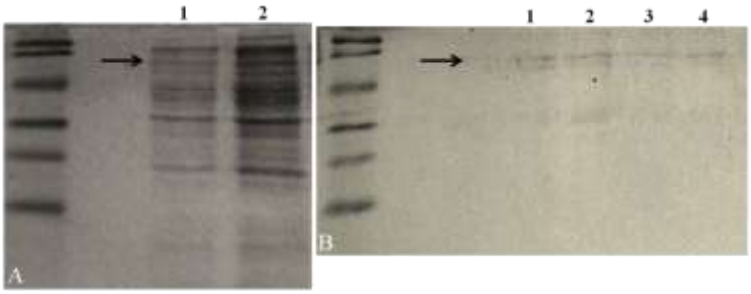

Fig. 3.5. Isolation and purification of H36-169 from H36-169pMal c2x/Nova Blue DE3 cells

A. SDS-PAGE gel, uninduced (lane 1) and induced (lane 2) cells. Protein band proposed to be H36-169 fused to the maltose binding protein (MBP) indicated by the arrow. B. SDS-PAGE gel with fractions for amylose bead purification column. (Lanes 1-4) faint bands (indicated by arrow) which would be associated with the H36-169-MBP.

Expression was very poor, and to answer the question whether H36-169 was being expressed at all, Western Blotting was done, Fig. 3.6.

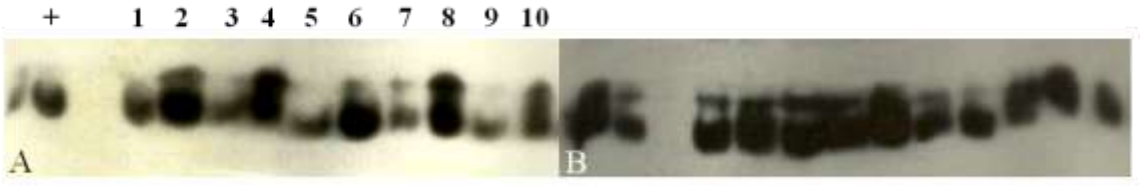

Fig. 3.6. Western Blots of induced and uninduced H36-169pMal c2x/Nova Blue DE3 cells

A. SDS-PAGE gel with uninduced (odd numbered lanes) and induced (even numbered lanes) cells. Positive control is H179 isolated by M. Kunkel. The protein band proposed to be H36-169 is fused to the maltose binding protein (MBP). Note, expression is present in both induced and uninduced cultures, verified by Western blotting later. B. Western blot of fractions for amylose bead purification column.

STRUCTURAL STUDIES OF H158

Circular Dichroism (CD) studies rationale Using similar methods to Kunkel in (Kunkel and Watowich, 2004), it was determined whether H158 was structured. This question is critical to whether H158 could be used for crystallization trials.

CD studies showed H158 was unstructured. CD studies, shown in Fig. 3.7, indicated that H158 was largely unstructured from 1 mg/mL through serial dilutions.

Dynamic Light Scattering studies rationale Again, following similar studies to Kunkel's work with H124 and H179 (Kunkel and Watowich, 2004), Dynamic Light Scattering studies were done to determine whether H158 tended to aggregate in concentrations which would be necessary for crystallization trials.

Dynamic Light Scattering studies showed H158 likely aggregates at minimal amount of concentrated protein necessary for crystallization trials. Dynamic Light Scattering results, shown in (A) in Fig. 3.8, indicated that at 0.5 mg/mL, H158 exists one of a three major species, indicated by the three populations at different radii. The majority, 99%, of the protein mass is situated at low radii of ~2.7 nm. Merely doubling the concentration of the protein, however, yields a different result. At 1 mg/mL, H158 exists as a largely homologous species, (B) in Fig. 3.8, situated at ~6.7 nm, suggesting it is multimeric.

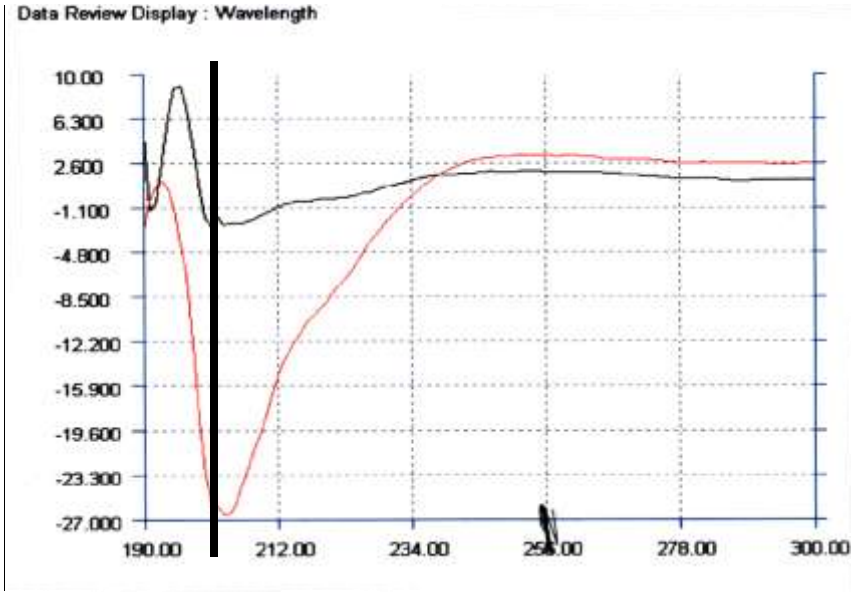

Fig. 3.7. CD study of purified H158

H158 is in 10 mM potassium phosphate buffer pH 7.0, 150 mM potassium chloride. The buffer alone absorbs at wavelengths below 200 nm. Line indicates where absorptions related to H158 begin. Dilutions began at H158 (1 mg/mL) and was diluted down to 6-fold diluted sample.

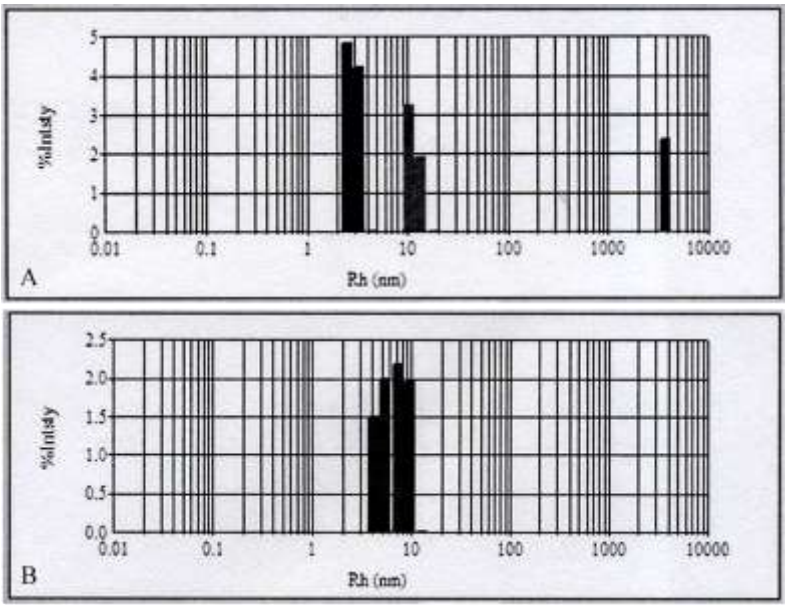

Fig. 3.8. Dynamic light scattering experiments of purified H158

H158 is in 10 mM potassium phosphate buffer pH 7.0, 50 mM potassium sulfate. A. H158 at 0.5 mg/mL concentration light scattering data. Protein exists as a heterologous species centered at a low radius. B. H158 at 1.0 mg/mL concentration light scattering data. Protein exists as a homologous species centered at a high radius.

HCV NLP ASSEMBLY- EM AND IMMUNO-GOLD STUDIES

Rationale for NLP studies At the time when these studies were begun, HCV cell culture systems were plagued with low-titer of virus. Given that, it seemed unlikely that large amounts of concentrated HCV nucleocapsids could be obtained from such systems, which would be necessary for obtaining a structure of the HCV nucleocapsid via Cryo-EM. Thus, nucleocapsid-like-particles were used as opposed to the cell culture systems available at the time.

NLP studies results in more uniform NLPs, but would require purification

NLP assembly using rabbit reticulocyte lysate, Fig. 3.9, seemed to yield more nlps given negative stain EM samples of both the nlps assembled in rabbit reticulocyte lysate

(RRL) and those assembled in buffer using the protocol from (Kunkel *et al*., 2001). Given the negative-stain EM images of the nlps assembled in rabbit reticulocyte and the control with the reticulocyte alone, the nlp reaction sample does have a mixture of particles which includes nlps, as confirmed by immuno-gold labeling in Fig. 3.10, as well particles, likely ribosomes in the reticulocyte alone. The yield of the nlps even in the rabbit reticulocyte reactions was low comparable to what would be needed for purification and then cryo-EM attempts.

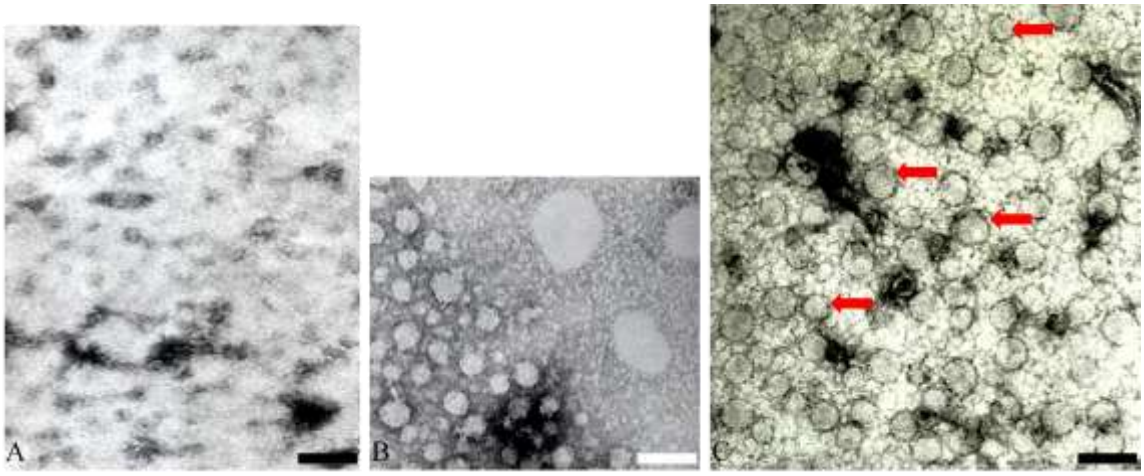

Fig. 3.9. Negatively stained nucleocapsid-like-particles (nlps)

A. Control nlp reaction with no HCVC content. No particles resembling the HCV nlps are found. B. Control nlp reaction with no HCVC content done with rabbit reticulocyte lysate. Particles of similar size and shape to the nlps are found (indicated by arrow). C. NLPs (indicated by arrows) were produced from purified H124 or H158 with tRNA incubated in rabbit reticulocyte lysate. Arrows in red indicate diversity of particle sizes. Scale bars= 50 nm.

Given the ambiguous results of the nlp production in RRL, the question remains as to whether the RRL system was able to produce nlps at all. Immuno-gold labeling showed that the RRL system did produce nlps, Fig. 3.10.

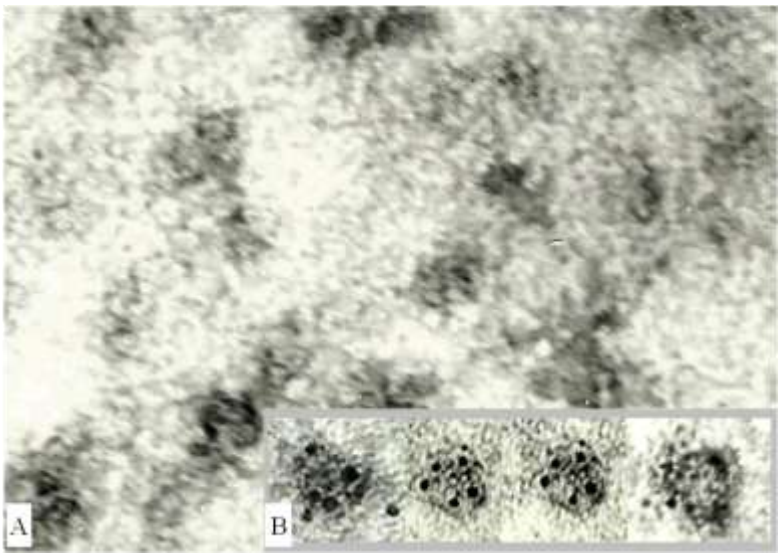

Fig. 3.10. Immuno-gold labeling of nucleocapsid-like-particles (nlps)

A. Negative control, immuno-gold labeling of nlp reaction without H124 or H158. B. Panel showing isolated immuno-labeled nlp particles from nlp reactions with H124 or H158.

While the nlp system was being attempted, it was suggested that I try to examine some of the new HCV cell culture systems becoming available at the time.

NEGATIVE STAIN EM OF HCV H77-JFH AND J6CFNS2-NS3JFH CULTURE SAMPLES

Rationale for HCV cell culture observation studies Ultimately, biologists want to utilize experimental systems as directly relevant to *in vivo* systems as possible. The concern with using any nlp system is whether the result would mimic what is seen in life accurately. Thus, it compelled me to examine whether the newly available HCV cell culture systems would yield enough virus for structural studies. The initial observations were simple uranyl acetate staining studies.

Uranyl acetate staining of HCV in cell culture showed particles consistent with HCV virions. Few HCV virions were present, Fig. 3.11, identity verified by immuno-gold labeling, in the HCV culture samples. Background was very heavily, indicative that further purification would be imperative for a pure HCV sample.

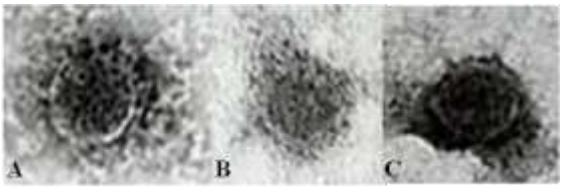

Fig. 3.11. Negative staining of HCV from tissue cultures

(A-C) Negatively stained virions (all ~60 nm in diameter). Virion particles were sparse in TEM.

CHANGING SYSTEMS FROM HCV TO VEEV

Dead-ends with HCV studies The two main goals of the HCV project was to find a crystal structure of an HCVC construct and to find a Cryo-EM structure of an HCV nucleocapsid. Given the results above, it seemed that the current studies were not going in positive directions which would lead to achieving these goals.

VEEV as a system to study simple ssRNA enveloped virus nucleocapsids may be more promising route. VEEV has a well-established cell culture system which produces virus at high titer, making isolation of nucleocapsids of various maturation stages *in vivo* obtainable. The mature nucleocapsid is solved, but the pre-viral nc and post-entry nc stages have not been. There is an isolated nc structure (Paredes *et al.*, 2003) which shows differences between it and the mature nc (Paredes *et al.*, 2001). This suggests that the nucleocapsid is likely to show variations in structural arrangements in

the other two biologically relevant maturation stages. There is a crystal structure for the C-terminus of the capsid protein. The question here would not be what the structure is of the capsid protein which makes up the nucleocapsid protein shell, but rather how does its position change due to changes in its environment. This system would still allow us to ask questions about the nucleocapsid of a simple ssRNA virus, but the aims have shifted from questions aimed at determining the structures of components of HCV nucleocapsids to comprehending changes which nucleocapsids can undergo in the VEE system.

Chapter 4: VEEV Nucleocapsid Results

ISOLATION AND PURIFICATION OF PRE-VIRAL NCS

Rationale for purification of pre-viral nc's There are only scant examples of pre-viral nc's isolated *in vivo* from any system. Isolating and studying these particles would offer a unique chance to answer a couple of questions: if pre-viral nc's adopt icosahedral structure in vivo prior to interacting with the E2 protein, and if it forms a structure different from the mature nc within the whole virion (Paredes *et al.*, 2003).

Purification of pre-viral nc's from lysed cells was successful. Pre-viral nc's could be purified from iodixanol or sucrose gradients between 35-45% iodixanol or sucrose, Fig. 4.1. RNase inhibitors were changed in later preps from vanadyl complexes to RNase inhibitor from human placenta, due to the fact that pre-viral nc's isolated with RNase inhibitor from human placenta lasted longer at 4°C and because vanadyl complexes left a structural artifact in the sample. Pre-viral nc's from the cushion stage of isolation were used for cryo, due to there being more particles per volume, and concentration attempts with the percent iodixanol or sucrose gradient fractions lead to further loss of particles as opposed to concentration thereof.

Pre-viral nc's are just one maturation stage for which there is no structure available. To better understand additional changes which the nucleocapsid undergoes during its "life cycle" the post-entry nc would have to be purified from harvested whole virions. Thus, the next step was to purify whole virus.

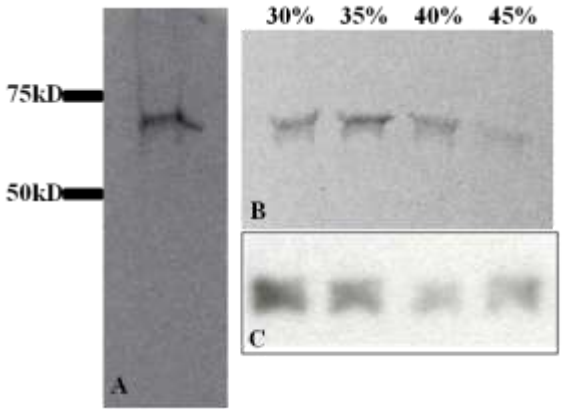

Fig. 4.1. SDS-PAGE gels-protein composition of purified pre-viral nucleocapsids

A. Coomassie blue staining of proteins from pre-viral nucleocapsid particles recovered from the cushion stage of particle purification and separated with SDS-PAGE. Molecular weight markers are shown along the left-hand side. B. Coomassie blue staining of proteins from pre-viral nucleocapsid particles recovered from iodixanol gradient fractions and separated with SDS-PAGE. The iodixanol concentration of each fraction is listed above each lane. C. Western blot (anti-VEEV capsid antibody) of proteins from pre-viral nucleocapsid particles recovered from iodixanol gradient fractions and separated with SDS-PAGE.

ISOLATION AND PURIFICATION OF VEEV-TC83

Rationale for the purification of VEEV-TC83 whole virions The isolation of whole virions was necessary for producing isolated nc's as well as post-entry nc's (Chapter 7). In addition, these isolated virions were used for diagnostic and EM training purposes.

VEEV-TC83 was purified successfully. Virion isolation was repeated from known protocols, as described above. Virion morphology and size were as previously described (Paredes *et al.*, 2001).

ISOLATION AND PURIFICATION OF ISOLATED NCS AT PH 7.4

Rationale for purification of isolated nc's It was requested that I attempt to isolate nucleocapsid in the same manner as Paredes (Paredes *et al.*, 2003) and attempt to find additional structures which the nucleocapsid could adopt after only the envelope was stripped off. It does not give us biologically relevant structures, but at least it did offer a chance to look at nucleocapsid particles from which a successful reconstruction had been done and compare some of their characteristics with that of the pre-viral nc's.

Comparison of isolated nc's with pre-viral nc's during purification

Isolated nc's, as described in (Paredes *et al*., 2003) were subjected to an iodixanol or sucrose gradient, similar to that for purifying pre-viral nc's, (A) in Fig. 4.2. The isolated nc's at pH 7.4 were present in sucrose or iodixanol fractions of 30-35%. In comparison with a parallel isolated of pre-viral nc's, (B) in Fig. 4.2, this distribution of density variations between the two shows that the isolated nc's are less diverse in their densities than pre-viral nc's.

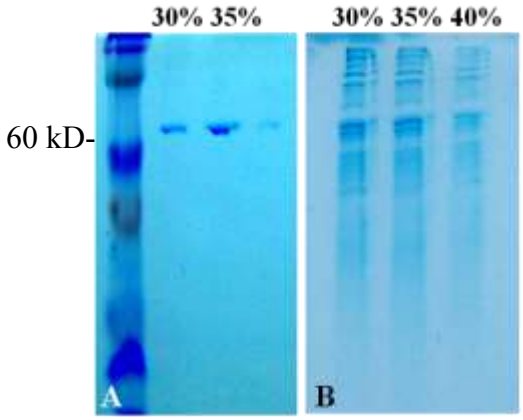

Fig. 4.2. SDS-PAGE gels of iodixanol gradient fractions of isolated nc's at pH 7.4 and pre-viral nc's

Capsid protein band runs as dimer at ~60 kD in both gels. A. SDS-PAGE gel isolated nc's at pH 7.4 iodixanol gradient. B. SDS-PAGE gel of iodixanol gradient of pre-viral nc's.

The pre-viral nc's seem to have a wider distribution of densities they are capable of occupying as opposed to the isolated nc's, seen in Fig. 4.2. As a note to Fig. 4.2 (B), previous gels have seen a small band at 45% iodixanol as well.

THIN-SECTIONS OF VEEV-TC83-INFECTED BHK CELLS

Rationale for thin-sections Thin-sections should show if pre-viral nc's are being produced in the cells in adequate amounts for purification attempts.

Thin-section observations Small, ~40 nm round objects were noticed in the infected BHK cells' thin-sections (B, D, F) in Fig. 4.3, which were absent in the uninfected BHK cells' thin-sections (A, C, E) in Fig. 4.3. The gold particles congregated around these areas where these ~40 nm round objects were found when immuno-gold labeling of the thin-sections was attempted, suggesting their identity to be VEEV nucleocapsids. Few virions were seen budding at this point. The nucleocapsids were congregated in the cell around liposomes, seemingly part of a secretory system leading to the cell membrane. Few particles were independent of the nucleocapsids clustered around the liposomes.

Pre-viral nc's are apparent in thin-sections 18 hours post-infection according to Fig. 4.3 (B, D, F). The question now is whether this is the most optimal time for isolating these particles.

PRE-VIRAL NCS ISOLATED AT 12, 18, AND 24 HOURS POST-INFECTION

Rationale for isolating at various time points Pre-viral nc's were apparent in the cells 18 hours post-infection. However, the efficiency of the purification procedure in extracting these particles post-cell lysis can yield fewer particles than would be expected by simply looking at the thin-sections. In addition, there is the concern that

waiting an excessive amount of time to isolate pre-viral nc's may result in a substantially mixed population of pre-viral and post-entry nc's, thus if pre-viral nc's could be isolated in adequate amounts prior to 18 hours, it would reduce the chance of that occurring.

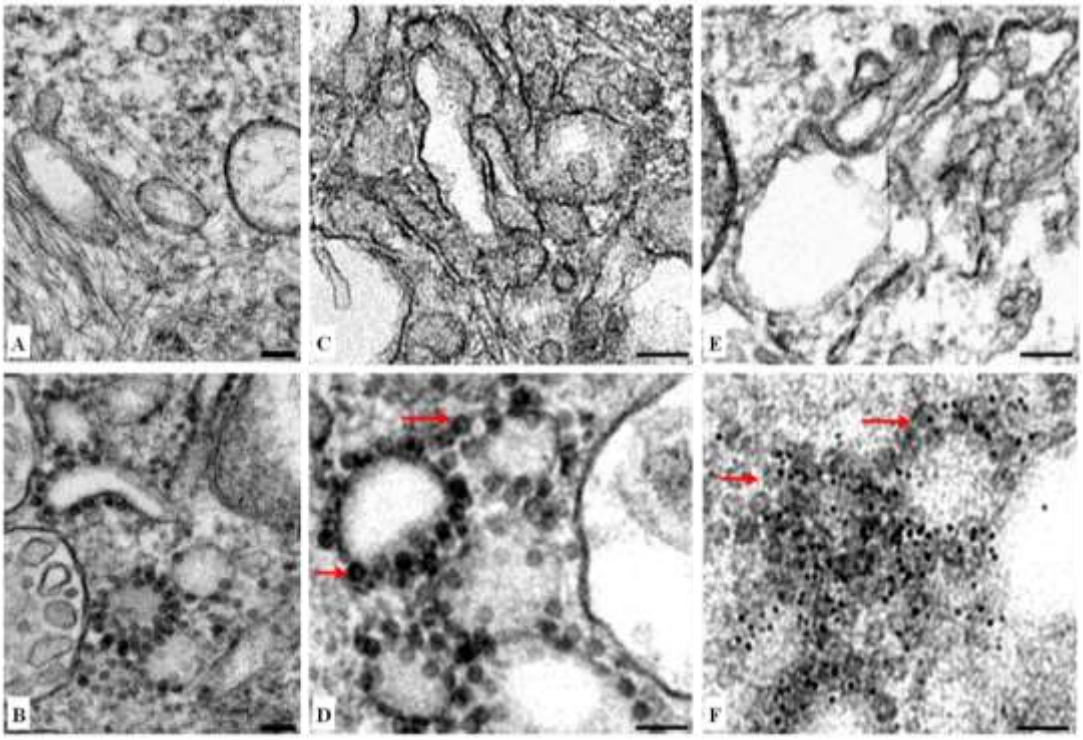

Fig. 4.3. Negatively-stained thin-sections of VEEV-TC83 infected BHK cells

Electron micrographs of negatively stained thin-sections of BHK cells. (A, C) Uninfected BHK cells. (B, D) Sections of BHK cells 19 hr post-infection with VEEV TC-83. E. Immuno-gold labeled thin-section of uninfected BHK cells. F. Immuno-gold labeled thin-section of BHK cells infected with VEEV TC-83. The sections of BHK cells were labeled with primary antibody against the C-terminus of VEEV capsid protein and 5 nm gold-conjugated secondary antibody. (D, F) Arrows point to pre-viral VEEV nucleocapsids. Scale bars = 100 nm.

Comparisons between the isolation times Pre-viral nc's were isolated from BHK cells at 12, 18, and 24 hours post-infection with VEEV TC-83. The amount of

particles capable of being purified at the given time point, the level of CPE (cytopathic effects) of cells, and the amount of whole virus budding from infected cells were the main factors taken into consideration for determining the optimal time for harvesting pre-viral nc's from cells.

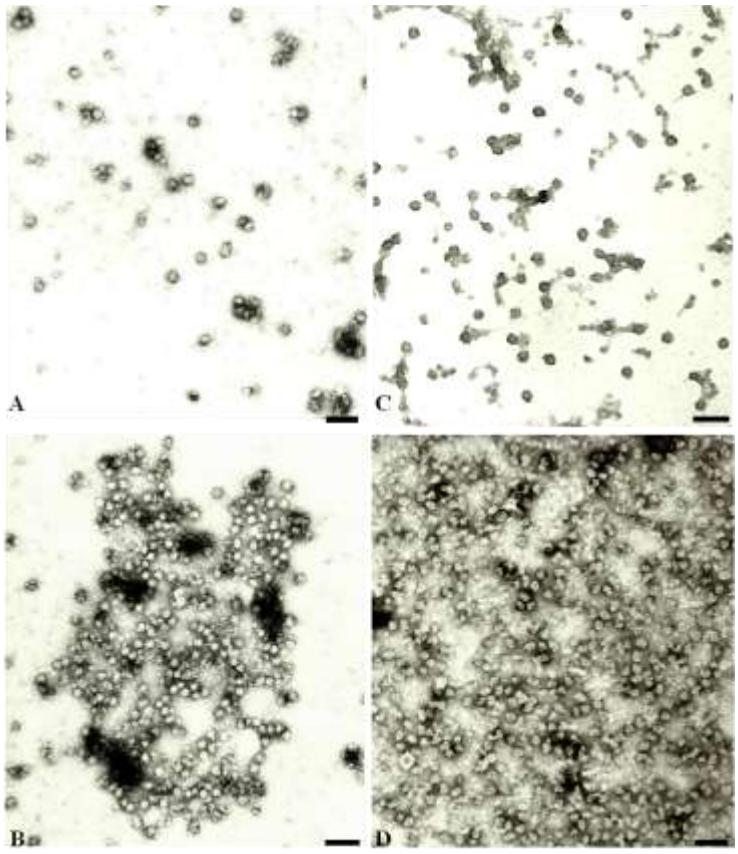

Fig. 4.4. Negatively stained pre-viral nc particles isolated from infected BHK cells after 12 or 18 hours post-infection

Electron micrographs of negatively stained purified pre-viral nc's. (A, C) Purified after 12 hours post-infection. (B, D) Purified after 18 hours post-infection. (A , B) are from correlating fractions in iodixanol gradients, as are (C, D). Scale bars = 100 nm.

Purifying pre-viral nc particles at 12 hours post-infection, (A, C) Fig. 4.4, yielded substantially fewer particles than doing so at 18 hours, (B, D) Fig. 4.4.

CPE became noticeable at 24 hours, so the isolation of pre-viral nc's at this time point was aborted. At this point, it was probable, too, that the amount of secondary infection would render the nucleocapsid particles as a mixture of pre-viral and post-entry nucleocapsids. This would make assigning where in the assembly process any reconstruction from this population would belong and implications thereof, ambiguous. The mean diameter of particles isolated at the 18 hour infection time was 40 nm. Identity of nucleocapsids had to be confirmed prior to structural studies.

IMMUNO-GOLD LABELING OF PRE-VIRAL AND ISOLATED NCS

Rationale for immuno-gold labeling of purified nucleocapsids Pre-viral nc's were isolated from lysed cells. It is possible that the particles isolated from the lysed sample are artifacts. To exclude this as a possibility, immuno-gold labeling, which is similar conceptually to western blotting in TEM, of the isolated pre-viral nc's was necessary. As for the isolated nc's from whole virions, it was necessary to ensure, again, that the isolated particles were nucleocapsids. Again, though less likely in the case of the isolated nc's, it is possible that the isolation of nucleocapsids from whole viruses may produce some artifact.

Successful immuno-gold labeling of VEE nucleocapsid particles validates nc identity. 5 nm gold particles congregated around the isolated particles in buffer for pre-viral, (B) Fig. 4.5, and isolated nc's, (B) Fig. 4.6. In both cases, though the diameter sizes varied within the samples, the gold particles labeled throughout the distributions. The general size distribution of isolated nc's is given in (C) Fig. 4.6.

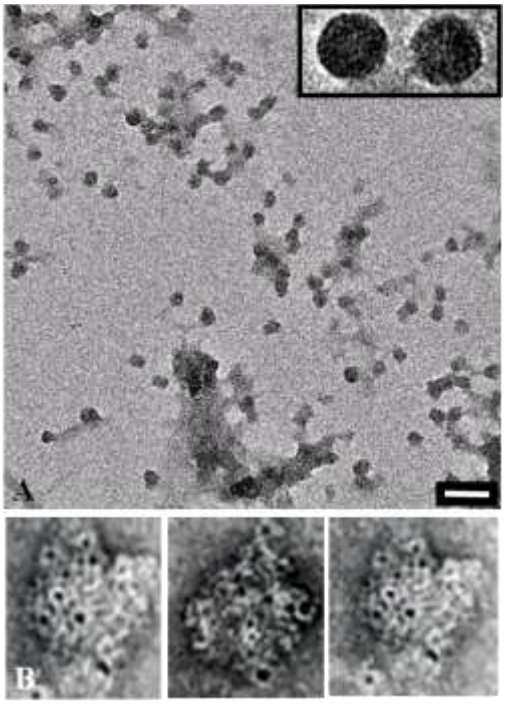

Fig. 4.5. Negatively stained and immuno-gold labeled pre-viral nc's

A. Negatively stained pre-viral nc's. Scale bar= 100 nm. Insert is a close-up on two negatively stained particles. B. Immuno-gold labeled pre-viral nc's, verifying the identity of proposed pre-viral viral nc's.

Given that particles, both pre-viral and post-entry, tended to clump together, so did the labeling. Labeling of the particles was in clear contrast to the negative controls, suggesting that the labeling was specific for the VEEV capsid-containing particles.

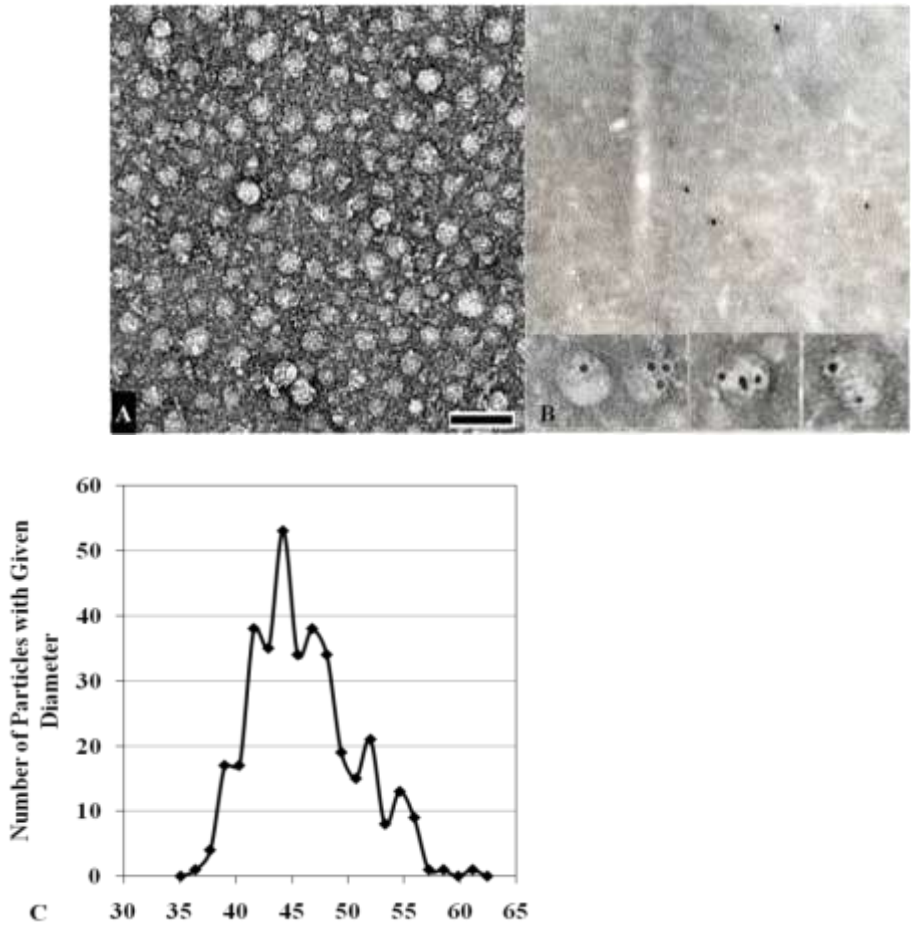

Fig. 4.6. Negatively stained and immuno-gold labeled isolated nc's with size distribution

A. Negatively stained isolated nc's. Scale bar= 100 nm. B. Immuno-gold labeled isolated nc's in the caption beneath the control for the same immuno-labeling. C. Size distribution of isolated nc's.

After confirmation of their identities, the samples could confidently be vitrified for structural determination, which was the original aim at their purifications.

VITRIFIED CRYO-EM SAMPLES- PRE-VIRAL NCS, ISOLATED NCS, AND VEEV-TC83

Rationale for vitrification and structural studies of pre-viral nc's, isolated nc's, and VEEV-TC83 Vitification is a step inherent to Cryo-EM structural determination. The rationale behind structural studies and Cryo-EM for pre-viral nc's has already been discussed. Cryo-EM of isolated nc's was pursued due to the heterogeneity of the isolated nc's observed by Paredes during his own reconstruction of isolated nc's (personal communication S. Watowich). The rationale behind vitrifying VEEV-TC83 at the time was largely a Cryo-EM training exercise. The whole virus should be the easiest to vitrify.

Samples were successful vitrified. Vitrification of pre-viral and isolated nc's was unsuccessful atop fenestrated carbon mesh copper grids. Pre-viral, isolated, and post-entry particles, discussed in Chapter 7, attached only to continuous carbon-coated mesh copper grids. The successful vitrification of pre-viral nc is shown in Fig. 4.7, and is shown for isolated nc's in Fig. 4.8. VEEV-TC83 was vitrified on the fenestrated carbon mesh copper grids, Fig. 4.9. Whole virions tended to be predominant at the edges of the grid's holes.

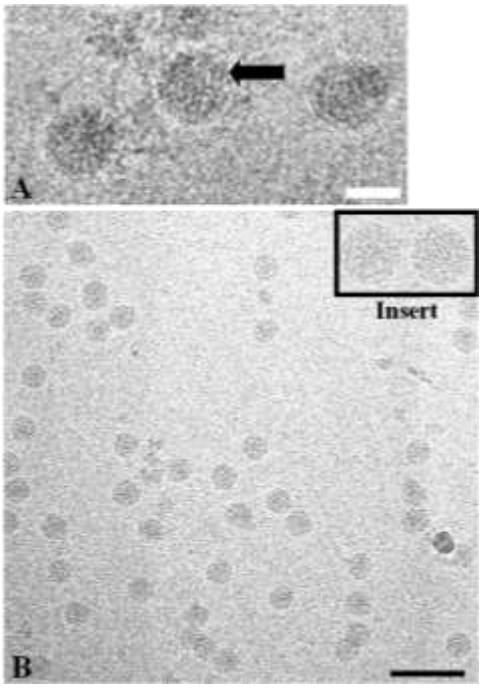

Fig. 4.7. Vitrified pre-viral nc's

A. Vitrified pre-viral nc's in cryo-EM. B. Representative Cryo-EM micrograph used in pre-viral nc reconstructions. Insert shows a magnified view of the particles. Scale bar= 100 nm.

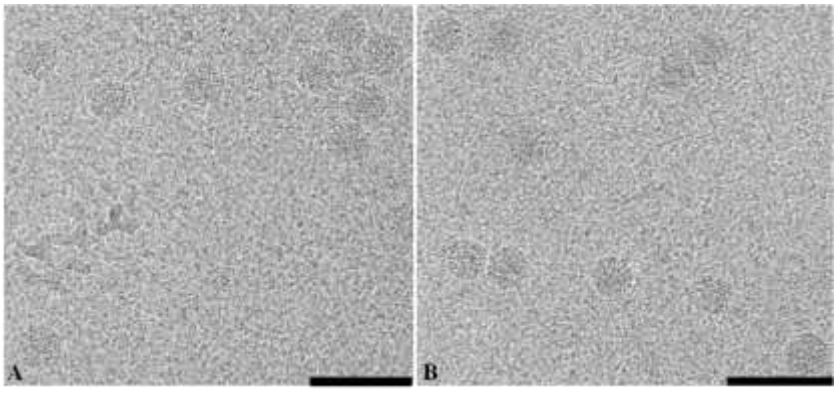

Fig. 4.8. Vitrified isolated nc's

(A-B) Vitrified isolated nc's in cryo-EM. Sample vitrified on continuous carbon coated holey film. Images taken on CCD camera on a JEM2100. Scale bar= 100 nm.

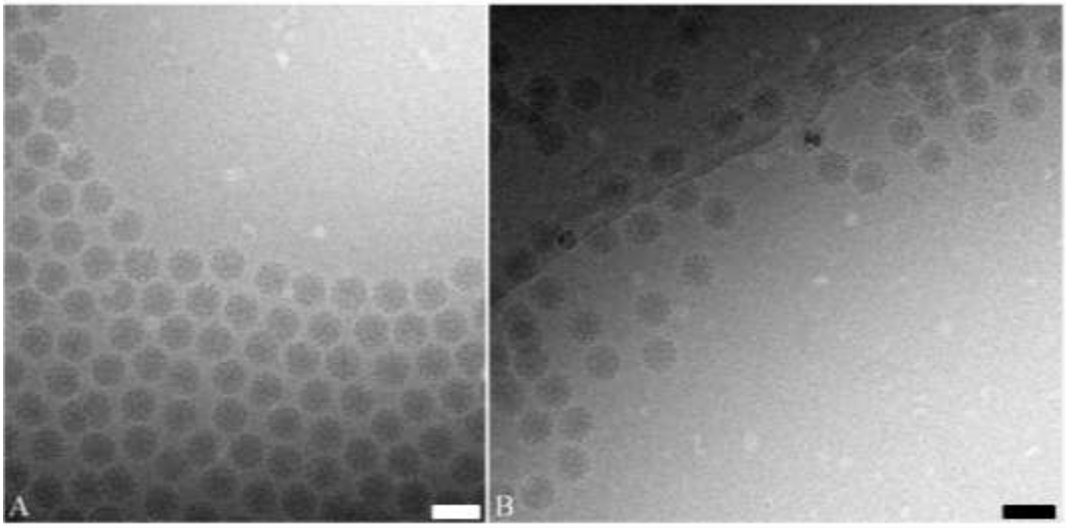

Fig. 4.9. Vitrified VEEV-TC83

(A-B) Micrographs of isolated and vitrified VEEV TC-83 particles. Scale bar= 100 nm. Images were taken on a JEM 2100 on CCD camera.

The whole virions here, Fig. 4.9, were capable of being vitrified on fenestrated holey carbon film grids. They do attach, however, attach to the continuous carbon portions of the grid more readily than they lie in the holes. In the case of pre-viral, isolated, and post-entry nc's, all attempts to vitrify the samples on holey carbon film grids, commercially (Quantifoil and C-Flat grids) or manually produced, failed. This was tried in conjunction, at some point with plasma cleaning, which was not suspected to be a factor, given the nucleocapsids' presumed hydrophobic exteriors. In all trials using plasma cleaning, even with wait-cycles, post-cleaning, plasma cleaning yielded no benefit in helping vitrify nucleocapsid particles. Successful nucleocapsid vitrifications were possible only with continuous carbon grids. Manually produced continuous carbon grids were, therefore, the choice for nucleocapsid vitrifications. As a note, isolated nc's

were vitrified in the presence of 2% Triton-X100 and had a better success rate during vitrification than pre-viral nc's.

CRYO-EM RECONSTRUCTIONS

Rationale for Cryo-EM reconstructions The rationale for the pre-viral and isolated nc's reconstructions was discussed above in describing the rationale for vitrifying the samples.

Pre-viral NC (39 nm diameter) cryo-EM The pre-viral nc (39 nm diameter) cryo-EM map, Fig. 4.10, is ~39 nm in diameter, which is within the error of using different microscopes for data collection to the mature nucleocapsid. The capsid shell has a thickness of 5.5 nm. The pre-viral nc map has a diameter which is <2% larger than the mature nc (Paredes *et al.*, 2001) and 7% less than the isolated nc (Paredes *et al.*, 2003). The thickness is ~7% less than the mature nc, and 42% less than the isolated nc (Paredes *et al.*, 2003).

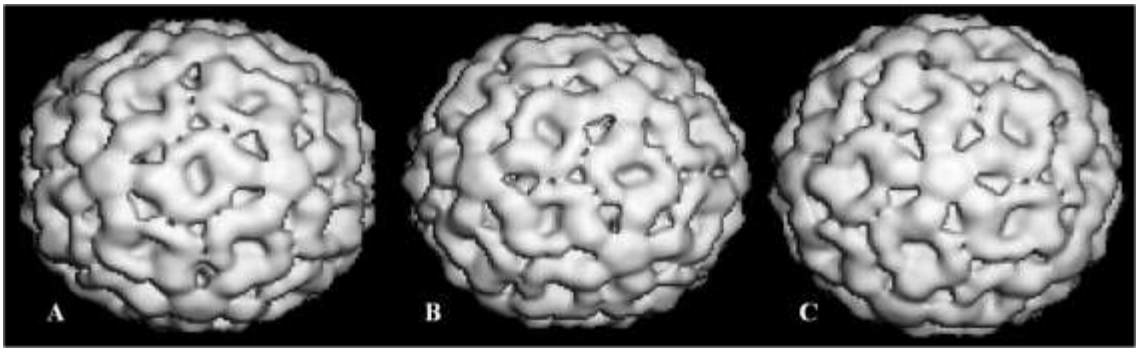

Fig. 4.10. Cryo-EM reconstruction (39 nm diameter) of pre-viral nc

(A-C) 39 nm diameter pre-viral nc shown at its 2, 3, and 5-fold axes of symmetry, respectively. Map was produced using CTF correction and VEEV mature nc as a starting model.

The 39 nm pre-viral nc has a rhombus-like structure at its two-fold axis, strong pentamers at the five-fold axis, and a clear triangular structure at the three-fold axis. Holes were apparent in the middle of the two- and three-fold axes, but the middle of the five-fold axis was clearly bulbous. The estimated resolution of the map is 32 Å.

Pre-viral NC (43 nm diameter) Cryo-EM The pre-viral nc (43 nm diameter) cryo-EM map, (B-D) in Fig. 4.11, is 43.4 nm in diameter, or slightly larger than the 42 nm isolated nc at pH 7.4 reconstruction done by (Paredes *et al.*, 2003). Fig. 4.11 shows reconstruction done using the AUTO-3DEM-generated initial starting model.

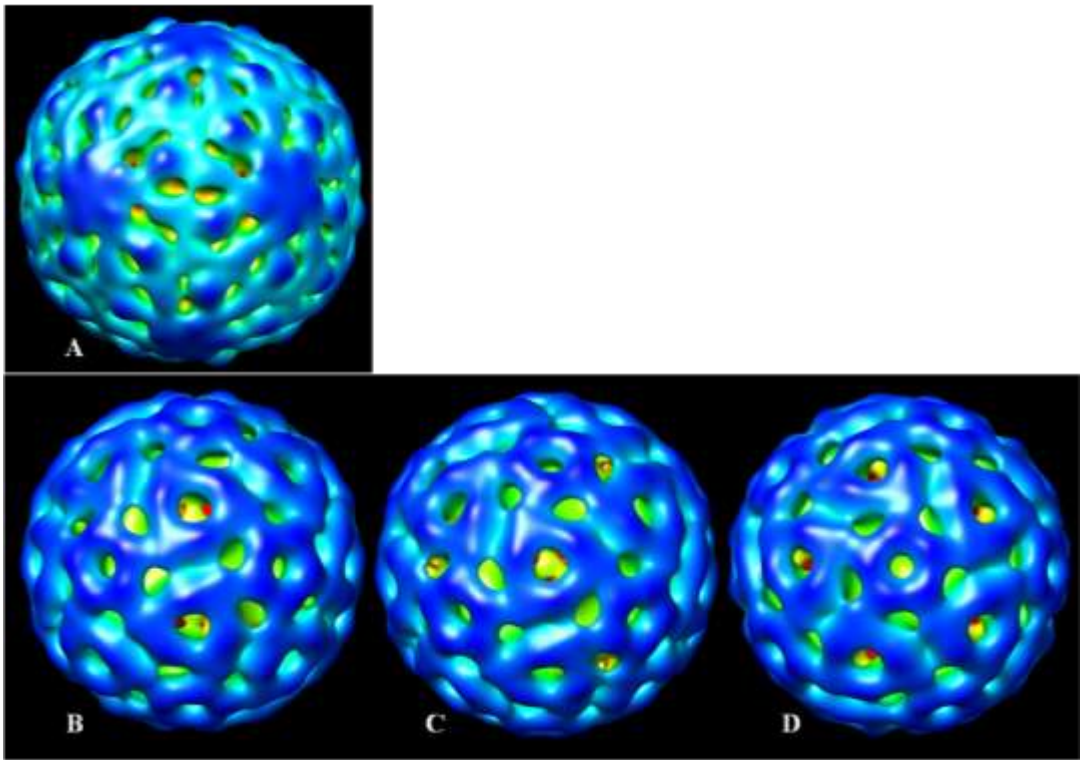

Fig. 4.11. Pre-viral nc reconstruction (43 nm diameter) from AUTO-3DEM-generated model

A. Initial model produced by AUTO-3DEM from 342 particles. (B-D) Pre-viral nc reconstruction using AUTO-3DEM-generated model as initial model and no CTF correction, shown at 2, 3, and 5-fold axes of symmetry.

The diameter of this pre-viral nc reconstruction is 12% greater than the mature nc (Paredes *et al.*, 2001). The capsid shell is 6.3 nm thick, or 5% thicker than the mature nucleocapsid (Paredes *et al.*, 2001) and 34% thinner than the isolated nc (Paredes *et al.*, 2003). Resolution is ~40 Å.

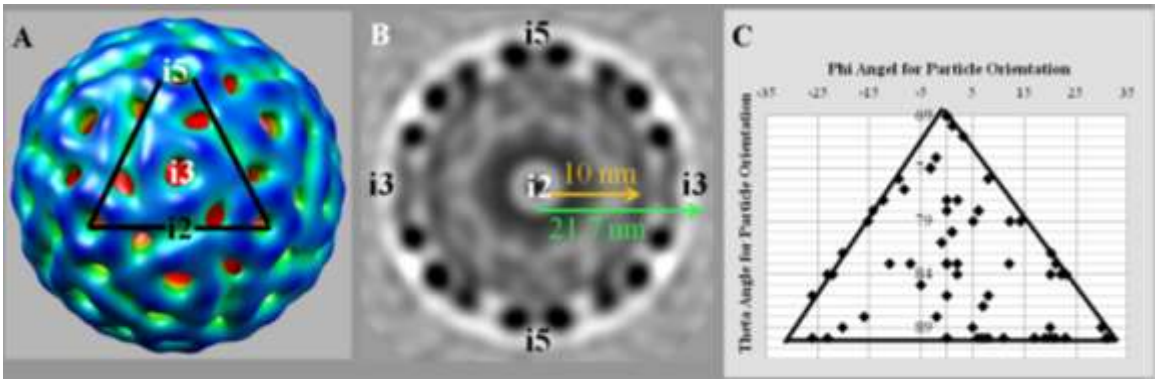

Fig. 4.12. Pre-viral nc reconstruction (43 nm diameter) analysis

A. Pre-viral nc reconstruction using initial model generated by AUTO-3DEM. The overlay highlights the 2, 3, and 5 fold axes of the map. B. Central section of the same map (A) looking down the 2 fold axis. This shows the thickness of the capsid protein shell in the map, extending from 10 nm to 21.7 nm from the center of the map. C. Shows the coverage of the asymmetric unit for the reconstruction (A), given the information from the ~80 particles which constituted the map.

Icosahedral symmetry was imposed in this case, but the holes in the center of the axes, Fig. 4.12 (A) as well as the reproducibility give the symmetry credibility. The thickness of the capsid shell was determined by looking at the central section, Fig. 4.12 (B). Although relatively few particles were used in the 43 nm diameter pre-viral nc reconstruction, the data still covered the asu well, Fig. 4.12 (C).

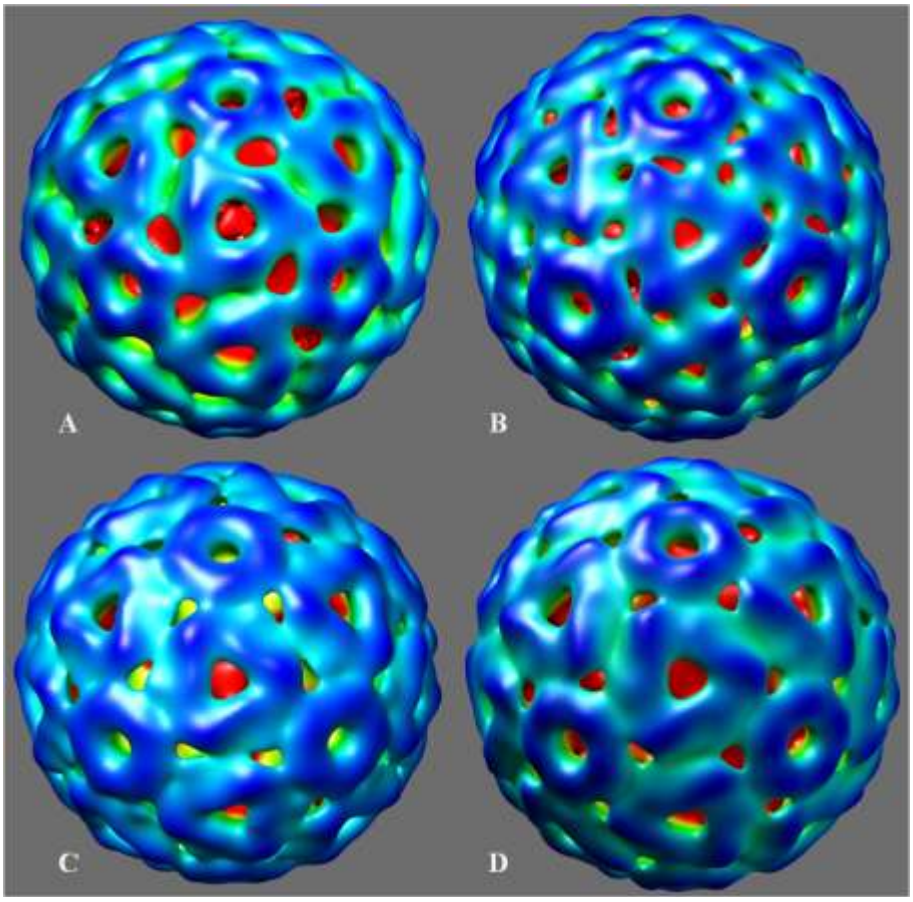

Fig. 4.13. Cryo-EM reconstructions from different initial models

Three-dimensional reconstruction of a VEEV pre-viral nucleocapsid assembly state. All reconstructions are shown at the 3 fold axis of symmetry. (A) Pre-viral nucleocapsid reconstruction produced using AUTO-3DEM-generated starting model. (B) Similar to (A) but with RCNMV map used as a starting model. (C) Similar to (A) but with VEEV mature nucleocapsids used as a starting model. (D) Similar to (A) but with WEEV mature nucleocapsid used as a starting model. None of the above reconstructions used CTF correction in its rendering.

Radial density distributions of pre-viral nc (43 nm diameter) reconstructions

Radial density plots of the four pre-viral, no-CTF correction employed, reconstructions from different initial starting models provided detailed descriptions of radial density distributions within the 3D reconstructions. These plots were similar for the

four independent reconstructions of the pre-viral nucleocapsid (Fig. 4.14), thus confirming the similarity between the independent reconstructions. A trough in the density plot, representing a local density minimum, at 10 nm radius (labeled “a” in Fig. 4.14) matched the boundary between density associated with viral RNA and the protein shell. Three local density peaks were observed between 10 and 21.7 nm on each spherical average plot, and were located at similar radial distances in the maps. The AUTO-3DEM reconstruction had a smaller density peak at 11.6 nm (labeled “b” in Fig. 4.14) relative to the other three reconstructions. This radial distance marked the maximum depth of the surface holes that penetrated through the capsid shell. Density peaks located at a radial distance of 15.5 nm (labeled “c” in Fig. 4.14) corresponded to the inner boundary of the capsid shell, whereas the density peak at 19 nm (labeled “d” in Fig. 4.14) was located midway through the capsid shell of the pre-viral nucleocapsid. The outer edge of the capsid shell for each map was indicated at a density of zero a radial distance of 21.7 nm (labeled “e” in Fig. 4.14). Only the inner core (radius 0-10 nm) of the pre-viral nucleocapsid, which corresponds to density associated with the vRNA in the maps, showed variations in the density profiles between different reconstructions (Fig. 4.14). This could suggest that the RNA at this stage is disordered. In contrast to the pre-viral nc’s three major peaks in the protein shell density, the mature nucleocapsid forms only two major peaks in a more concise range, from ~12 nm to ~19 nm. This gives the appearance of the nucleocapsid being expanded at the pre-viral stage and becoming compressed into the mature nc.

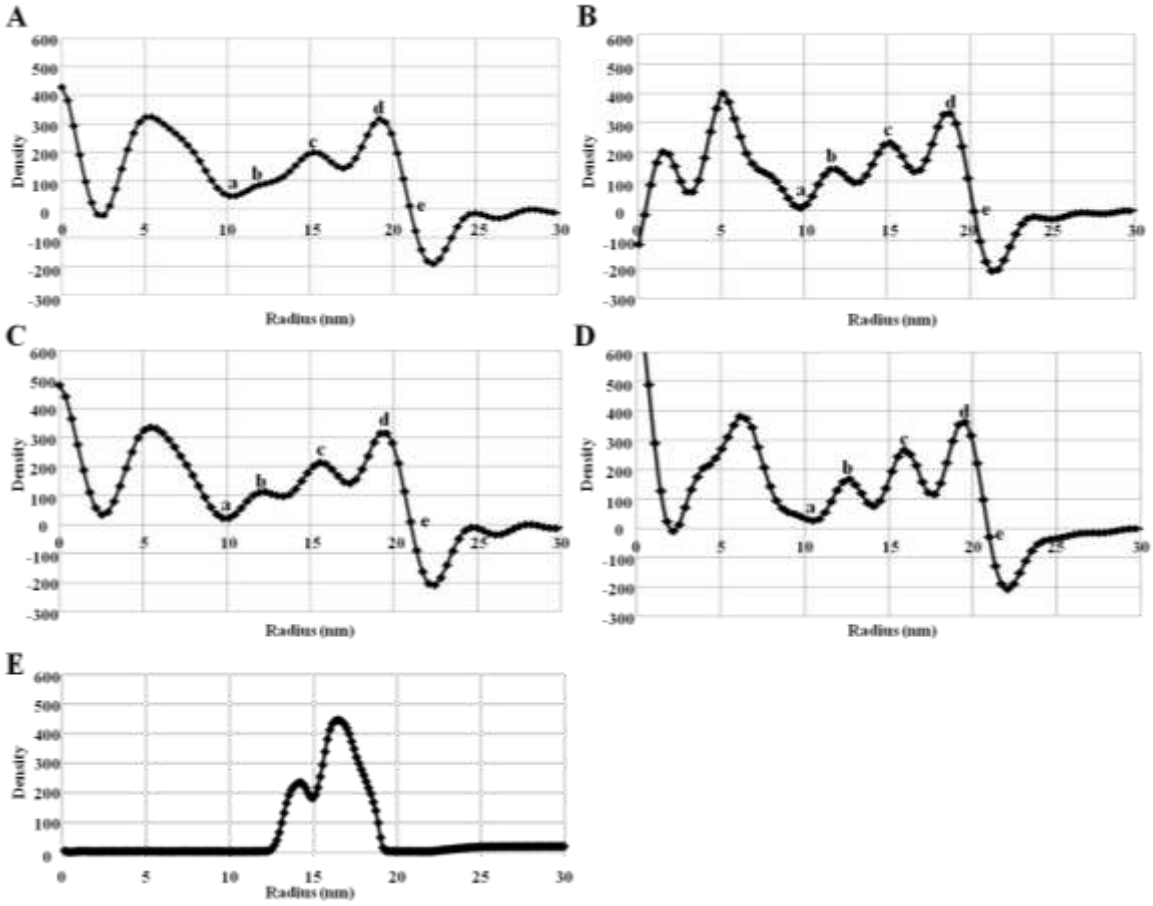

Fig. 4.14. Radial density plots of pre-viral nc reconstructions (43 nm diameter) and the mature nc

Radial density plots of pre-viral nucleocapsid reconstructions produced from each of four starting models, (A) AUTO-3DEM-generated, (B) WEEV mature nucleocapsid, (C) VEEV mature nucleocapsid, and (D) RCNMV. (E) The radial density plot of VEEV mature nucleocapsid without RNA content at comparable resolution. Note that the pre-viral reconstructions have the RNA content still in their plots. The protein shells all begin at (a.) for the pre-viral nc reconstructions.

Pre-viral nc alternate reconstruction methods unsuccessful at generating additional maps or improving existing reconstruction. Attempts to find additional reconstructions and/or increase the resolution of the existing map accomplished neither

by these additional methods. Methods for additional methods are illustrated in Fig. 4.15. In the case in which the goal was to find additional reconstructions, the particles used to reconstruct the above four reconstructions was omitted from the dataset prior to beginning. In the case in which the goal was to increase the resolution of the existing model, two main strategies existed, either the particles used to reconstruct the four pre-viral nc reconstructions above were the entire dataset used, or they remained mixed with the other particles as the "full" dataset. Various percentages of "best correlating" particles were used in the selection process in both cases. The end result was the same, reconstructions with poor features, which failed to converge into stable reconstructions. To illustrate this, and example of such results is shown in Fig. 4.15.

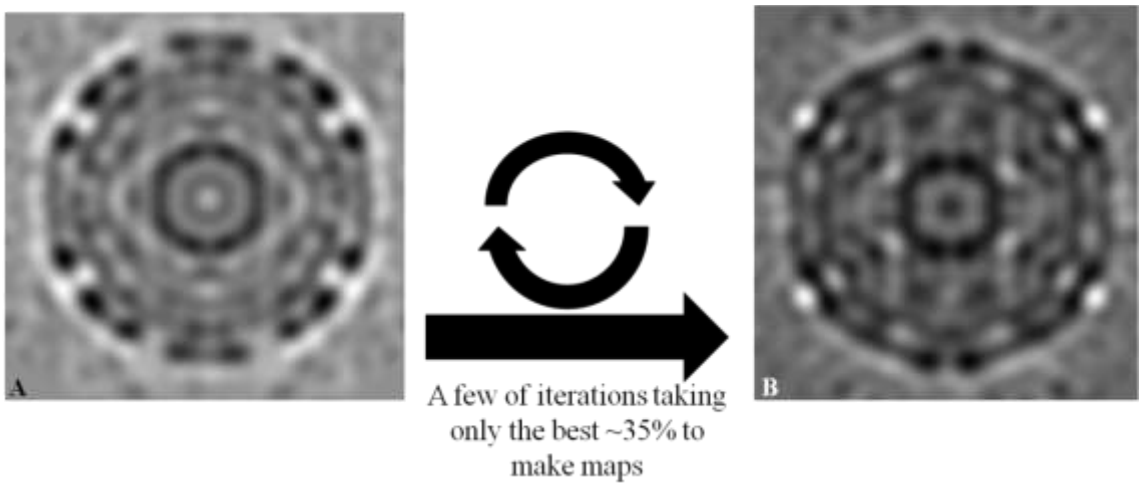

Fig. 4.15. Example result of "alternate" reconstruction method

Central sections of a beginning model and a reconstruction a few iterations after using the alternate method. In this case, the best 35% of the 342 particle dataset were used to produce the reconstruction with central section (B) after a few iterations. Note the changes in definition of detail and the presence of "streaks" through the central section. Central section (A) was initially from the pre-viral nc reconstruction produced with WEEV mature nc as its initial model.

Central section (A) in Fig. 4.16 has more concise densities, which by the time the reconstruction resulting in central section (B) is produced, is rounded and the independent "bulbs" of density get stretched out into layers.

Isolated NC (pH 7.4) cryo-EM Reconstructions from the first two reconstructions showed what looked like "structures within structures" and lacked clear 2, 3, and 5-fold features which were seen in A. Paredes's structure (Paredes *et al.*, 2003). Thus, the diameter cut-offs were altered to separate these "structures" into separate reconstructions. The result was reconstructions which seemed to be lacking in features and data spanning the asymmetric unit. Subsets were small, and perhaps too small to do this. Some of the groups of particles had 30 or fewer particles. The number of particles per dataset can be derived from the size distribution graph, (C) in Fig. 4.6.

EXPASY VEEV CAPSID SEQUENCE ALIGNMENTS WITH OTHER ALPHAVIRUS CAPSID SEQUENCES

Rationale for sequence alignments Whether or not VEEV, like Sindbis and Semliki Forest virus, has a ribosome binding site on the capsid protein which may aid in its disassembly and ultimately the release in ssRNA into a newly infected cell, is still a question. It is a question related to the overall goal of comprehending nucleocapsid assembly, maturation, and disassembly, which could be addressed through easily obtainable amino acid sequences and alignment tools, and thus was pursued. Ultimately, if Eliquos and Sculptor are capable of accurately docking the C-terminal VEE capsid protein into the low-resolution Cryo-EM maps, then it could have been determined if the

presumed ribosome binding site on the VEE capsid protein, if it potentially exists, given the alignment results, becomes more exposed in different maturation stages.

Sequence alignments results give credence that there may be a ribosome binding domain on the VEE capsid protein There was a 58.3% sequence identity in a 12 residue overlap between the putative Sindbis capsid protein ribosome binding site (Wengler and Wurkner, 1992), gln 94 to arg 105 and the VEEV capsid protein, beginning at aa 105 and aa 116. There was an 87.5% sequence identity in an 8 residue overlap between the putative Semliki Forest virus capsid protein ribosome binding site at lys 101 to arg 110. This overlap spans the VEEV capsid protein sequence from aa 110-117.

RADIAL SLICES OF PRE-VIRAL (39 NM DIAMETER) AND MATURE NC MAPS

Rationale for radial slices of 39 nm pre-viral nc and mature nc maps Radial slices of each map were made in order to determine whether there were structural differences between the two maps beyond the superficial differences. In addition, it was also of interest to determine whether the holes observed in the pre-viral nucleocapsid structure penetrate through the capsid shell.

Observations of radial slices Radial slices towards the center of the pre-viral nucleocapsid structure were made with the Chimera program (Fig. 4.16). I observed from the intact structure that there were holes on the surface and the interior of the structure. After cutting through the structure, producing "onion layers" towards the structure's interior, we notice that none of the holes we observed on the intact structure penetrate through the capsid shell. Looking from the exterior surface of the structure there were holes between the protruding capsomeres forming the hexameric, pentameric, or triangular-shaped structures along the axes of symmetry, and holes visible just beneath

the more superficial gaps which do not correspond directly to the more superficial ones. The holes dividing the hexamers and triangles, along the two and three-fold axes of symmetries are lost after removing ~43% of the protein shell. This superficial layer correlates with the protein density that makes the pentamers, hexamers, and triangles on the protein surface at the 5, 2, and 3-fold axes of symmetry, Fig. 4.16 (A-C). Beneath this layer, shown in Fig. 4.16 (D-E) is a middle layer through the nucleocapsid protein shell. At the top of this layer, shown in Fig. 4.16 (D), which is after ~51% of the protein shell volume has been removed, holes are present at approximately the five and three-fold axes of symmetry. The holes at the three-fold axis form a triangle, which does not line up with the triangle at the pre-viral nc's surface; it is twisted by ~10°. The holes in this protein layer form a pentamer structure, but, again, this does not line up with the pentamer we see at the nc's surface. It is twisted by ~37° Fig. 4.16 (D). After 64% of the capsid protein shell volume has been removed, there is a layer through which no holes penetrate, Fig. 4.16 (E). Holes reemerge in the structure after ~73% of the capsid protein shell volume has been removed (data not shown). The first holes make a pentamer structure at approximately the five-fold axis of symmetry. These holes expand as more shell volume is removed (sections not shown), and holes corresponding to approximately where the three-fold axis of symmetry is on the surface emerge (~77% protein shell volume removed), Fig. 4.16 (F). By the time 94% of the capsid shell volume is removed, again, there are holes at approximately where the pentamers and triangles are on the structure's surface at the five and three-fold axes of symmetry. Interestingly, at the five-fold axis, there are holes, which mimic the holes between the arms extending from the pentamers on the nc's surface, and a pentamer-shaped protein density with extensions, again, mimicking what we see on the nc's surface, Fig. 4.16 (F).

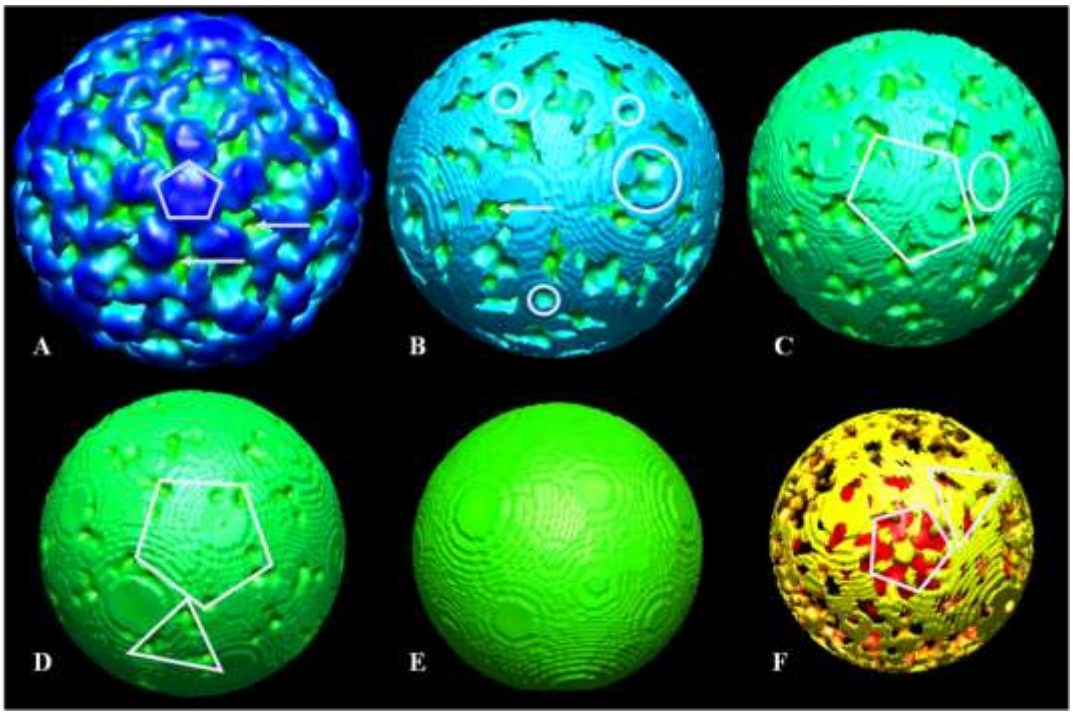

Fig. 4.16. Radial slices into 39 nm diameter pre-viral nc map

Slices made with Chimera. All structures are looking down the 5-fold axis. A. Corresponds to the uncut pre-viral nucleocapsid map. (B-F) radial cuts into the structure by: 1.7, 2.8, 3.3, 4.2, and 5.6. Arrows in (A) point to the holes seen in radial cuts. Pentamer overlays denote points of interest at 5-fold axis. Circle overlays show where notable holes in previous cuts were. Triangles denote points of interest at 3-fold axis. Colors range from warmest colors closest to the radial center to coolest at the furthest from the radial center. "Ripples" in sliced models are an artifact of the volume eraser.

Like the exterior of the pre-viral nc, the interior appears to be twisted internally at its axes. At this resolution, holes and other details are likely missing from the radial cuts, so the continuous layer at 2.8-3.3 nm inside the protein shell may not be proven to be so at higher resolution.

"REFOLDING" OF ISOLATED TC83 vRNA

Rationale for attempts at "refolding" isolated TC83 vRNA These experiments address another question about the nucleation event for alphaviruses, which was still in question at the time the experiments were conducted. The question addressed here was whether the vRNA becomes structured and forms a scaffold for nucleocapsid assembly.

Evidence does not support idea for vRNA forming structures without capsid protein vRNA in negative stain EM looked random with no apparent structure. Some round structures were seen and predominated in the 2 hour 32°C incubation time. They seemed to be ~10 nm in diameter. There were also round objects in the EMs with a densely stained center and halo around it with diameters of ~15 nm, Fig. 4.17 (B-D).

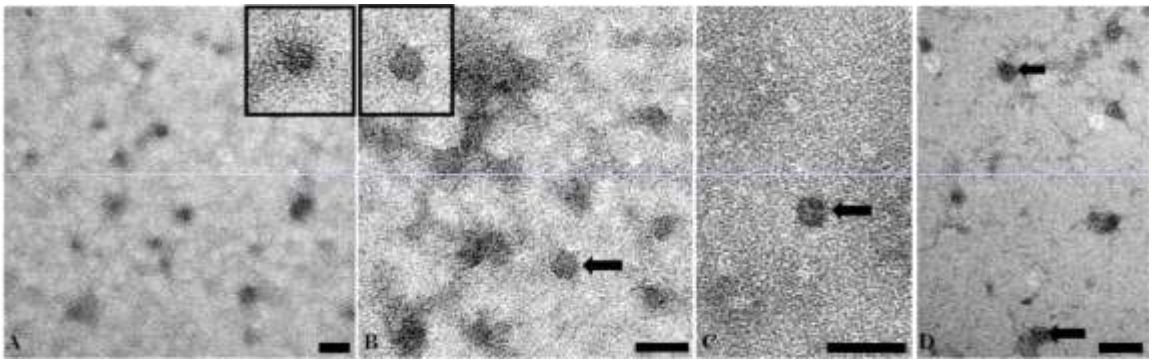

Fig. 4.17. Negatively stained vRNA "folding" experiments

A. Control vRNA-assembly folding experiment, no vRNA content. B. vRNA folding experiment, post-10 minute incubation on ice. C. vRNA folding experiment, post-2 hour on ice. D. vRNA folding experiment, after tube was allowed to incubate on ice for 10 minutes, and then at 4ºC.

These objects seen in the vRNA "refolding" reactions were similar to some similar artifacts in controls, Fig. 4.17 (A). Similar results were seen in the vRNA

reactions in the rabbit reticulocyte lysate. Given the objects in the controls, the round "particles" seen in the any of these vRNA folding experiments cannot be attributed necessarily to vRNA folding in on itself to conform to any structure with the conditions attempted.

DOCKING CAPSID PROTEIN INTO MATURE NC MAPS USING ELIQUOS AND SCULPTOR

Rationale for docking with Eliquos/Sculptor system The resulting pre-viral cryo-EM reconstructions were, despite my best efforts, low resolution maps. Given that, the current docking programs habitually fail to accurately dock crystal structures into Cryo-EM densities with resolutions poorer than 15 Å. During the course of my studies, J.J. Heyed developed the programs Eliquos and Sculptor, which showed more promise at docking crystal structures into low resolution cryo-EM maps, depending on the system (personal communication). Given that and the requests of reviewers and advisors, this system was attempted to dock the C-terminal VEE capsid protein crystal structure into the mature nc reconstruction at increasingly lower resolutions to test where the programs failed to accurately dock the crystal structure.

Eliquos and Sculptor fail to accurately dock the crystal structure in cryo-EM reconstructions of the mature nc at 20 Å resolution Of the three C-terminal capsid chains in the crystal structure (PDB file 1EP5), chain C, the third of the C-termini, was used for docking with Eliquos and Sculptor programs after an initial docking with each of the C-terminus chains independently into the mature nc 3-fold axis at 8.7 Å resolution. The results were compared with Zhong Li's unpublished docking at the same resolution. All three chains, A-C in the crystal structure, docked into similar positions as Zhong Li (personal communication). However, chain C, seemed to fit the EM density

best, and was thus used for further docking attempts with the program. A run with chain C probing the two-fold axis hexamers was used to overlay with subsequent runs to determine the reliability of the program to dock the C-terminal capsid protein at the given resolution of the mature nc EM map.

Docking was attempted on mature nc's of resolutions 12, 16, 20, 24 Å resolutions, Fig. 4.18-20. The programs' ability to determine the correct positions of the C-termini in the EM density began to fall apart by 20 Å resolution, Fig. 4.20. Given this, these programs would yield unreliable results if we attempted to dock any of the pre-viral nc structures.

Fig. 4.18 shows that Eliquos and Sculptor, while the most adept programs to date at docking proteins into low-resolution EM densities, is unable to accurately dock the VEEV C-terminal protein segment into a VEEV nucleocapsid density at 28 Å resolution. Different kinds of filtering were used in these cases, as was the instruction by J.J. Heyd (personal communication), who developed the programs, Laplacian and Hessian filtering methods. To further analyze whether it is the filtering method itself which causes the inaccuracies at lower resolutions, 12, 16, and 20 Å mature nc maps were also docked using the same programs and protocols, but with Hessian filtering even though it is not required at 12 and 16 Å resolutions. Given that the docking results did not vary in this case, the filtering aspect at those resolutions is an insignificant point.

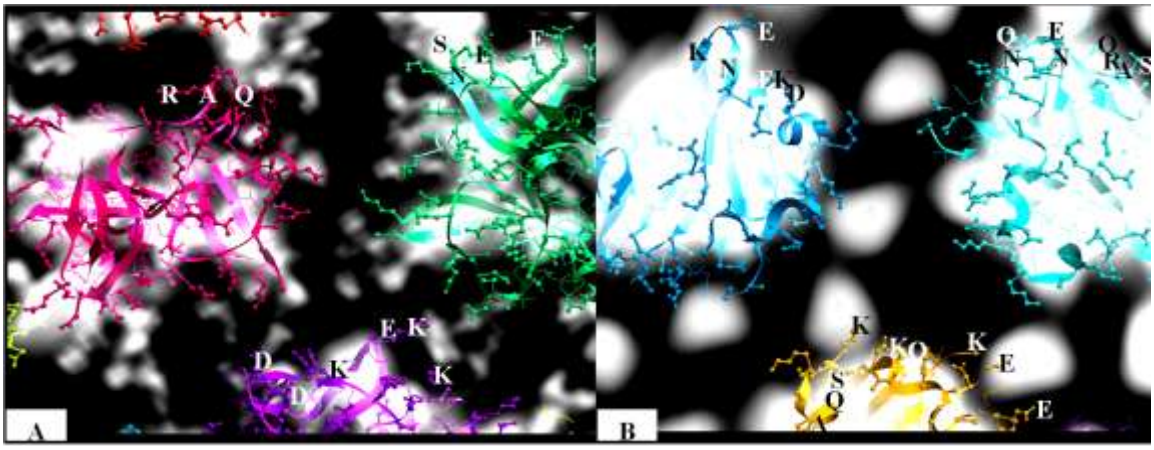

Fig. 4.18. Docking of C-term VEEV capsid protein into mature nc 8.7 and 28 Å resolution map

Docking of 3-fold axes of A. C-terminal of VEEV capsid protein docked into 3-fold axis of the mature nc at 8.7 Å resolution using Laplacian-filtering in Eliquos. Amino-acids at interfaces are marked according to their accepted abbreviations. B. C-terminal of VEEV capsid protein docked into 3-fold axis of mature nc at 28 Å resolution using Hessian-filtering in Eliquos.

Hessian filtering was used in docking the C-terminal capsid protein segment into the 16 Å resolution mature nc map, shown in Fig. 4.19. The result overlapped well with the accepted result from docking the protein with the mature nc at 8.7 Å resolution.

The docking of the C-terminal protein into the 20 Å resolution mature nc map does not overlap with the accepted docking at 8.7 Å, shown in Fig. 4.20. Thus, docking using these programs and procedures fails at this point.

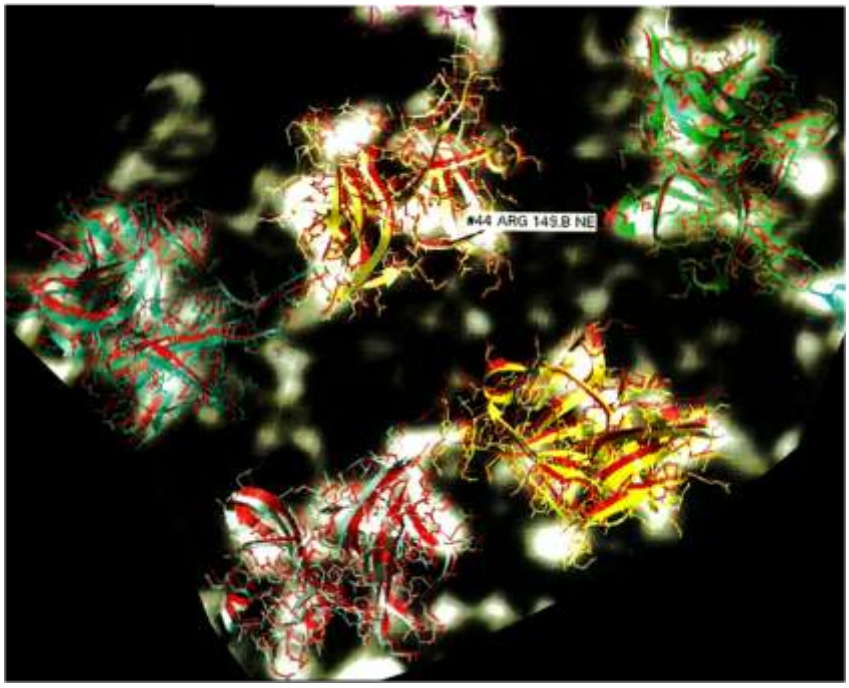

Fig. 4.19. Docking overlay of C-term VEEV capsid protein docked into mature nc 8.7 and 16 Å resolution maps

Docking in red is the 8.7 Å results. All other colored C-terminal proteins are as a result of the docking into the 16 Å mature nc map.

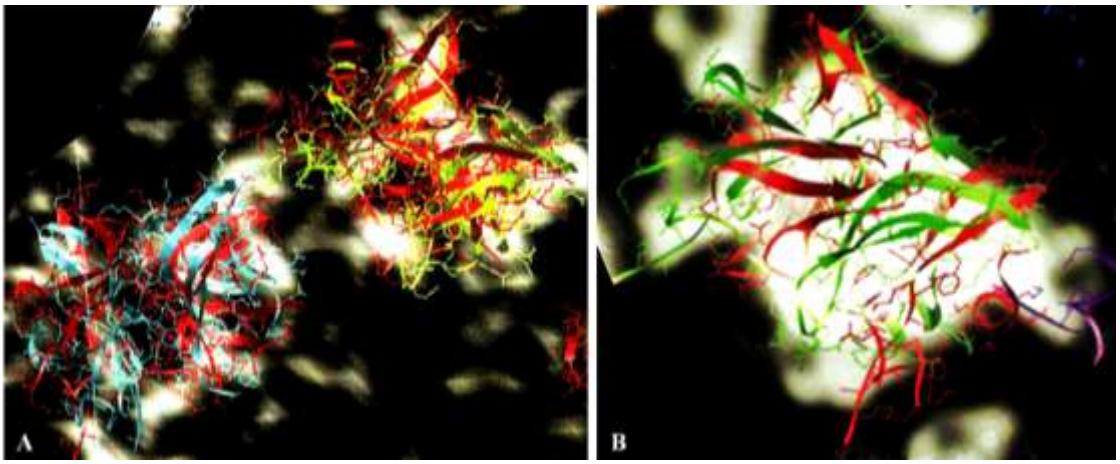

Fig. 4.20. Docking overlay of C-term VEEV capsid protein into mature nc 8.7 and 20 Å resolution maps

Docking in red is the 8.7 Å results. All other colored C-terminal proteins are as a result of the docking into the 16 Å mature nc map.

DOCKING OF CAPSID PROTEIN INTO PRE-VIRAL NC (43 NM DIAMETER MAP) USING CHIMERA

Rationale behind docking the capsid protein into the 43 nm diameter pre-viral nc map The question remains, given the divergence of the 43 nm in diameter pre-viral nc reconstruction from a clear T=4 structure, as to whether the same number of proteins can fit into this pre-viral nc reconstruction as the mature nc. Thus, docking with Chimera was done to see if twelve VEEV capsid protein C-termini were able to fit into three-fold axis, as it would be seen in a classic T=4 structure.

Twelve- VEEV capsid protein C-termini were able to fit without overlapping into the three-fold axis. Docking showed that twelve C-termini were able to fit into the 43 nm diameter pre-viral nc density, but this fit does not give as much empty room between C-termini when this is repeated for the mature nc.

The positions are not intended to reflect accurate positioning, given the resolution and reasons stated in the previous Eliquos/Sculptor docking section. The Chimera docking data, seen in Fig. 4.21, suggests that 240 C-terminal capsid proteins can fit in the pre-viral nc reconstruction from the AUTO-3DEM generated model. This is important to ascertain whether the reconstruction was part of a dead-end assembly pathway or could still, potentially, be part of the viable assembly process.

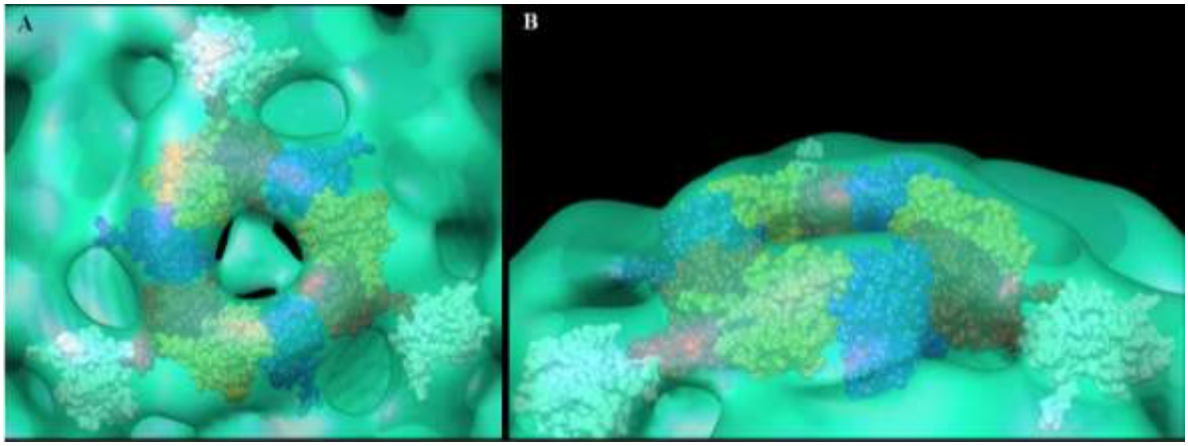

Fig. 4.21. Capsid protein C-termini docked into pre-viral nc reconstruction (43 nm diameter map) using Chimera

Capsid proteins modeled within the pre-viral nucleocapsid. (A) Twelve C-terminal domains of the VEEV capsid protein positioned within an icosahedral face of the pre-viral nucleocapsid particle and viewed along an icosahedral 3-fold axis. (B) Side view of the pre-viral nucleocapsid highlighting the arrangement of twelve C-terminal domains of the VEEV capsid protein within an icosahedral face of the particle.

VOLUME CALCULATION OF PRE-VIRAL NC (43 NM DIAMETER) MAP

Rationale behind volume calculation of 43 nm diameter pre-viral nc map

The limited resolution of the pre-viral nucleocapsid assembly intermediate made it difficult to definitively assign capsid protein positions and stoichiometry. However, determining the stoichiometry of pre-viral nucleocapsids was important for unraveling VEEV assembly pathways and mechanisms. Two independent and complementary approaches were used to estimate the number of capsid proteins that formed the pre-viral nucleocapsid. Both approaches showed that this pre-viral nucleocapsid assembly intermediate likely contained 240 capsid proteins, identical to the number of capsid protein that form the mature VEEV nucleocapsid. The first approach, described earlier, involved monomers of the C-terminal domain of VEEV capsid protein being docked into

the electron density that defined an icosahedral face of the pre-viral nucleocapsid capsid shell. Twelve capsid C-termini, could be contained in the 3-fold symmetry axis density without steric clashes (intersection of protein surfaces) between docked subunits, Fig. 4.23. This was attempted with the mature VEEV (Watowich and Paredes, personal communication), which is known to have 240 of the C-terminal protein subunits, using the same program, electron density thresholds, and map resolution. Consistent with its T=4 symmetry, twelve capsid proteins could be in the mature VEEV nucleocapsid (Paredes *et al.*, 2001). The docking experiments suggest that the same number of capsid proteins formed the pre-viral assembly intermediates and mature virus nucleocapsids.

In the second approach, the electron density volume corresponding to the capsid shell was calculated for pre-viral and mature VEEV nucleocapsids. These calculations used comparable density threshold values to delineate the protein envelope and accounted for the different density distributions in the reconstructions.

Density calculations suggest that the 43 nm diameter pre-viral nc reconstruction can hold 240 capsid proteins. A density cutoff of 2.8 σ was sufficient to enclose a volume in the mature nucleocapsid equal to the volume of 240 C-terminal domains of the VEEV capsid protein (5.08×10^6 A^3). At this electron density threshold, the total electron density volume of the pre-viral nucleocapsid capsid shell was greater than that of the mature nucleocapsid capsid shell. Thus, the electron density volume of the pre-viral nucleocapsid capsid shell was sufficient to enclose at least 240 C-terminal domains of the VEEV capsid protein.

The limited resolution of the pre-viral nucleocapsid structure prevented definitive localization of the capsid proteins within the surface capsomers. Although the pre-viral nucleocapsid could accommodate 240 capsid proteins, these proteins did not adopt the

classic T=4 capsomer lattice observed in VEEV mature nucleocapsids (Paredes *et al.*, 2001) and VEEV nucleocapsids isolated from whole virions (Paredes *et al.*, 2003), with quasi-hexons centered on the 2-fold axis of symmetry. Higher resolution will be necessary to determine accurately how the 240 VEEV capsid proteins are arranged within the pre-viral nucleocapsid.

Chapter 5: HCVC Conclusions

HCVC Constructs Unsuitable for Crystallization Trails/Useful Protein Structure Analysis

The HCVC constructs, H158 and H36-169 were chosen in an effort to accomplish one or both of two goals: obtain a suitable construct for protein crystallization trials and/or analyze the structure of the protein. H36-169 expressed poorly, and therefore the yields after purification attempts were miserable. What was not attempted which may have helped expression was to try to express H36-169 without the MBP fused to it and try to express and purify it as the other constructs had been. Perhaps, too, we could have added HCVC aa1-36 which was included in the other constructs expressed previously in the laboratory and yielded better results, H124, H158, and H179 (purified by Kunkel and Lorinczi). While it was not published at the time that these experiments were being performed, H1-169, along with H1-117, was used to identify the structural characteristics of HCVC (Boulant *et al.*, 2005). It is interesting to note, that in this publication, they found, comparable to what we found with H158, the protein tended to aggregate. However, it was found that a small amount of detergent could solubilize the protein better, and that the protein behaves more as a membrane protein. Basically, the aggregation properties which we found with H158 at even moderate concentrations would have dispersed, according to the results in (Boulant *et al.*, 2005), given the addition of a small amount of detergent.

HCV NLP and Cell Culture Samples Were Insufficient for Cryo-EM Attempts

HCV NLP reactions The HCV NLP reactions resulted in heterogeneous populations and, in the case of using rabbit reticulocyte lysate, had additional purification which would have to be done to isolated the NLPs from the lysate contents. The reactions using the rabbit reticulocyte lysate were small, given the commercially available volume, so scaling the reaction up to accommodate loss in the purification process is not practical. Thus, the NLP reactions which were done in buffer, as described in (Kunkel *et al.*, 2001) could be used, but the heterogeneity problem would have to be approached as it was later approached with the VEEV pre-viral nc's, with separation of different particles after images were taken. Alternatively, the small NLP reactions could have been used to find agents for disruption.

HCV NLP characteristics implications The nucleocapsid-like-particles were heterogeneous in size and shape. The question is comparable to the same question which will be asked later of the representative alphavirus nucleocapsids, VEEV nc's. The nucleocapsids' heterogeneity either conforms during the interaction with E1, it conforms to a structure *in vivo* on its own, or it goes through a selection process. These suggestions are contingent on the validation that HCV nucleocapsids do conform to a uniform structure within the virus. Given that the current low-resolution HCV cryo-EM reconstruction (Yu *et al.*, 2007) does not describe the nucleocapsid within the whole virion, this is not known. Multiple structures of these particles was not done, so it is not known if their spherical average plots at the nucleocapsid radii overlap or suggest comparable characteristics.

HCV whole virion cell culture The yield of virions within the concentrated cell culture mediums alone was insufficient for cryo-EM trials. Further attempts using a heparin-binding column were attempted, but fractions containing virus were widely scattered throughout the elution. This suggests one of two possibilities: either the culture supernatant needed a more extended exposure to the beads for the virions to bind to the beads sufficiently, or the virions are only capable weakly binding to heparin beads, largely due to the beads as opposed to the heparin. My attempt to isolate the virions using this method is contrary to that used by (Yu *et al.*, 2007), which used methods more comparable to what I later used to isolate VEEV. They yielded a heterogeneous population of virus which clung to lipids, resulting in a reconstruction with few distinct features. Two problems are still apparent in achieving an HCV structure with well-defined features: the inherent heterogeneity of the particles and their pervasive lipophilic nature. The inherent heterogeneity will likely have to be addressed, as it has been, during particle selection during the reconstruction process, just as I did with the pre-viral nc and post-entry at pH 5.5 reconstructions and as Yu did (Yu *et al.*, 2007). The virion's lipids will have to be stripped, and the virions quickly resuspended in maybe an agent such as n-dodecyl β-D-maltoside, which has been used to refold Membrane Protein F (Visudtiphole *et al.*, 2005). Attempts to remove the lipid associated with the virion may be similar conceptually to removing the lipid from VEEV for isolated nc's. That would mean subjecting the whole virion to concentrations, smaller than that used for removal of the virion envelope, of detergents, like Triton-X100 or Tween. The actual concentration at would have to be worked out by subjecting aliquots of the same isolated virus sample to a series of detergent concentrations and observing the results via negative stain and TEM. The amount of lipid may not be readily recognizable with this method, but the

stability of the virion will be. Thus, the concentration to use would be the slightly less than the maximum concentration of detergent, which caused absolutely no virion structural deformities or disruption.

Chapter 6: VEEV Nucleocapsids Conclusions

PRE-VIRAL NUCLEOCAPSID RECONSTRUCTIONS AND THEIR IMPLICATIONS ON ASSEMBLY

Pre-viral NCs initial assembly As a small aside, experiments aimed at addressing whether or not there was a possibility that the ssRNA folded and formed a scaffold for pre-viral nc assembly. Given the results in Fig. 4.17, this suggestion is not supported by the data, at least under the conditions attempted. It was confirmed during the course of these experiments that another group had confirmed that the "seed" for alphavirus nucleocapsid assembly occurred with ssRNA-capsid interactions *(*Warrier *et al.*, 2008). ssRNA structural elements do play a role in nucleocapsid assembly, as described previously in the introduction, but it is more instrumental in capsid-RNA recognition and stability of the capsid-RNA interactions.

Pre-viral NCs in thin-sections and implications As it was noted originally for Semliki Forest virus (Acheson and Tamm, 1967), another alphavirus, the pre-viral nucleocapsids, as we call them, bind a secretory pathway to migrate to the cell surface, and are thus found in clusters and attached to liposomes in the cell. To my knowledge, the identity and the requisite for this secretory pathway for pre-viral nc shuttling to the cell membrane has yet to be described. It does show low the pre-viral nc's are continually attached to lipids, even at this stage. This suggests that the orientation at this stage would readily accommodate lipophilic interactions necessary for binding to newly budded virion's membrane. Heterogeneity, even at this stage has been noted, first by Acheson (Acheson and Tamm, 1967), as well as by us. The mean diameter of pre-viral nc's in Acheson's thin-sections was ~28 nm, while mine was ~40 nm. However, Acheson

was using chick embryo cells and observing the pre-viral nc's at 5-9 hours post-infection. In my case, I was using BHK cells and observing the pre-viral nc's at 18 hours post-infection, when I made the diameter observations. The main question is, then, do the size distributions change during the course of infection and would predominant structures differ at these stages? Acheson noted that pre-viral nucleocapsids' placement or affinity to cellular constituents were indiscriminant very early in infection (Acheson and Tamm, 1967). At this early stage, perhaps the structure has to undergo changes to become more lipophilic, thus sending it on its cellular path to the edge of the cell. So, the pre-viral nucleocapsids go through stages even from the time of their first appearance into the cell until the time at which I was capable of isolating enough from lysed cells for reconstructions. To answer these questions, pre-viral nc isolations would have to be done at time increments, and structures would have to be attempted with these. This would likely be a more daunting task than attempting to do so at a later time point, when pre-viral nc's are more abundant. It is possible that the initial stages lack even more structural elements than the one(s) I found. The size distributions at each stage could easily be done with negative staining. Finding density distributions of may be more of a challenge, given what I previously stated. Another question is, do all of the pre-viral nc's form viable precursor nucleocapsids capable of interacting with E2 and eventually being encased within whole virions? This would answer whether the nucleocapsid precursor assembly is nearly perfect or has byproducts. A summary of these suggestions is in Fig. 6.1.

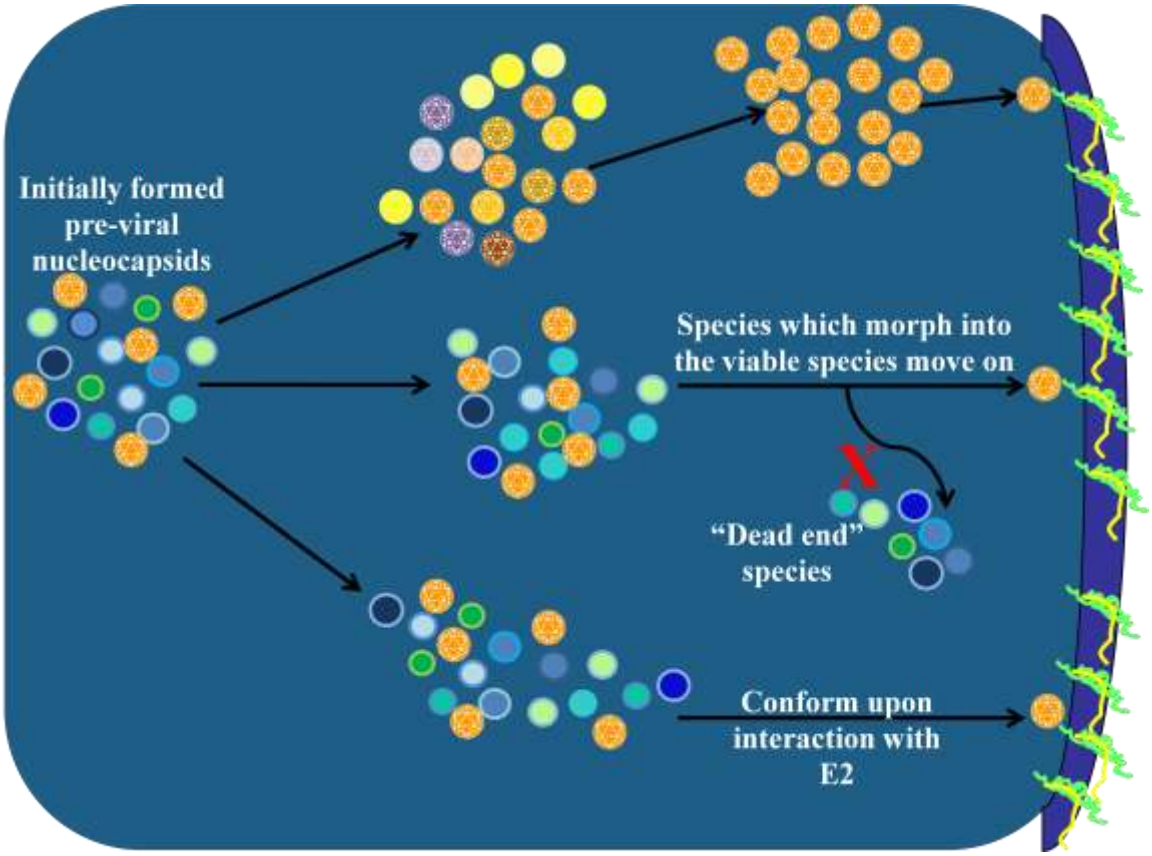

Fig. 6.1. Possible outcomes of assembled pre-viral nc's

Three possible outcomes are described for the known heterogeneous population of pre-viral nc's. In the first possibility, at the top of the image, the particles change conformation and morph into one viable pre-viral nucleocapsid, capable of binding to E2 proteins at the cell surface and becoming encased in whole virions. The second option, in the middle suggests that there are some pre-viral nc's which are incapable of conforming to a/the viable pre-viral nucleocapsid species and are therefore "dead end" species. The third option, presented at the bottom of the image suggests that the heterogeneity persists until the pre-viral nc's meet the E2, which upon interaction, conforms their structures to the viable one, capable of becoming the encased mature nc.

Pre-viral NCs reconstructions Two major pre-viral nc reconstructions have been presented, one which utilized CTF correction (39 nm diameter pre-viral nc reconstruction), and one with did not (43 nm pre-viral nc reconstruction). The former has

no parallel map to validate it, but it uses particles which were not included in the 43 nm diameter pre-viral reconstruction which did not use CTF correction. The appropriate CTF correction, according to the programs' instructions, available at http://cryoem.ucsd.edu/programs/pftsearch.pdf and http://bilbo.bio.purdue.edu/~baker/programs/doc/current/em3dr.html, is dependent on the system itself, and it is advised that users try different ones to determine which is appropriate for their system. The CTF experiments done with the whole virion, Fig. A1.1-2 (Appendix 1,VEEV-TC83 Reconstructions Using Different CTF Methods), would suggest that using the CTF correction applied to the 39 nm diameter pre-viral nc map would cause distortions. This may or may not be entirely true, because even the pre-viral nc reconstruction without CTF correction and with the validation of four maps from different initial starting models, was a very different structure than the whole virion used for the CTF correction experiment. What this experiment does show, however, is that caution must be taken in applying CTF corrections, given that some of the CTF correction applications can lead to distortions in the maps, as it can clearly be seen with the VEEV maps, Fig. 4.16. The only way to tell for certain if the CTF correction used on the 39 nm diameter pre-viral nc map was valid for the pre-viral nc system would have been to repeat the pre-viral reconstruction with the same particles and initial starting map, altering only the CTF correction methods.

Both the maps appear suitable, but the lack of a hole at the five-fold axis of the CTF-corrected map is potentially suspicious of over-emphasizing a local minimum where the 5-fold symmetry is imposed. However, other structures are available, which do not have holes in the center of an axis (Cheng *et al*., 1994; Chipman *et al*., 1996; Rossmann *et al.*, 1994). If this is another potential structure within the pre-viral nc population, then

it is in a twisted confirmation relative to the mature nc reconstruction (Paredes *et al.*, 2001). This sort of twisting and untwisting in response to a change in environment, or in my case interaction with the E2 protein or, more generally, additional unknown maturation stages, has been seen before in verse sequence in CCMV (Liepold *et al.*, 2005). This "twisting" can interestingly be seen through radial cuts into the reconstruction Fig. 4.16. That would suggest an "untwisting" event occurring to conform this structure to that of the mature nc (Paredes *et al.*, 2001). Adding to the possibility that this is another structure within the population, this reconstruction is smaller than the one pre-viral nc reconstruction produced without CTF correction. Thus, this one would be from a different species of pre-viral nc within the heterogeneous population.

Confirmed by having four different maps from different starting models, including one from the AUTO-3DEM-generated initial model, free of model bias, the pre-viral nc model with no CTF correction does not appear twisted in appearance as the CTF corrected model. It is also larger in diameter, which according to sizing of pre-viral nc particles from thin-sections to isolated pre-viral nc's, is the dominant size of the pre-viral nc particles. This and the fact that it could be reproduced by initial models with disparate structures suggest that this is a dominant structure within the population. Despite my best efforts, this structure remains at low resolution, ~42 Å. The suggestion could be that at this stage of maturation, the icosahedral symmetry elements are weak. It has been shown *in vitro* capsid-like-particles (CLPs) can assemble into a 30 Å reconstruction comparable to the mature nc and 42 nm in diameter, though 70% of the original data had to be discarded (Mukhopadhyay *et al*., 2002). This would suggest that the system is capable of forming a structure more comparable to the mature nc, though it, perhaps, is not capable of forming a strong, uniform icosahedral structure, given the

resolution. The pre-viral nc reconstruction produced here without CTF correction (39 nm diameter map) has a diameter which is within a nanometer of theirs. Despite the difference in structure, docking attempts have shown that 240 C-termini of the capsid protein can fit into the density of our pre-viral nc reconstruction, Fig. 4.21. This suggests that in the cell our pre-viral nc may be a precursor which is capable of undergoing conformational changes on its own to become like the *in vitro* structure (Mukhopadhyay *et al.*, 2002). The lower resolution of the pre-viral nc structure may be a reflection of the slight variances of structures within the dataset which within the cell may me still undergoing rearrangements and conformational changes which would lead it to the *in vitro* structure. The questions, though, still would be, what conditions would cause it to rearrange into the *in vitro* structure on its own within the cell, and what inhibits it from forming more readily?

Pre-viral NCs (43 nm diameter) docking with Sculptor and Eliquos

Attempts were made to determine whether docking the low resolution pre-viral nc structures was possible using the Eliquos and Sculptor programs. While most docking fails to reliably position protein crystal structures in cryo-EM densities at medium resolution, Eliquose with Hessian filtering has been shown to surpass this limit to dock proteins in low resolution cryo-EM densities (personal communication). After testing this system with the mature nucleocapsid and the capsid protein C-terminus, it was clear that, even with Hessian filtering, the program failed to accurately predict the docking positions of the capsid protein C-terminus into the mature nc EM density by 20 Å resolution Fig. 4.18-20. The low resolution of the pre-viral nucleocapsid made prospects to describe the structural changes occurring between the different maturation stages and potentially placement of a putative ribosome binding site bleak. Unfortunately, these are likely to

remain indeterminate unless a higher resolution pre-viral nc reconstruction can be achieved. Given the fragility of the pre-viral nc particles experienced working with these particles, and also further described in (Mukhopadhyay *et al*., 2002), this will at least require additional or alternative isolation procedures. One consideration for this could be the addition of a small concentration of detergent, which post-entry nc's at pH 5.5 are sustained in. The addition of a fixative throughout the isolation procedure could be another consideration to stabilize the vulnerable, frail structures.

Chapter 7: Future Direction

AIM AT A MORE BIOLOGICALLY RELEVANT POST-ENTRY NC RECONSTRUCTION

Rationale The current isolated nc reconstruction (Paredes *et al.*, 2003) does not mimic the pH change which biologically occurs in order to release the VEE nucleocapsid into the newly infected cell; it only mimics the stripping of the membrane from the whole virion. Exposure of the virus to acidic conditions is more imperative to the post-entry nc's release than membrane fusion (Paredes *et al.*, 2004). Thus, in order to discover what structural changes are occurring at this maturation stage, a cryo-EM reconstruction needs to be done in which the nucleocapsid is isolated from the whole virus which has been exposed to the pH change which occurs in nature.

Methods The post-entry nc's were isolated in a nearly identical procedure to those for the isolated nc's listed previously in the Methods section. However, in this case, prior to the addition of detergent, the buffer which the whole virus was dialyzed into was at pH 5.5, as opposed to pH 7.4. This required using MES, as opposed to Tris for the buffer. After the addition of detergent, the resulting particles were stained with 2% uranyl acetate and examined for size distribution. In addition, the identity of the particles were verified, as was done with the pre-viral nc's, by immuno-gold labeling.

Post-entry nc's at pH 5.5 reconstructions were produced as described for pre-viral nc (39 nm diameter). In this case, however, there were focal pairs. Both the further from focus images and the closer to focus images were used in the reconstruction at the same time, so the number of original particles in these reconstructions is half of total number of boxed particles. Seven-hundred fifty original particles were initially boxed out. Only ~300 original particles remained in the final reconstructions. No CTF correction was

employed. Starting models included VEEV mature nc, taken from (Paredes *et al.*, 2001), and Sindbis mature nc cryo-EM reconstructions.

Results The SDS-PAGE gel was used again to show the proteins within the post-entry nc sample. Major bands consistent with capsid protein are apparent.

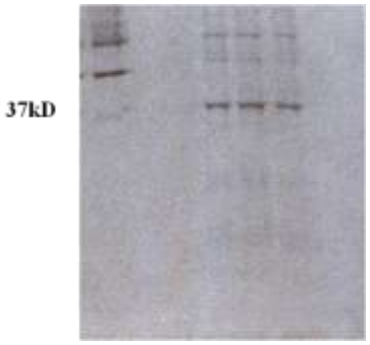

Fig. 7.1. SDS-PAGE gel of post-entry nc's at pH 5.5

A. SDS-PAGE gel of post-entry nc's produced by changing the buffer of isolated VEEV TC-83 and then exposing it to detergent. The capsid protein band occurred just above the 36 kD marker, and is estimated at ~37 kD.

Staining with 2% uranyl acetate was used to determine whether the results of the pH change and exposure to detergent yielded nucleocapsid particles as expected. In addition, the identity of the particles was verified by immuno-gold labeling. Shown below, the resulting post-entry nc's were varying in size. The immuno-gold labeling clustered around the particles, with very little background, suggesting that the particles seen in the staining images were VEE nucleocapsids.

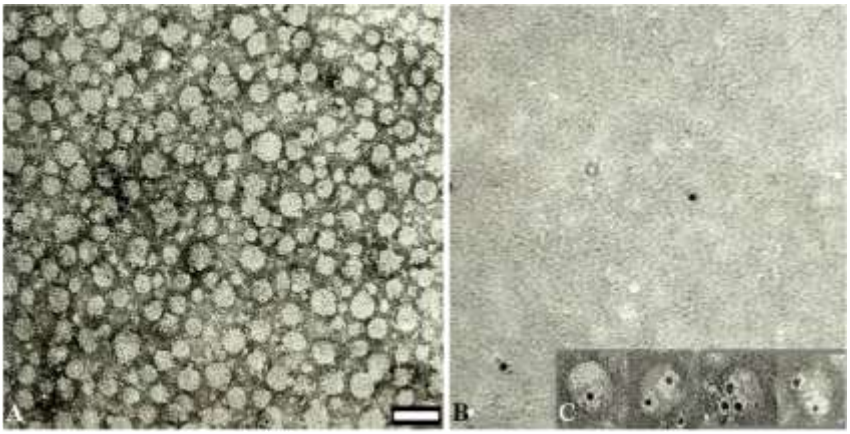

Fig. 7.2. Negatively stained and immuno-labeled post-entry nc's

A. Negative staining of post-entry nc particles at pH 5.5. Particles at this stage been produced by exposing isolated VEEV-TC83 in pH 5.5 buffer to Triton-X100 and have not undergone any gradient purification. Scale bar= 50 nm. B. Immuno-gold labeling control, no post-entry nc's. C. Immuno-gold labeled post-entry nc's at pH 5.5.

Post-entry nc's were measured from their uranyl acetate staining images. The sample, as suggested by visual inspection of the uranyl acetate staining images, is shown to be heterogeneous in size, with the majority being about 41 nm in diameter. The range is comparable to what was seen with the pre-viral nc, but the maximum diameter exceeds that which was seen for the pre-viral nc's.

Post-entry nc's were vitrified onto holey carbon grids covered with continuous carbon. Grids were prepared within the laboratory, as opposed to those available commercially, as was the case for the isolated nc's and whole viruses.

The post-entry pH 5.5 reconstructions have similar features to each other and agree relatively well. The main feature of interest in this preliminary reconstruction is the presence of large holes at the two-fold axis and the spikes in the center of these. The resolution estimations are ~35 Å.

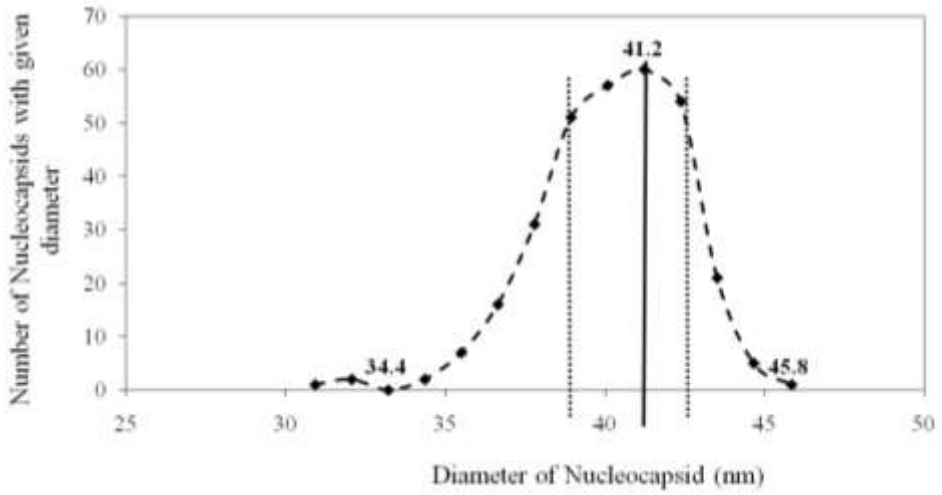

Fig. 7.3. Size distribution of post-entry nc's at pH 5.5

The majority of particles were centered around 41.2 nm in diameter. The minimum diameter was 34.4 nm in diameter. The maximum diameter was 45.8 nm in diameter. The vertical dotted lines indicate the size distribution chosen for Cryo-EM reconstruction later.

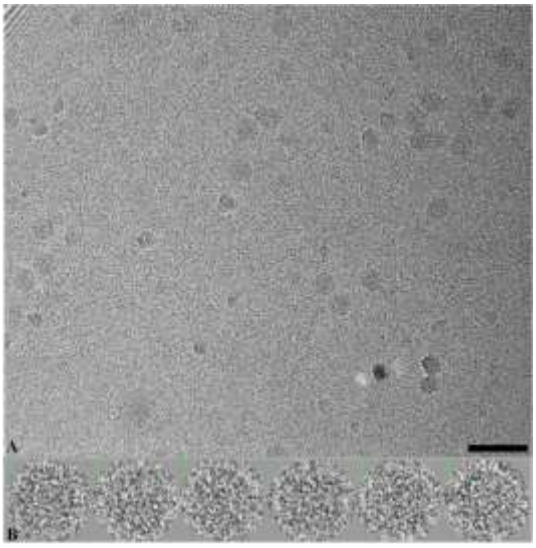

Fig. 7.4. Vitrified post-entry nc's

A. Vitrified post-entry nc's in cryo-EM. Sample vitrified on continuous carbon coated holey film. Images taken on CCD camera on a JEM2100. Scale bar= 100 nm. B. Boxed particles from vitrified micrographs in the same dataset.

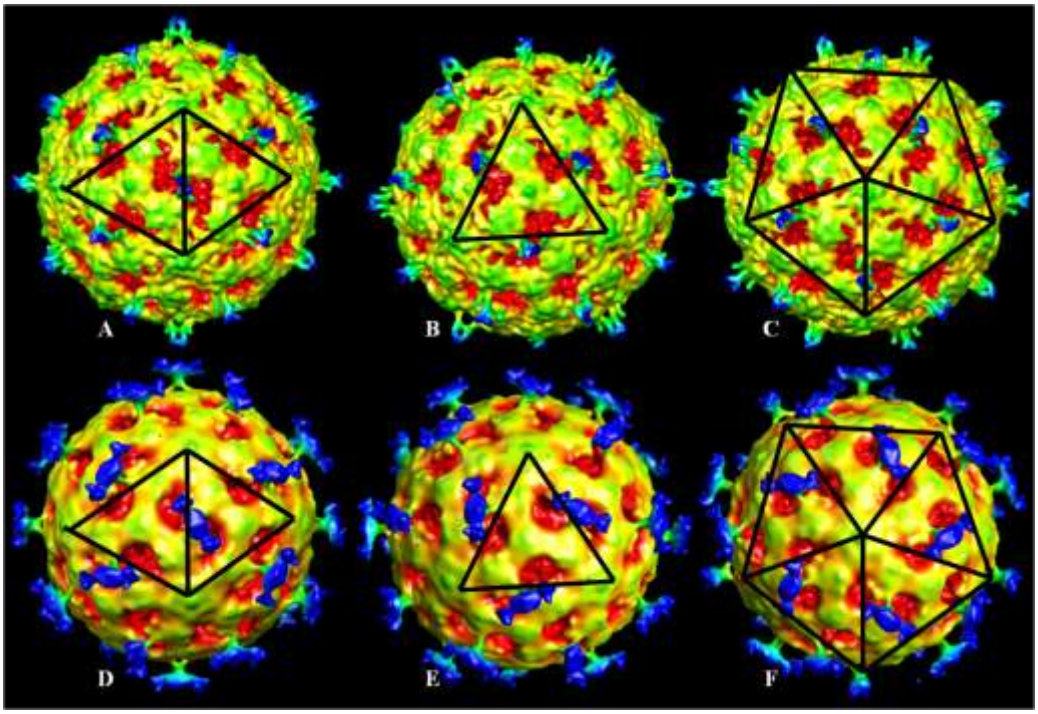

Fig. 7.5. Post-entry nc at pH 5.5 Cryo-EM reconstructions

(A-C) Post-entry nc at pH 5.5 reconstruction using VEEV mature nc as initial starting model, shown at its 2, 3, and 5 fold axes of symmetry, respectively. (D-F) Post-entry nc at pH 5.5 reconstruction using Sindbis mature nc as initial starting model, shown at its 2, 3, and 5 fold axes of symmetry, respectively. Neither reconstruction was produced using any CTF correction.

Conclusions The parallel preliminary p ost-entry nc reconstructions, from the two initial models, VEE mature nc and Sindbis mature nc, are comparable and show the beginnings of the same structural characteristics. The most noteworthy features of these maps are the gaping pores at the two-fold axis and a sharp spike in the middle Fig. 4.20. These pores and elevated feature at an axis is similar to what is seen at the five-

fold axis of bacteriophage phix174 (empty) (Bernal *et al*., 2003), which is the procapsid phase of the ssDNA phage. This would suggest that the two-fold axis of the post-entry nc is or has released the ssRNA through the large pores at the two-fold axis in a similar but inverse manner in which the phix174 procapsid's pores at the five-fold axis allows entry to its nucleic acid. Confidence in this deduction would be pending refinement of these structures.

Appendix 1: VEEV-TC83 Reconstructions Using Different CTF Methods

Rationale The rationale for the cryo-EM reconstructions of the VEEV-TC83 with different CTF corrections was an attempt to address whether CTF corrections caused distortions in a reconstruction with a known, correction structure.

Results: VEEV-TC83 cryo-EM Reconstructions done with altering the CTF mode in the map-generating program, EM3DR, did not alter the results of the map, Fig. A1.1 (B-E). The major features of the VEEV-TC83 maps matched with what is currently known about the whole virus structure (Paredes *et al.*, 2001), Fig. A1.1 (A). Reconstructions resulting from differences in CTF modes in the particle origin and orientation determination program, PFTSEARCH, did show differences between each other and, in the case of CTF modes 1 and 3, with the known VEEV-TC83 structure, Fig. A1.1 (F-I).

Spherical averages of the VEEV maps which correlated well with the accepted map have highly overlapping spherical average plots, Fig. A1.2. The least correlating of those structures also corresponds to the one with the most variant spherical average plot.

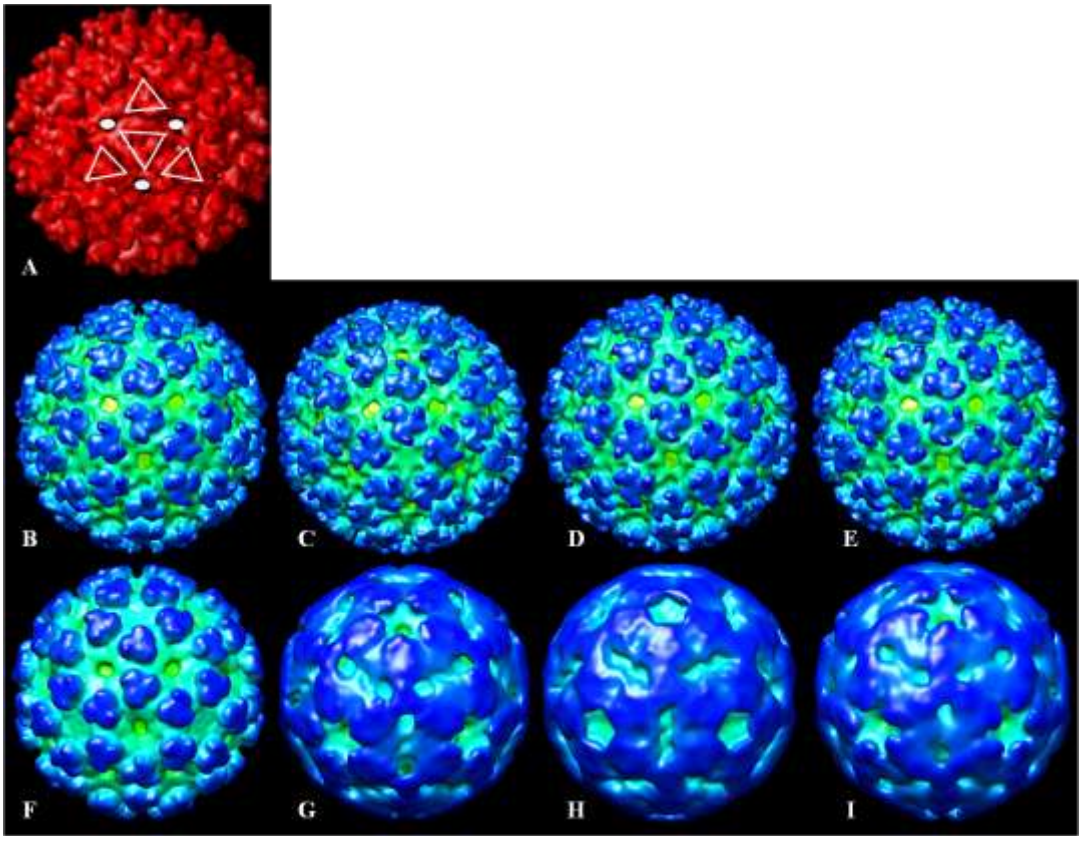

Fig. A1.1. Cryo-EM reconstructions of VEEV-TC83 using different CTF corrections

A. The accepted TC83 map (Paredes *et al*., 2001) reduced to ~30 Å resolution for comparison to the other VEEV maps (B-I). The shapes overlaying the structure show are highlight structural features the other reconstructions should have to be comparable to the accepted map (A). In reconstructions (B-E), no CTF correction was used to produce the newly produced map via EM3DR, but varying CTF correction in PFTsearch to find origins and orientations were employed. B. VEEV reconstruction using no CTF correction in either PFTsearch or EM3DR. C. VEEV reconstruction using CTF correction mode= 1 (model projections are multiplied by the CTF)* in PFTsearch. D. VEEV reconstruction using CTF correction mode= 2 (raw image is multipied by CTF)* in PFTsearch. E. VEEV reconstruction using CTF correction mode= 3 (raw image is multiplied by 1/CTF)* in PFTsearch. In reconstructions (F-I), CTF correction was used in EM3DR for producing the newly produced maps, but varying CTF corrections were, again, used in PFTsearch to find origins and orientations. F. VEEV reconstruction using no CTF correction in PFTsearch. G. VEEV reconstruction using CTF mode= 1 in PFTsearch. H. VEEV reconstruction using CTF mode=2 in PFTsearch. I. VEEV reconstruction using CTF mode= 3 in PFTsearch. Information on CTF modes in PFTsearch available at http://cryoem.ucsd.edu/programs/pftsearch.pdf.

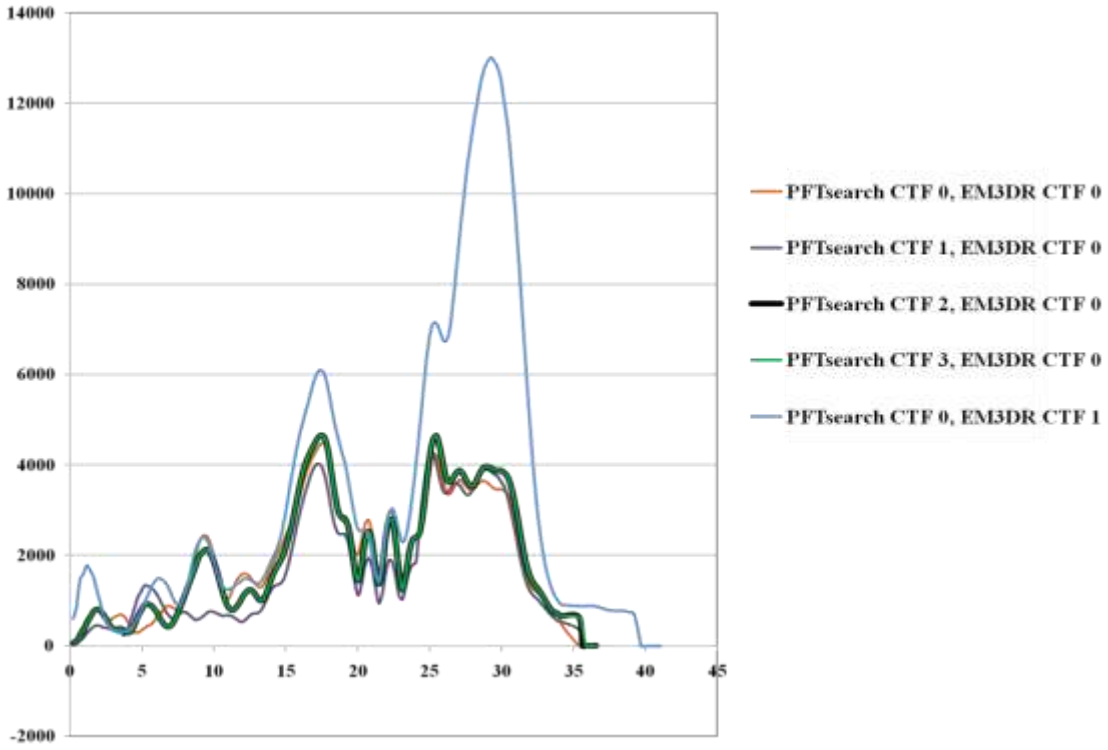

Fig. A1.2. Overlap of correlating VEEV-TC83 maps' spherical average plots

VEEV maps from Fig. A1.1 (B-F) which corresponded well with the accepted map (Paredes *et al*., 2001) are included.

Conclusions This shows that CTF corrections can distort resulting cryo-EM single particle reconstructions. The results found here for CTF corrections which distrorted the TC83 maps would likely be the same for similar maps, such as another alphavirus whole virion reconstruction. This agrees with what the authors of the reconstruction programs say about their programs on their website, http://cryoem.ucsd.edu/programs/pftsearch.pdf. This is to say that I agree that one must proceed with caution when applying CTF corrections and try all available options before choosing one to use.

References

Acheson, N. H., and Tamm, I. (1967). Replication of Semliki Forest virus: an electron microscopic study. *Virology* **32,** 128-143.

Adrian, M., Dubochet, J., Lepault, J., and McDowall, A.W. (1984). Cryo-electron microscopy of viruses. *Nature* **308,** 32-36.

Aguilar, P. V., Greene, I. P., Coffey, L. L., Medina, G., Moncayo, A. C., Anishchenko, M., Ludwig, G. V., Turell, M. J., O'Guinn, M. L., Lee, J., Tesh, R. B., Watts, D. M., Russell, K. L., Hice, C., Yanoviak, S., Morrison, A. C., Klein, T. A., Dohm, D. J., Guzman, H., Travassos da Rosa, A. P., Guevara, C., Kochel, T., Olson, J., Cabezas, C., and Weaver, S. C. (2004). Endemic Venezuelan equine encephalitis in northern Peru. *Emerg Infect Dis* **10,** 880-888.

Alter, M. J., Coleman, P. J., Alexander, W. J., Kramer, E., Miller, J. K., Mandel, E., Hadler, S. C., and Margolis, H. S. (1989). Importance of heterosexual activity in the transmission of hepatitis B and non-A, non-B hepatitis. *JAMA* **262,** 1201-1205.

Alter, M. J., Hadler, S. C., Judson, F. N., Mares, A., Alexander, W. J., Hu, P. Y., Miller, J. K., Moyer, L. A., Fields, H. A., Bradley, D. W., and Margolis, H. S. (1990). Risk factors for acute non-A, non-B hepatitis in the United States and association with hepatitis C virus infection. *JAMA* **264,** 2231-2235.

Alter, M. J., and Moyer, L. A. (1998). The importance of preventing hepatitis C virus infection among injection drug users in the United States. *J Acquir Immune Defic Syndr Hum Retrovirol* **18,** S6-S10.

Amos, L. A., Henderson, R., and Unwin, P. N. (1982). Three-dimensional structure determination by electron microscopy of two-dimensional crystals. *Prog Biophys Mol Biol* **39,** 183-231.

Anderson, L. E., Wang, X., Gibbon, J. T. (2005). Three enzymes of carbon metabolism or their antigenic analogs in pea leaf nuclei. *Plant Physiol* **105**, 659-667.

Baker, T. S., and Cheng, R. H. (1996). A model-based approach for determining orientations of biological macromolecules imaged by cryoelectron microscopy. *J Struct Biol* **116,** 120-130.

Baker, T. S., and Johnson, J. E. (1996). Low resolution meets high: towards a resolution continuum from cells to atoms. *Curr Opin Struc Biol* **6,** 585-594.

Baker, T. S., Olson, N. H., and Fuller, S. D. (1999). Adding the third dimension to virus life cycles: three-dimensional reconstruction of icosahedral viruses from cryo-electron micrographs. *Microbiol Mol Biol Rev* **63,** 862-922.

Barth, H., Cerino, R., Arcuri, M., Hoffmann, M., Schurmann, P., Adah, M. I., Gissler, B., Zhao, X., Ghisetti, V., Lavezzo, B., Blum, H. E., von Weizsacker, F., Vitelli, A., Scarselli, E., and Baumert, T. F. (2005). Scavenger receptor class B type I and hepatitis C virus infection of primary tupaia hepatocytes. *J Virol* **79,** 5774-5785.

Baumeister, W. (1982). Towards higher resolution in biomolecular electron microscopy. *Ultramicroscopy* **9,** 151-158.

Berger, B., Shor, P. W., Tucker-Kellogg, L., and King, J. (1994). Local rule-based theory of virus shell assembly. *Proc Natl Acad Sci U S A* **91,** 7732-7736.

Bernal, R. A., Hafenstein, S., Olson, N. H., Bowman, V. D., Chipman, P. R., Baker, T. S., Fane, B. A., and Rossmann, M. G. (2003). Structural studies of bacteriophage alpha3 assembly. *J Mol Biol* **325,** 11-24.

Bernard, K. A., Klimstra, W. B., and Johnston, R. E. (2000). Mutations in the E2 glycoprotein of Venezuelan equine encephalitis virus confer heparan sulfate interaction, low morbidity, and rapid clearance from blood of mice. *Virology* **276,** 93-103.

Blanchard, E., Belouzard, S., Goueslain, L., Wakita, T., Dubuisson, J., Wychowski, C., and Rouille, Y. (2006). Hepatitis C virus entry depends on clathrin-mediated endocytosis. *J Virol* **80,** 6964-6972.

Bolumar, F., Hernandez-Aguado, I., Ferrer, L., Ruiz, I., Avino, M. J., and Rebagliato, M. (1996). Prevalence of antibiotics to hepatitis C in a population of intravenous drug users in Valencia, Spain, 1990-1992. *Int J Epidemiol* **25,** 204-209.

Böttcher, B., Wynne, S. A., and Crowther, R. A. (1997). Determination of the fold of the core protein of hepatitis B virus by electron cryomicroscopy. *Nature* **386,** 88-91.

Boulant, S., Vanbelle, C., Ebel, C., Penin, F., and Lavergne, J. P. (2005). Hepatitis C virus core protein is a dimeric alpha-helical protein exhibiting membrane protein features. *J Virol* **79,** 11353-11365.

Bradley, D., McCaustland, K., Krawczynski, K., Spelbring, J., Humphrey, C., and Cook, E. H. (1991). Hepatitis C virus: buoyant density of the factor VIII-derived isolate in sucrose. *J Med Virol* **34,** 206-208.

Bradley, D. W., Maynard, J. E., Popper, H., Cook, E. H., Ebert, J. W., McCaustland, K. A., Schable, C. A., and Fields, H. A. (1983). Posttransfusion non-A, non-B hepatitis: physicochemical properties of two distinct agents. *J Infect Dis* **148,** 254-265.

Bradley, D. W., McCaustland, K. A., Cook, E. H., Schable, C. A., Ebert, J. W., and Maynard, J. E. (1985). Posttransfusion non-A, non-B hepatitis in chimpanzees. Physicochemical evidence that the tubule-forming agent is a small, enveloped virus. *Gastroenterology* **88,** 773-779.

Bukh, J., Purcell, R. H., and Miller, R. H. (1994). Sequence analysis of the core gene of 14 hepatitis C virus genotypes. *Proc Natl Acad Sci U S A* **91,** 8239-8243.

Bykovsky, A. F., Yershov, F. I., and Zhdanov, V. M. (1969). Morphogenesis of Venezuelan equine encephalomyelitis virus. *J Virol* **4,** 496-504.

Carrillo-Tripp, M., Shepherd, C. M., Borelli, I. A., Venkataraman, S., Lander, G., Natarajan, P., Johnson, J. E., Brooks, C. L., 3rd, and Reddy, V. S. (2009). VIPERdb2: an enhanced and web API enabled relational database for structural virology. *Nucleic Acids Res* **37,** D436-D442.

Carruthers, S., and Loxley, W. (1995). Hepatitis C and young drug users: are they about to join the epidemic? *Aust J Public Health* **19,** 421-424.

Caspar, D. L., and Klug, A. (1962). Physical principles in the construction of regular viruses. *Cold Spring Harb Symp Quant Biol* **27,** 1-24.

Caston, J. R., Trus, B. L., Booy, F. P., Wickner, R. B., Wall, J. S., and Steven, A. C. (1997). Structure of L-A virus: a specialized compartment for the transcription and replication of double-stranded RNA. *J Cell Biol* **138,** 975-985.

Cheng, R. H., Reddy, V. S., Olson, N. H., Fisher, A. J., Baker, T. S., and Johnson, J. E. (1994). Functional implications of quasi-equivalence in a T = 3 icosahedral animal virus established by cryo-electron microscopy and X-ray crystallography. *Structure* **2,** 271-282.

Chetwynd, J., Brunton, C., Blank, M., Plumridge, E., and Baldwin, D. (1995). Hepatitis C seroprevalence amongst injecting drug users attending a methadone programme. *N Z Med J* **108,** 364-366.

Chipman, P. R., Agbandje-McKenna, M., Kajigaya, S., Brown, K. E., Young, N. S., Baker, T. S., and Rossmann, M. G. (1996). Cryo-electron microscopy studies of empty capsids of human parvovirus B19 complexed with its cellular receptor. *Proc Natl Acad Sci U S A* **93,** 7502-7506.

Chiu, W., Burnett, R. M., and Garcea, R. L. (1997). "Structural biology of viruses." Oxford University Press, New York, NY.

Choi, Y. G., and Rao, A. L. (2000). Molecular studies on bromovirus capsid protein. VII. Selective packaging on BMV RNA4 by specific N-terminal arginine residuals. *Virology* **275,** 207-217.

Chromy, L. R., Pipas, J. M., and Garcea, R. L. (2003). Chaperone-mediated in vitro assembly of Polyomavirus capsids. *Proc Natl Acad Sci U S A* **100,** 10477-10482.

Cosslett, V. E. (1947). Conditions for extending the resolution limit of the electron microscope. *J Sci Instrum* **23,** 40-43.

Cotton, P. (1991). Tests help nail down HCV--but not entirely. *JAMA* **265,** 312.

Courouce, A. M., Le Marrec, N., Girault, A., Ducamp, S., and Simon, N. (1994). Anti-hepatitis C virus (anti-HCV) seroconversion in patients undergoing hemodialysis: comparison of second- and third-generation anti-HCV assays. *Transfusion* **34,** 790-795.

Cremers, A. F., Fischer, J. C., Schilstra, M. J., and Mellema, J. E. (1979). Low-dose electron image reconstruction of negatively stained contractile phage sheath from Bacillus subtilis (PBS-Z). *Ultramicroscopy* **4,** 395-412.

Cristofari, G., Ivanyi-Nagy, R., Gabus, C., Boulant, S., Lavergne, J. P., Penin, F., and Darlix, J. L. (2004). The hepatitis C virus Core protein is a potent nucleic acid chaperone that directs dimerization of the viral (+) strand RNA in vitro. *Nucleic Acids Res* **32,** 2623-2631.

Crowther, R. A. (1971). Procedures for three-dimensional reconstruction of spherical viruses by fourier synthesis from electron micrographs. *Phil Trans R Soc Lond B* **261,** 221-230.

Crowther, R. A., Amos, L. A., Finch, J. T., De Rosier, D. J., and Klug, A. (1970). Three dimensional reconstructions of spherical viruses by fourier synthesis from electron micrographs. *Nature* **226,** 421-425.

Deny, P., Roulot, D., Asselot, C., Rauzy, M., Rautureau, J., and Coste, T. (1992). Low rate of hepatitis C virus (HCV) transmission within the family. *J Hepatol* **14,** 409-410.

Dierksen, K., Typke, D., Hegerl, R., and Baumeister, W. (1993). Towards automatic electron microscopy. II. implementations of autofocus and low-dose procedures. *Ultramicroscopy* **49,** 109-120.

Di Bisceglie, A. M., and Hoofnagle, J. H. (2002). Optimal therapy of hepatitis C. *Hepatology* **36,** S121-S127.

Dokland, T. (2000). Freedom and restraint: themes in virus capsid assembly. *Structure* **8,** R157-R162.

Dokland, T., and Murialdo, H. (1993). Structural transitions during maturation of bacteriophage lambda capsids. *J Mol Biol* **233,** 682-694.

Dupraz, P., and Spahr, P. F. (1992). Specificity of Rous sarcoma virus nucleocapsid protein in genomic RNA packaging. *J Virol* **66,** 4662-4670.

Duret, L., Gasteiger, E., and Perriere, G. (1996). LALNVIEW: a graphical viewer for pairwise sequence alignments. *Comput Appl Biosci* **12,** 507-510.

Esteban, J. I., Esteban, R., Viladomiu, L., Lopez-Talavera, J. C., Gonzalez, A., Hernandez, J. M., Roget, M., Vargas, V., Genesca, J., Buti, M., and et al. (1989). Hepatitis C virus antibodies among risk groups in Spain. *Lancet* **2,** 294-297.

Estrada-Franco, J. G., Navarro-Lopez, R., Beasley, D. W., Coffey, L., Carrara, A. S., Travassos da Rosa, A., Clements, T., Wang, E., Ludwig, G. V., Cortes, A. C., Ramirez, P. P., Tesh, R. B., Barrett, A. D., and Weaver, S. C. (2003). West Nile virus in Mexico: evidence of widespread circulation since July 2002. *Emerg Infect Dis* **9,** 1604-1607.

Evans, M. J., von Hahn, T., Tscherne, D. M., Syder, A. J., Panis, M., Wolk, B., Hatziioannou, T., McKeating, J. A., Bieniasz, P. D., and Rice, C. M. (2007). Claudin-1 is a hepatitis C virus co-receptor required for a late step in entry. *Nature* **446,** 801-805.

Fields, B. N., Knipe, D. M., and Howley, P. M. (1996). "Fields Virology." 3rd ed. Lippincott-Raven Publishers, Philadelphia, PA.

Flint, M., Thomas, J. M., Maidens, C. M., Shotton, C., Levy, S., Barclay, W. S., and McKeating, J. A. (1999). Functional analysis of cell surface-expressed hepatitis C virus E2 glycoprotein. *J Virol* **73,** 6782-6790.

Forsell, K., Griffiths, G., and Garoff, H. (1996). Preformed cytoplasmic nucleocapsids are not necessary for alphavirus budding. *EMBO J* **15,** 6495-6505.

Freundlich, M. M. (1963). Origin of the electron microscope: the history of a great invention, and of a misconception concerning the inventors, is reviewed. *Science* **142,** 185-188.

Frolov, I., Frolova, E., and Schlesinger, S. (1997). Sindbis virus replicons and Sindbis virus: assembly of chimeras and of particles deficient in virus RNA. *J Virol* **71,** 2819-2829.

Fromentin, R., Majeau, N., Laliberte Gagne, M. E., Boivin, A., Duvignaud, J. B., and Leclerc, D. (2007). A method for in vitro assembly of hepatitis C virus core protein and for screening of inhibitors. *Anal Biochem* **366,** 37-45.

Fukushi, S., Katayama, K., Kurihara, C., Ishiyama, N., Hoshino, F. B., Ando, T., and Oya, A. (1994). Complete 5' noncoding region is necessary for the efficient internal initiation of hepatitis C virus RNA. *Biochem Biophys Res Commun* **199,** 425-432.

Fuller, S. D., Butcher, S. J., Cheng, R. H., and Baker, T. S. (1996). Three-dimensional reconstruction of icosahedral particles--the uncommon line. *J Struct Biol* **116,** 48-55.

Gardner, J. P., Durso, R. J., Arrigale, R. R., Donovan, G. P., Maddon, P. J., Dragic, T., and Olson, W. C. (2003). L-SIGN (CD 209L) is a liver-specific capture receptor for hepatitis C virus. *Proc Natl Acad Sci U S A* **100,** 4498-4503.

Garoff, H. (1974). Cross-linking of the spike glycoproteins in Semliki Forest virus with dimethylsuberimidate. *Virology* **62,** 385-392.

Garoff, H., and Simons, K. (1974). Location of the spike glycoproteins in the Semliki Forest virus membrane. *Proc Natl Acad Sci U S A* **71,** 3988-3992.

Garoff, H., Simons, K., and Renkonen, O. (1974). Isolation and characterization of the membrane proteins of Semliki Forest virus. *Virology* **61,** 493-504.

Grakoui, A., Wychowski, C., Lin, C., Feinstone, S. M., and Rice, C. M. (1993). Expression and identification of hepatitis C virus polyprotein cleavage products. *J Virol* **67,** 1385-1395.

Hadziyannis, S. J., Sette, H., Jr., Morgan, T. R., Balan, V., Diago, M., Marcellin, P., Ramadori, G., Bodenheimer, H., Jr., Bernstein, D., Rizzetto, M., Zeuzem, S., Pockros, P. J., Lin, A., and Ackrill, A. M. (2004). Peginterferon-alpha2a and ribavirin combination therapy in chronic hepatitis C: a randomized study of treatment duration and ribavirin dose. *Ann Intern Med* **140,** 346-355.

Hainfeld, J. F., Wall, J. S., and Desmond, E. J. (1982). A small computer system for micrograph analysis. *Ultramicroscopy* **8,** 263-270.

Hawley, R. J., and Eitzen, E. M., Jr. (2001). Biological weapons--a primer for microbiologists. *Annu Rev Microbiol* **55,** 235-253.

Herschlag, D. (1995). RNA chaperones and the RNA folding problem. *J Biol Chem* **270,** 20871-20874.

Hewan-Lowe, K. (1992). Diagnostic electron microscopy: future development. *Ultrastruct Pathol* **16,** 259-261.

Hilleman, M. R. (2002). Overview: cause and prevention in biowarfare and bioterrorism. *Vaccine* **20,** 3055-3067.

Hofmann, H., and Kunz, C. (1990). Low risk of health care workers for infection with hepatitis C virus. *Infection* **18,** 286-288.

Honda, M., Brown, E. A., and Lemon, S. M. (1996). Stability of a stem-loop involving the initiator AUG controls the efficiency of internal initiation of translation on hepatitis C virus RNA. *RNA* **2,** 955-968.

Hong, E. M., Perera, R., and Kuhn, R. J. (2006). Alphavirus capsid protein helix I controls a checkpoint in nucleocapsid core assembly. *J Virol* **80,** 8848-8855.

Hoofnagle, J. H., and Seeff, L. B. (2006). Peginterferon and ribavirin for chronic hepatitis C. *N Engl J Med* **355,** 2444-2451.

Hopf, U., Moller, B., Kuther, D., Stemerowicz, R., Lobeck, H., Ludtke-Handjery, A., Walter, E., Blum, H. E., Roggendorf, M., and Deinhardt, F. (1990). Long-term follow-up of posttransfusion and sporadic chronic hepatitis non-A, non-B and frequency of circulating antibodies to hepatitis C virus (HCV). *J Hepatol* **10,** 69-76.

http://authors.library.caltech.edu/5456/1/hrst.mit.edu/hrs/materials/public/ElectronMicroscope/EM_HistOverview.htm Produced by Tim Patucka 07/19/2002, California Technical Institute, Website last updated by Arne Hessenbruch 12/10/2002, Accessed 09/2010.

http://bilbo.bio.purdue.edu/~baker/programs/doc/current/em3dr.html Maintained by Tim Baker laboratory, UCSD, Website last update 06/20/2002, Accessed 10/2005.

http://cryoem.ucsd.edu/programs-old.shtm Produced by the Timothy S. Baker Cryoelectron Microscopy Laboratory, UCSD, Website last updated 10/30/2006, Accessed 09/2010.

http://cryoem.ucsd.edu/programs/robem_usersguide_v3.15.pdf Maintained by Robert Sinkovits, UCSD, Website update 02/16/2010, Accessed (previous version) 10/2005.

http://cryoem.ucsd.edu/programs/pftsearch.pdf Maintained by Tim Baker laboratory, UCSD, Website update 11/14/2003, Accessed 10/2005.

http://www.neb.com/nebecomm/products/protocol31.asp Maintained by New England BioLab Inc., Website last update not listed, Accessed Spring 2004.

http://viperdb.scripps.edu/data_analy.php Maintained by The Scripps Research Institute, Website last updated 2008, Accessed 09/2010.

http://www.virology.wisc.edu/virusworld/tri_number.php Maintained by Jean-Yves Sgro, Institute for Molecular Virology University of Wisconsin-Madison, Website update 2010, Accessed 01/2010.

http://www.who.int/csr/disease/hepatitis/whocdscsrlyo2003/en/print.html Maintained by the World Health Organization, Website last update 2002, Accessed 01/2010.

Huang, Z., Baldwin, P. R., Mullapudi, S., and Penczek, P. A. (2003). Automated determination of parameters describing power spectra of micrograph images in electron microscopy. *J Struct Biol* **144,** 79-94.

Huang, Z. S., and Wu, H. N. (1998). Identification and characterization of the RNA chaperone activity of hepatitis delta antigen peptides. *J Biol Chem* **273,** 26455-26461.

Hussy, P., Langen, H., Mous, J., and Jacobsen, H. (1996). Hepatitis C virus core protein: carboxy-terminal boundaries of two processed species suggest cleavage by a signal peptide peptidase. *Virology* **224,** 93-104.

Ivanyi-Nagy, R., Kanevsky, I., Gabus, C., Lavergne, J. P., Ficheux, D., Penin, F., Fosse, P., and Darlix, J. L. (2006). Analysis of hepatitis C virus RNA dimerization and core-RNA interactions. *Nucleic Acids Res* **34,** 2618-2633.

Jubin, R., Vantuno, N. E., Kieft, J. S., Murray, M. G., Doudna, J. A., Lau, J. Y., and Baroudy, B. M. (2000). Hepatitis C virus internal ribosome entry site (IRES) stem loop IIId contains a phylogenetically conserved GGG triplet essential for translation and IRES folding. *J Virol* **74,** 10430-10437.

Kaper, J. M., and Geelen, J. L. (1971). Studies on the stabilizing forces of simple RNA viruses. II. Stability, dissociation and reassembly of cucumber mosaic virus. *J Mol Biol* **56,** 277-294.

Keef, T., Taormina, A., and Twarock, R. (2005). Assembly models for Papovaviridae based on tiling theory. *Phys Biol* **2,** 175-188.

Kellenberger, E. (1976). DNA viruses: cooperativity and regulation through conformational changes as features of phage assembly. *Philos Trans R Soc Lond B Biol Sci* **276,** 3-13.

Kerner, R. (2008). Classification and evolutionary trends of icosahedral viral capsids. *Computational and Math Methods in Med* **9,** 175-181.

Khromykh, A. A., and Westaway, E. G. (1996). RNA binding properties of core protein of the flavivirus Kunjin. *Arch Virol* **141,** 685-699.

Kim, Y. K., Kim, C. S., Lee, S. H., and Jang, S. K. (2002). Domains I and II in the 5' nontranslated region of the HCV genome are required for RNA replication. *Biochem Biophys Res Commun* **290,** 105-112.

Kinney, R. M., Chang, G. J., Tsuchiya, K. R., Sneider, J. M., Roehrig, J. T., Woodward, T. M., and Trent, D. W. (1993). Attenuation of Venezuelan equine encephalitis virus strain TC-83 is encoded by the 5'-noncoding region and the E2 envelope glycoprotein. *J Virol* **67,** 1269-1277.

Klein, K. C., Dellos, S. R., and Lingappa, J. R. (2005). Identification of residues in the hepatitis C virus core protein that are critical for capsid assembly in a cell-free system. *J Virol* **79,** 6814-6826.

Klietmann, W. F., and Ruoff, K. L. (2001). Bioterrorism: implications for the clinical microbiologist. *Clin Microbiol Rev* **14,** 364-381.

Koster, A. J., Chen, H., Sedat, J. W., and Agard, D. (1992). Automated microsocpy for electron tomography. *Ultramicroscopy* **3,** 207-227.

Knipe, D. M., Howley, P. M., and Griffin, D. E. (2001). "Fundamental virology." 4th ed. Lippincott Williams & Wilkins, Philadelphia, PA.

Krol, M. A., Olson, N. H., Tate, J., Johnson, J. E., Baker, T. S., and Ahlquist, P. (1999). RNA-controlled polymorphism in the in vivo assembly of 180-subunit and 120-subunit virions from a single capsid protein. *Proc Natl Acad Sci U S A* **96,** 13650-13655.

Kunkel, M., Lorinczi, M., Rijnbrand, R., Lemon, S. M., and Watowich, S. J. (2001). Self-assembly of nucleocapsid-like particles from recombinant hepatitis C virus core protein. *J Virol* **75,** 2119-2129.

Kunkel, M., and Watowich, S. J. (2002). Conformational changes accompanying self-assembly of the hepatitis C virus core protein. *Virology* **294,** 239-245.

Kunkel, M., and Watowich, S. J. (2004). Biophysical characterization of hepatitis C virus core protein: implications for interactions within the virus and host. *FEBS Lett* **557,** 174-180.

Larson, S. B., Day, J., Greenwood, A., and McPherson, A. (1998). Refined structure of satellite tobacco mosaic virus at 1.8 A resolution. *J Mol Biol* **277,** 37-59.

Larson, S. B., Lucas, R. W., Greenwood, A., and McPherson, A. (2005). The RNA of turnip yellow mosaic virus exhibits icosahedral order. *Virology* **334,** 245-254.

Larson, S. B., and McPherson, A. (2001). Satellite tobacco mosaic virus RNA: structure and implications for assembly. *Curr Opin Struc Biol* **11,** 59-65.

Lata, R., Conway, J. F., Cheng, N., Duda, R. L., Hendrix, R. W., Wikoff, W. R., Johnson, J. E., Tsuruta, H., and Steven, A. C. (2000). Maturation dynamics of a viral capsid: visualization of transitional intermediate states. *Cell* **100,** 253-263.

Lentzen, M., and Urban, K. (2006). Contrast transfer and resolution limits for sub-angstrom high-resolution transmission electron microscopy. *Microsc Microanal* **12,** 1456-1457.

Lepault, J., Booy, F. P., and Dubochet, J. (1983). Electron microscopy of frozen biological suspensions. *J Microsc* **129,** 89-102.

Liepold, L. O., Revis, J., Allen, M., Oltrogge, L., Young, M., and Douglas, T. (2005). Structural transitions in Cowpea chlorotic mottle virus (CCMV). *Phys Biol* **2,** S166-S172.

Linger, B. R., Kunovska, L., Kuhn, R. J., and Golden, B. L. (2004). Sindbis virus nucleocapsid assembly: RNA folding promotes capsid protein dimerization. *RNA* **10,** 128-138.

Lo, S. Y., Selby, M. J., and Ou, J. H. (1996). Interaction between hepatitis C virus core protein and E1 envelope protein. *J Virol* **70,** 5177-5182.

Lopez, C., Gil, L., Lazo, L., Menendez, I., Marcos, E., Sanchez, J., Valdes, I., Falcon, V., de la Rosa, M. C., Marquez, G., Guillen, G., and Hermida, L. (2009). In vitro assembly of nucleocapsid-like particles from purified recombinant capsid protein of dengue-2 virus. *Arch Virol* **154,** 695-698.

Lozach, P. Y., Lortat-Jacob, H., de Lacroix de Lavalette, A., Staropoli, I., Foung, S., Amara, A., Houles, C., Fieschi, F., Schwartz, O., Virelizier, J. L., Arenzana-Seisdedos, F., and Altmeyer, R. (2003). DC-SIGN and L-SIGN are high affinity binding receptors for hepatitis C virus glycoprotein E2. *J Biol Chem* **278,** 20358-20366.

Ludlam, C. A., Chapman, D., Cohen, B., and Litton, P. A. (1989). Antibodies to hepatitis C virus in haemophilia. *Lancet* **2,** 560-561.

Ludtke, S. J., Baldwin, P. R., and Chiu, W. (1999). EMAN: semiautomated software for high-resolution single-particle reconstructions. *J Struct Biol* **128,** 82-97.

Ludwig, G. V., Kondig, J. P., and Smith, J. F. (1996). A putative receptor for Venezuelan equine encephalitis virus from mosquito cells. *J Virol* **70,** 5592-5599.

Lyons, A. J., Lytle, J. R., Gomez, J., and Robertson, H. D. (2001). Hepatitis C virus internal ribosome entry site RNA contains a tertiary structural element in a functional domain of stem-loop II. *Nucleic Acids Res* **29,** 2535-2541.

Maisonneuve, P., Courouce, A. M., Ferrer le Coeur, F., Guerois, C., Laurian, Y., Magniez, M., Parquet-Gernez, A., Verroust, F., and Noel, L. (1992). Anti-HCV and recipients: situation in hemophiliacs in 1991. *Rev Fr Transfus Hemobiol* **35,** 193-198.

Maisonneuve, P., Laurian, Y., Noel, L., Guerois, C., Assouvie-Gomez, I., Ferrer-Le Coeur, F., Verroust, F., Courouce, A. M., and Saint-Paul, B. (1990). Antibodies against hepatitis C virus in French hemophiliacs. *Rev Fr Transfus Hemobiol* **33,** 375-377.

Majeau, N., Gagne, V., Boivin, A., Bolduc, M., Majeau, J. A., Ouellet, D., and Leclerc, D. (2004). The N-terminal half of the core protein of hepatitis C virus is sufficient for nucleocapsid formation. *J Gen Virol* **85,** 971-981.

Mandell, G. L., Douglas, R. G., and Bennett, J. E. (1995). "Mandell, Douglas and Bennett's principles and practice of infectious diseases." 4th ed. 2 vols. Churchill Livingstone, New York, NY.

Mannige, R. V., and Brooks, C. L., 3rd (2008). Tilable nature of virus capsids and the role of topological constraints in natural capsid design. *Phys Rev E Stat Nonlin Soft Matter Phys* **77,** 051902.

Marcellin, P. (1999). Hepatitis C: the clinical spectrum of the disease. *J Hepatol* **31,** 9-16.

Matsumoto, M., Hwang, S. B., Jeng, K. S., Zhu, N., and Lai, M. M. (1996). Homotypic interaction and multimerization of hepatitis C virus core protein. *Virology* **218,** 43-51.

Melancon, P., and Garoff, H. (1987). Processing of the Semliki Forest virus structural polyprotein: role of the capsid protease. *J Virol* **61,** 1301-1309.

Melbye, M., Biggar, R. J., Wantzin, P., Krogsgaard, K., Ebbesen, P., and Becker, N. G. (1990). Sexual transmission of hepatitis C virus: cohort study (1981-9) among European homosexual men. *BMJ* **301,** 210-212.

Miller, R. H., and Purcell, R. H. (1990). Hepatitis C virus shares amino acid sequence similarity with pestiviruses and flaviviruses as well as members of two plant virus supergroups. *Proc Natl Acad Sci U S A* **87,** 2057-2061.

Monazahian, M., Bohme, I., Bonk, S., Koch, A., Scholz, C., Grethe, S., and Thomssen, R. (1999). Low density lipoprotein receptor as a candidate receptor for hepatitis C virus. *J Med Virol* **57,** 223-229.

Mukhopadhyay, S., Chipman, P. R., Hong, E. M., Kuhn, R. J., and Rossmann, M. G. (2002). In vitro-assembled alphavirus core-like particles maintain a structure similar to that of nucleocapsid cores in mature virus. *J Virol* **76,** 11128-11132.

Myers, T. M., Smallwood, S., and Moyer, S. A. (1999). Identification of nucleocapsid protein residues required for Sendai virus nucleocapsid formation and genome replication. *J Gen Virol* **80,** 1383-1391.

Nakagawa, A., Miyazaki, N., Taka, J., Naitow, H., Ogawa, A., Fujimoto, Z., Mizuno, H., Higashi, T., Watanabe, Y., Omura, T., Cheng, R. H., and Tsukihara, T. (2003). The atomic structure of rice dwarf virus reveals the self-assembly mechanism of component proteins. *Structure* **11,** 1227-1238.

Namba, K., and Stubbs, G. (1986). Structure of tobacco mosaic virus at 3.6 A resolution: implications for assembly. *Science* **231,** 1401-1406.

Newcomb, W. W., Homa, F. L., Thomsen, D. R., and Brown, J. C. (2001). In vitro assembly of the herpes simplex virus procapsid: formation of small procapsids at reduced scaffolding protein concentration. *J Struct Biol* **133,** 23-31.

Newcomb, W. W., Trus, B. L., Cheng, N., Steven, A. C., Sheaffer, A. K., Tenney, D. J., Weller, S. K., and Brown, J. C. (2000). Isolation of herpes simplex virus procapsids from cells infected with a protease-deficient mutant virus. *J Virol* **74,** 1663-1673.

Nguyen, H. D., Reddy, V. S., and Brooks, C. L., 3rd (2009). Invariant polymorphism in virus capsid assembly. *J Am Chem Soc* **131,** 2606-2614.

Nolandt, O., Kern, V., Muller, H., Pfaff, E., Theilmann, L., Welker, R., and Krausslich, H. G. (1997). Analysis of hepatitis C virus core protein interaction domains. *J Gen Virol* **78,** 1331-1340.

Paredes, A., Alwell-Warda, K., Weaver, S. C., Chiu, W., and Watowich, S. J. (2001). Venezuelan equine encephalomyelitis virus structure and its divergence from old world alphaviruses. *J Virol* **75,** 9532-9537.

Paredes, A., Alwell-Warda, K., Weaver, S. C., Chiu, W., and Watowich, S. J. (2003). Structure of isolated nucleocapsids from Venezuelan equine encephalitis virus and implications for assembly and disassembly of enveloped virus. *J Virol* **7,** 659-664.

Pettersen, E. F., Goddard, T. D., Huang, C. C., Couch, G. S., Greenblatt, D. M., Meng, E. C., and Ferrin, T. E. (2004). UCSF Chimera--a visualization system for exploratory research and analysis. *J Comput Chem* **25,** 1605-1612.

Pileri, P., Uematsu, Y., Campagnoli, S., Galli, G., Falugi, F., Petracca, R., Weiner, A. J., Houghton, M., Rosa, D., Grandi, G., and Abrignani, S. (1998). Binding of hepatitis C virus to CD81. *Science* **282,** 938-941.

Pohlmann, S., Zhang, J., Baribaud, F., Chen, Z., Leslie, G. J., Lin, G., Granelli-Piperno, A., Doms, R. W., Rice, C. M., and McKeating, J. A. (2003). Hepatitis C virus glycoproteins interact with DC-SIGN and DC-SIGNR. *J Virol* **77,** 4070-4080.

Ponz, E., Campistol, J. M., Barrera, J. M., Gil, C., Pinto, J., Andreu, J., and Bruguera, M. (1991). Hepatitis C virus antibodies in patients on hemodialysis and after kidney transplantation. *Transplant Proc* **23,** 1371-1372.

Poynard, T., Ratziu, V., Benhamou, Y., Opolon, P., Cacoub, P., and Bedossa, P. (2000). Natural history of HCV infection. *Baillieres Best Pract Res Clin Gastroenterol* **14,** 211-228.

Prevelige, P. E., Jr., Thomas, D., and King, J. (1993). Nucleation and growth phases in the polymerization of coat and scaffolding subunits into icosahedral procapsid shells. *Biophys J* **64,** 824-835.

Prince, A. M., Huima-Byron, T., Parker, T. S., and Levine, D. M. (1996). Visualization of hepatitis C virions and putative defective interfering particles isolated from low-density lipoproteins. *J Viral Hepat* **3,** 11-17.

Rayment, I., Baker, T. S., Caspar, D. L., and Murakami, W. T. (1982). Polyoma virus capsid structure at 22.5 A resolution. *Nature* **295,** 110-115.

Reddy, V. S., Giesing, H. A., Morton, R. T., Kumar, A., Post, C. B., Brooks, C. L., 3rd, and Johnson, J. E. (1998). Energetics of quasiequivalence: computational analysis of protein-protein interactions in icosahedral viruses. *Biophys J* **74,** 546-558.

Rein, A., Henderson, L. E., and Levin, J. G. (1998). Nucleic-acid-chaperone activity of retroviral nucleocapsid proteins: significance for viral replication. *Trends Biochem Sci* **23,** 297-301.

Rico-Hesse, R., Weaver, S. C., de Siger, J., Medina, G., and Salas, R. A. (1995). Emergence of a new epidemic/epizootic Venezuelan equine encephalitis virus in South America. *Proc Natl Acad Sci U S A* **92,** 5278-5281.

Robertson, B., Myers, G., Howard, C., Brettin, T., Bukh, J., Gaschen, B., Gojobori, T., Maertens, G., Mizokami, M., Nainan, O., Netesov, S., Nishioka, K., Shin i, T., Simmonds, P., Smith, D., Stuyver, L., and Weiner, A. (1998). Classification, nomenclature, and database development for hepatitis C virus (HCV) and related viruses: proposals for standardization. International Committee on Virus Taxonomy. *Arch Virol* **143,** 2493-2503.

Roggendorf, M., Deinhardt, F., Rasshofer, R., Eberle, J., Hopf, U., Moller, B., Zachoval, R., Pape, G., Schramm, W., and Rommel, F. (1989). Antibodies to hepatitis C virus. *Lancet* **2,** 324-325.

Rosenthal, P. B., and Henderson, R. (2003). Optimal determination of particle orientation, absolute hand, and contrast loss in single-particle electron cryomicroscopy. *J Mol Biol* **333,** 721-745.

Rossmann, M. G., and Johnson, J. E. (1989). Icosahedral RNA virus structure. *Annu Rev Biochem* **58,** 533-573.

Rossmann, M. G., Olson, N. H., Kolatkar, P. R., Oliveira, M. A., Cheng, R. H., Greve, J. M., McClelland, A., and Baker, T. S. (1994). Crystallographic and cryo EM analysis of virion-receptor interactions. *Arch Virol Suppl* **9,** 531-541.

Sabahi, A. (2009). Hepatitis C virus entry: the early steps in the viral replication cycle. *Virol J* **6,** 117-128.

Salunke, D. M., Caspar, D. L., and Garcea, R. L. (1989). Polymorphism in the assembly of polyomavirus capsid protein VP1. *Biophys J* **56,** 887-900.

Santolini, E., Migliaccio, G., and La Monica, N. (1994). Biosynthesis and biochemical properties of the hepatitis C virus core protein. *J Virol* **68,** 3631-3641.

Sarkar, N. H., and Moore, D. H. (1970). Electron microscopy of the nucleic acid of mouse mammary tumor virus. *J Virol* **5,** 230-236.

Satyanarayana, T., Gowda, S., Mawassi, M., Albiach-Marti, M. R., Ayllon, M. A., Robertson, C., Garnsey, S. M., and Dawson, W. O. (2000). Closterovirus encoded HSP70 homolog and p61 in addition to both coat proteins function in efficient virion assembly. *Virology* **278,** 253-265.

Savithri, H. S., and Erickson, J. W. (1983). The self-assembly of the cowpea strain of southern bean mosaic virus: formation of T = 1 and T = 3 nucleoprotein particles. *Virology* **126,** 328-335.

Scarselli, E., Ansuini, H., Cerino, R., Roccasecca, R. M., Acali, S., Filocamo, G., Traboni, C., Nicosia, A., Cortese, R., and Vitelli, A. (2002). The human scavenger receptor class B type I is a novel candidate receptor for the hepatitis C virus. *EMBO J* **21,** 5017-5025.

Schneemann, A. (2006). The structural and functional role of RNA in icosahedral virus assembly. *Annu Rev Microbiol* **60,** 51-67.

Schroder, R. R., Hofmann, W., Menetret, J. (1990). Zero-loss energy filtering as improved imaging mode in cryoelectronmicroscopy of frozen-hydrated specimens. *J Struct Biol* **105,** 28-34.

Schwartz, R., Garcea, R. L., and Berger, B. (2000). "Local rules" theory applied to polyomavirus polymorphic capsid assemblies. *Virology* **268,** 461-470.

Seeff, L. B., and Dienstag, J. L. (1988). Transfusion-associated non-A, non-B hepatitis. Where do we go from here? *Gastroenterology* **95,** 530-533.

Selby, M. J., Choo, Q. L., Berger, K., Kuo, G., Glazer, E., Eckart, M., Lee, C., Chien, D., Kuo, C., and Houghton, M. (1993). Expression, identification and subcellular localization of the proteins encoded by the hepatitis C viral genome. *J Gen Virol* **74,** 1103-1113.

Severson, W., Xu, X., Kuhn, M., Senutovitch, N., Thokala, M., Ferron, F., Longhi, S., Canard, B., and Jonsson, C. B. (2005). Essential amino acids of the hantaan virus N protein in its interaction with RNA. *J Virol* **79,** 10032-10039.

Shaikh, T. R., Hegerl, R., and Frank, J. (2003). An approach to examining model dependence in EM reconstructions using cross-validation. *J Struct Biol* **142,** 301-310.

Sherman, M. B., Guenther, R. H., Tama, F., Sit, T. L., Brooks, C. L., Mikhailov, A. M., Orlova, E. V., Baker, T. S., and Lommel, S. A. (2006). Removal of divalent cations induces structural transitions in red clover necrotic mosaic virus, revealing a potential mechanism for RNA release. *J Virol* **80,** 10395-10406.

Smith, P.R. (1978). An integrated set of computer programs for processing electron micrographs of biological studies. *Ultramicroscopy* **3,** 153-160.

Sorzano, C. O., de la Fraga, L. G., Clackdoyle, R., and Carazo, J. M. (2004). Normalizing projection images: a study of image normalizing procedures for single particle three-dimensional electron microscopy. *Ultramicroscopy* **101,** 129-138.

Strauss, J. H., and Strauss, E. G. (1994). The alphaviruses: gene expression, replication, and evolution. *Microbiol Rev* **58,** 491-562.

Takahashi, K., Kishimoto, S., Yoshizawa, H., Okamoto, H., Yoshikawa, A., and Mishiro, S. (1992). p26 protein and 33-nm particle associated with nucleocapsid of hepatitis C virus recovered from the circulation of infected hosts. *Virology* **191,** 431-434.

Tanaka, Y., Shimoike, T., Ishii, K., Suzuki, R., Suzuki, T., Ushijima, H., Matsuura, Y., and Miyamura, T. (2000). Selective binding of hepatitis C virus core protein to synthetic oligonucleotides corresponding to the 5' untranslated region of the viral genome. *Virology* **270,** 229-236.

Tang, G., Peng, L., Baldwin, P. R., Mann, D. S., Jiang, W., Rees, I., and Ludtke, S. J. (2007). EMAN2: an extensible image processing suite for electron microscopy. *J Struct Biol* **157,** 38-46.

Tellinghuisen, T. L., Hamburger, A. E., Fisher, B. R., Ostendorp, R., and Kuhn, R. J. (1999). In vitro assembly of alphavirus cores by using nucleocapsid protein expressed in Escherichia coli. *J Virol* **73,** 5309-5319.

Tellinghuisen, T. L., and Kuhn, R. J. (2000). Nucleic acid-dependent cross-linking of the nucleocapsid protein of Sindbis virus. *J Virol* **74,** 4302-4309.

Teoh, N. C., and Farrell, G. C. (2004). Management of chronic hepatitis C virus infection: a new era of disease control. *Intern Med J* **34,** 324-337.

Tong, M. J., el-Farra, N. S., Reikes, A. R., and Co, R. L. (1995). Clinical outcomes after transfusion-associated hepatitis C. *N Engl J Med* **332,** 1463-1466.

Tsai, T. F. (1991). Arboviral infections in the United States. *Infect Dis Clin North Am* **5,** 73-102.

Tsukiyama-Kohara, K., Iizuka, N., Kohara, M., and Nomoto, A. (1992). Internal ribosome entry site within hepatitis C virus RNA. *J Virol* **66,** 1476-1483.

Tuma, R., Tsuruta, H., Benevides, J. M., Prevelige, P. E., Jr., and Thomas, G. J., Jr. (2001). Characterization of subunit structural changes accompanying assembly of the bacteriophage P22 procapsid. *Biochemistry* **40,** 665-674.

Twarock, R. (2004). A tiling approach to virus capsid assembly explaining a structural puzzle in virology. *J Theor Biol* **226,** 477-482.

Twarock, R., and Hendrix, R. W. (2006). Crosslinking in viral capsids via tiling theory. *J Theor Biol* **240,** 419-424.

van der Vies, S. M., Gatenby, A. A., and Georgopoulos, C. (1994). Bacteriophage T4 encodes a co-chaperonin that can substitute for Escherichia coli GroES in protein folding. *Nature* **368,** 654-656.

van Heel, M. G. (1979). Imagic and its results. *Ultramicroscopy* **4,** 117.

Visudtiphole, V., Thomas, M. B., Chalton, D. A., and Lakey, J. H. (2005). Refolding of *Escherichia coli* outer membrane protein F in detergent creates LPS-free trimers and asymmetric dimers. *Biochem J* **392**, 375-381.

Wang, E., Brault, A. C., Powers, A. M., Kang, W., and Weaver, S. C. (2003). Glycosaminoglycan binding properties of natural Venezuelan equine encephalitis virus isolates. *J Virol* **77,** 1204-1210.

Warrier, R., Linger, B. R., Golden, B. L., and Kuhn, R. J. (2008). Role of Sindbis virus capsid protein region II in nucleocapsid core assembly and encapsidation of genomic RNA. *J Virol* **82,** 4461-4470.

Weaver, S. C., Ferro, C., Barrera, R., Boshell, J., and Navarro, J. C. (2004). Venezuelan equine encephalitis. *Annu Rev Entomol* **49,** 141-174.

Weaver, S. C., Salas, R., Rico-Hesse, R., Ludwig, G. V., Oberste, M. S., Boshell, J., and Tesh, R. B. (1996). Re-emergence of epidemic Venezuelan equine encephalomyelitis in South America. VEE Study Group. *Lancet* **348,** 436-440.

Weihofen, A., Binns, K., Lemberg, M. K., Ashman, K., and Martoglio, B. (2002). Identification of signal peptide peptidase, a presenilin-type aspartic protease. *Science* **296,** 2215-2218.

Wejstal, R. (1999). Sexual transmission of hepatitis C virus. *J Hepatol* **31,** 92-95.

Wengler, G., and Gros, C. (1996). Analyses of the role of structural changes in the regulation of uncoating and assembly of alphavirus cores. *Virology* **222,** 123-132.

Wengler, G., and Wurkner, D. (1992). Identification of a sequence element in the alphavirus core protein which mediates interaction of cores with ribosomes and the disassembly of cores. *Virology* **191,** 880-888.

Werling, K., and Tulassay, Z. (2006). New trend in treatment in patients with chronic hepatitis C. *Orv Hetil* **147,** 637-641.

WHO, and Viral Hepatitis Prevention Board Antworp, B. (1999). Global surveillance and control of hepatitis C. Report of a WHO Consultation organized in collaboration with the Viral Hepatitis Prevention Board, Antwerp, Belgium. *J Viral Hepat* **6,** 35-47.

Wilkinson, T. A., Tellinghuisen, T. L., Kuhn, R. J., and Post, C. B. (2005). Association of Sindbis virus capsid protein with phospholipid membranes and the E2 glycoprotein: implications for alphavirus assembly. *Biochemistry* **44,** 2800-2810.

Williams, A. E., and Dodd, R. Y. (1990). The serology of hepatitis C virus in relation to post-transfusion hepatitis. *Ann Clin Lab Sci* **20,** 192-199.

Wilson, H. R., Tollin, P., Sawyer, L., Robinson, D. J., Price, N. C., and Kelly, S. M. (1991). Secondary structures of narcissus mosaic virus coat protein. *J Gen Virol* **72,** 1479-1480.

Woodson, S. A. (2000). Compact but disordered states of RNA. *Nat Struct Biol* **7,** 349-352.

Wrobel, B., Yosef, Y., Oppenheim, A. B., and Oppenheim, A. (2000). Production and purification of SV40 major capsid protein (VP1) in Escherichia coli strains deficient for the GroELS chaperone machine. *J Biotechnol* **84,** 285-289.

Xie, Z., and Hendrix, R. W. (1995). Assembly in vitro of bacteriophage HK97 proheads. *J Mol Biol* **253,** 74-85.

Xu, X., Severson, W., Villegas, N., Schmaljohn, C. S., and Jonsson, C. B. (2002). The RNA binding domain of the hantaan virus N protein maps to a central, conserved region. *J Virol* **76,** 3301-3308.

Yafal, A. G., and Palma, E. L. (1979). Morphogenesis of foot-and-mouth disease virus. I. Role of procapsids as virion Precursors. *J Virol* **30,** 643-649.

Yan, X., Sinkovits, R. S., and Baker, T. S. (2007). AUTO3DEM--an automated and high throughput program for image reconstruction of icosahedral particles. *J Struct Biol* **157,** 73-82.

Yang, F., Wang, W., Chen, R. Z., and Xu, X. (1997). A simple and efficient method for purification of prawn baculovirus DNA. *J Virol Methods* **67,** 1-4.

Yu, X., Qiao, M., Atanasov, I., Hu, Z., Kato, T., Liang, T. J., and Zhou, Z. H. (2007). Cryo-electron microscopy and three-dimensional reconstructions of hepatitis C virus particles. *Virology* **367,** 126-134.

Zanetti, A. R., Tanzi, E., and Newell, M. L. (1999). Mother-to-infant transmission of hepatitis C virus. *J Hepatol* **31,** 96-100.

Zhang, X., Walker, S. B., Chipman, P. R., Nibert, M. L., and Baker, T. S. (2003). Reovirus polymerase lambda 3 localized by cryo-electron microscopy of virions at a resolution of 7.6 A. *Nat Struct Biol* **10,** 1011-1018.

Zhu, J., Penczek, P. A., Schroder, R., and Frank, J. (1997). Three-dimensional reconstruction with contrast transfer function correction from energy-filtered cryoelectron micrographs: procedure and application to the 70S Escherichia coli ribosome. *J Struct Biol* **118,** 197-219.

Zlotnick, A., Johnson, J. M., Wingfield, P. W., Stahl, S. J., and Endres, D. (1999). A theoretical model successfully identifies features of hepatitis B virus capsid assembly. *Biochemistry* **38,** 14644-14652.

Vita

Kristen Lamb was born on December 19th, 1980 at Fort Gordon, Georgia the daughter of Lt. Col. James T. Lamb and Annette B. Lamb. She studied for her Bachelor's degree in Chemistry (ACS certified) at West Georgia University in Carrollton, Georgia. Here she was a Chemistry workshop leader, a TA in Organic Chemistry, and participated in research on "Green Chemistry." After earning her bachelor's degree there, she matriculated at the University of Texas Medical Branch (UTMB) in Galveston, Texas. Upon her acceptance at UTMB, she received a scholarship for entering graduate students from the Pharmacology Department, given her undergraduate research. In 2005, she received the Keck Fellowship for Virus Imaging, which was renewed under a competitive renewal the following year.

Education

B.S., Chemistry, May 2003, University of West Georgia, Carrollton, GA

Publications

Lamb, K., Lokesh, G.L., Sherman, M., and Watowich, S. (2010). Structure of a Venezuelan equine encephalitis virus assembly intermediate from infected cells. *Virol* **406,** 261-269.

Dissertation Summary

The studies focused on two simple ssRNA viruses, hepatitis C virus (HCV) and Venezuelan equine encephalitis Virus (VEEV), and their early stages of structural development. In the HCV experiments, preliminary experiments aimed at structural determination of the core protein, and the structure of nucleocapsids formed *in vitro*. Constructs of the HCV core protein considered for possible structural determination were H158 and H36-169. H36-169 expressed poorly and attempts with it were abandoned, and H158 was found to be largely unstructured and existing as a multimer at just 1 mg/mL. Structural determination using these, therefore, seemed unlikely. Attempts to find the

structure of the *in vitro* assembled HCV nucleocapsid with nucleocapsid-like-particle reactions using H124 and H158 with tRNA yielded particles heterogeneous in size in only a small sample size. Attention was averted to VEEV nucleocapsid morphology changes during virus maturation, and cryo-EM structural determinations of two nucleocapsid stages were attempted. Results of these experiments opened up more questions as to what happens between nucleocapsid formation and the enveloping process for simple ssRNA enveloped viruses as were observed here.